Summer 9-1-2014

Dominant Mechanisms of Uranium(VI)–Phosphate Interactions in Subsurface Environments: An in situ remediation perspective

Vrajesh Sanat Mehta
Washington University in St. Louis

WASHINGTON UNIVERSITY IN ST. LOUIS

School of Engineering and Applied Science

Department of Energy, Environmental, and Chemical Engineering

Dissertation Examination Committee:
Daniel E. Giammar, Chair
Jeffrey G. Catalano
John D. Fortner
Young-Shin Jun
Jill Pasteris
Palghat Ramachandran

Dominant Mechanisms of Uranium(VI)–Phosphate Interactions in Subsurface Environments: An *in situ* remediation perspective

by

Vrajesh Sanat Mehta

A dissertation presented to the
Graduate School of Arts and Sciences
of Washington University in
partial fulfillment of the
requirements for the degree
of Doctor of Philosophy

August 2014

Saint Louis, Missouri

Table of Contents

List of Figures

List of Tables

Acknowledgements

I am extremely grateful to my advisor Daniel Giammar for his valuable guidance, constant encouragement and motivation throughout the course of this research. He has been a great source of inspiration for me and I remain indebted to him. His relentless dedication and commitment to quality research has made me a better and more efficient researcher. From him, I have learned the importance of fundamentals, and his mentorship has helped me mature as a pragmatic individual.

I would like to acknowledge Jeff Catalano, John Fortner, Young-Shin Jun, Jill Pasteris and Palghat Ramachandran for agreeing to be members of my thesis committee. Their insightful suggestions and inputs helped me stay focused on specific research goals and tailoring the research approach for the same. Special thanks are due to Jeff Catalano for all his help and support on various fronts throughout this collaborative project. Working with Zheming Wang from PNNL was a pleasure and I always enjoyed my conversations with him. I am immensely grateful to Sanjeev Chaudhari, who introduced me to the world of research and also led by example to show how research can be utilized as a tool for the benefit of society.

Over the course of last four years, I got a chance to work with a great group of people within and outside the university. Specifically, I will cherish the interactions, constructive arguments and the time spent with Fabien Maillot on the project work and during beamtime at the Stanford Synchrotron Radiation Laboratory. My sincere thanks to

Lyndsay Taylor, whose help made my life a lot easier during the last few months of my Ph.D. Many thanks are due to Patty Wurm, Sanmathi Chavalmane, Kate Nelson, Paul Carpenter, Tyrone Daulton for their help in training me on various analytical instruments.

The Aquatic Chemistry Laboratory (ACL) has been a fruitful place for me where I thoroughly enjoyed working. The insightful discussions that we had during our weekly group meetings were very helpful in receiving suggestions and feedbacks, and they also enabled me to stay up to date with other research areas. Working with Yin Wang on his thesis project was a pleasure and I learned a lot from him. Discussions with him and Zimeng Wang were very rewarding throughout my stay in the ACL. My sincere thanks to Jose Cerrato, Fei Wang, Lin Wang, Wei Xiong and Chao Pan who were always available and willing to help out whenever needed. I enjoyed the experience of mentoring and working with Lijie Zhang, Begum Karakocak and Zezhen Pan. I would like to thank Daniel Giammar and other instructors including Jay Turner, Robin Shephard and Robert Heider for giving me the opportunity to serve as a teaching assistant on various courses and for making those experiences so rewarding.

I find myself extremely honored on being a recipient of a McDonnell Academy scholarship. Being a McDonnell Scholar provided me with unique opportunities to interact with politicians, diplomats, journalists, entrepreneurs and talented scholars from different cultures through which I learned much more beyond research. Mary Wertsch and Jim Wertsch's warmth and loving nature made me feel as a part of their family. Their guidance and belief in my capabilities at all times was a morale booster, and I will always remain indebted to them. Carla, Kristin and Angie were always helpful and largely responsible for making my experience as a McDonnell Academy scholar so rewarding.

Many colleagues and friends within and outside the department are acknowledged for making my stint as a Ph.D. student enjoyable.

This work was supported by the U.S. Department of Energy (DOE) Subsurface Biogeochemical Research Program (Award No. DE-SC0006857). Thanks and best wishes are due to Charles and Marlene Buescher who donated the fellowship honoring Dr. Ryckman that supported my first year study.

I owe a lot to my little brother Bunti Mehta and his wife Nikita Mehta, who always stood by me and took care of our parents while I traveled through the journey of Ph.D. I am grateful to my parents-in-law Kalpana Shah and Jagdish Shah who supported me unreservedly in all the times and decisions that I took. I bow down my head at the feet of my parents Arti Mehta and Sanat Mehta with all veneration and gratitude for their selfless sacrifice in modeling my life. I imbibed the important lessons of life from them and wish their choicest blessing to be bestowed on me in coming years to come. I appreciate the encouragement provided by all the family members. Lastly, my deepest thanks go to my lovely wife Riddhi Mehta whose unconditional sacrifices always reminded me to keep going and not stop until the goal is achieved. Without her help and support, I have no doubts that this thesis would not have been completed.

Finally, I would like to dedicate this work to my daughter Aarna, whose arrival just days before the submission of this report has multiplied the joy of completion of Ph.D.

Vrajesh Mehta

Washington University in St. Louis

August 2014

ABSTRACT OF THE DISSERTATION

Dominant Mechanisms of Uranium(VI)–Phosphate Interactions in Subsurface Environments: An *In Situ* Remediation Perspective

by

Vrajesh Mehta

Doctor of Philosophy in Energy, Environmental, and Chemical Engineering

Washington University in St. Louis, 2014

Professor Daniel Giammar, Chair

Anthropogenic activities associated with the production of nuclear materials have resulted in uranium contaminated soil and groundwater. The carcinogenic and toxic effects of uranium contamination pose a significant risk to the environment and human health. Phosphate addition to uranium-contaminated subsurface environments has been proposed as a strategy for *in situ* remediation. Addition of phosphate amendments can result in uranium sequestration in its oxidized +VI state without sustaining reducing conditions as is needed for *in situ* immobilization via chemical or biological reduction of U(VI) to less soluble U(IV) species. Phosphate addition can be used as a stand-alone process or as a complementary process to bioremediation-based methods, especially for sites with naturally oxic conditions. Although recent studies have reported phosphate-induced precipitation of U(VI)-phosphates in laboratory and field-scale tests, the fundamental mechanisms controlling U(VI) immobilization are not well known. Hence understanding the mechanisms at the microscopic and molecular levels is imperative to

successfully designing and implementing phosphate-based *in situ* uranium immobilization.

Interactions with phosphate can result in uranium immobilization through various processes. This study investigated the dominant mechanisms of U(VI)-phosphate reactions using an integrated approach of aqueous phase and solid phase characterization techniques. Batch experiments were performed to study the effect of pH and co-solutes (dissolved inorganic carbon (DIC), Na^+ and Ca^{2+}) on the products and solubility of uranium(VI) precipitated with phosphate. The results suggested that in the absence of co-solute cations, chernikovite [$H_3O(UO_2)(PO_4)\cdot 3H_2O$] precipitated despite uranyl orthophosphate [$(UO_2)_3(PO_4)_2\cdot 4H_2O$] being thermodynamically more favorable under certain conditions. The presence of Na^+ as a co-solute led to the precipitation of sodium autunite [$Na_2(UO_2)_2(PO_4)_2$], and the dissolved U(VI) concentrations were generally in agreement with equilibrium predictions of sodium autunite solubility.

In the calcium-containing systems, the observed concentrations were below the predicted solubility of autunite [$Ca(UO_2)_2(PO_4)_2$]. Consequently, specific batch studies were conducted to investigate the dependence of U(VI) uptake mechanisms on the starting forms of calcium and phosphate at concentrations relevant to field sites. Depending on the experimental conditions, uranium uptake occurred through adsorption on calcium-phosphate solids, precipitation of autunite, or incorporation into a calcium-phosphate solid. Extended X-ray absorption fine structure (EXAFS) spectroscopy analysis using structural model fittings and linear combination fitting allowed quantification of the contribution of each uranium uptake mechanism mentioned above.

Following the batch experiments with simple systems, the effect of phosphate amendment on uranium immobilization was evaluated for sediments obtained from a field site in Rifle, Colorado using batch sorption studies and column experiments. Batch sorption studies showed that phosphate addition increased the U(VI) adsorption, however the net uranium uptake was limited due to the dominance of the aqueous speciation by Ca-U(VI)-carbonate complexes. Column experiments were performed under conditions that simulated the subsurface environment at the Rifle site. Remobilization experiments showed increased retention of uranium when phosphate was present in uranium-free influent. The response of dissolved uranium concentrations to stopped-flow events and the comparison of experimental data with a simple reactive transport model indicated that uranium transport was controlled by non-equilibrium processes. Intraparticle diffusion is thought to be acting as the rate-limiting process. Sequential extractions and laser induced fluorescence spectroscopy (LIFS) analysis indicated that adsorption was the dominant mode of uranium immobilization.

When uranium and phosphate were added concurrently to columns packed with sediments, significant uptake of uranium continued as long as phosphate was present in the influent. Even when phosphate was removed from the influent, the columns retained significant amounts (~ 67 %) of the accumulated uranium. Sequential extractions showed that the uranium accumulated transformed into less easily extractable (i.e., more immobile) species with the relative amounts of accumulated uranium extracted in the acetic acid and hot acid digestion step being highest for the column that was treated with phosphate for the longest duration. The uranium retained in the sediments after the phosphate was removed from the influent was primarily in a form that could be extracted

with acetic acid and ammonium acetate. The extraction results, aqueous phase analysis and LIFS analysis showed that uranium uptake occurred through multiple processes. For select conditions, EXAFS analysis was used to quantify the contribution of uranium uptake which confirmed that uranium uptake occurred through a combination of precipitation and adsorption.

The information gained from this research project improved our understanding of U(VI)-phosphate reactions that can be used to identify and manipulate the conditions that lead to the greatest decreases in U(VI) mobility. The results illustrate that precipitation of uranyl-phosphates is not the only means of *in situ* uranium remediation and that a wide range of uranium immobilization mechanisms can control uranium mobility following phosphate addition. Although phosphate addition led to significant retardation of uranium release and also resulted in increased net uptake of uranium for conditions of the Rifle site, phosphate amendments could be more beneficial at sites with lower pH and dissolved inorganic carbon concentrations.

|| Jai Shri Krishna ||

Chapter 1. Introduction

1.1 Background and Motivation

Programs associated with the production of nuclear materials have led to the generation of hazardous radioactive wastes at many places across the world. In the United States, following the shutdown of nuclear weapons production in 1990's, the Department of Energy [DOE] (DOE 1997) reported the contamination of over 1.7 trillion gallons of contaminated groundwater, 40 million cubic meters of contaminated soil and debris, and 3 million cubic meters of waste buried in landfills, trenches and spill areas. This legacy has contaminated groundwater and soil at more than 120 DOE sites across 36 states in the United States (Palmisano and Hazen 2003). The contamination of groundwater and soil at these sites occurred as a result of direct injection of mixed waste into the subsurface, leakage from storage tanks, and infiltration from unlined storage ponds into the surrounding media. These releases can lead to contamination that eventually migrates into surface water or groundwater sources used for water supplies. At least half of the contamination at most of these sites is comprised of heavy metals and radionuclides, with uranium being one of the major components of the waste.

The distributed nature of the contamination over vast areas makes it economically challenging to use pump-and-treat or excavation methods, so *in situ*

immobilization is an attractive approach. The objective of this route of remediation is to enhance the formation of stable solid forms of uranium, thus reducing its mobility. *In situ* remediation allows the possibility of manipulation of site geochemistry and hydrogeology to promote immobilization. Phosphate addition is one possible method for promoting *in situ* immobilization. To attain effective uranium containment strategies, a proper understanding of the immobilization mechanisms that affect uranium's fate and transport is necessary.

1.1.1 Aqueous Uranium Geochemistry

Being the most abundant of the naturally occurring actinides, uranium concentrations of 1.2 to 120 mg/kg have been reported in the enriched deposits of sedimentary rocks and phosphate rocks, respectively, in countries including Canada, Brazil, Australia, Namibia and the United States (Ewing 1999). In natural surface waters, concentrations range from 0.001 µM to 5 µM as compared to 0.03 µM in seawater (Finch and Murakami 1999, Langmuir 1997). The three main isotopes of uranium are ^{238}U, ^{235}U and ^{234}U with the natural abundance of 99.2745%, 0.720%, and 0.0055% respectively. While uranium can exist in oxidation states of 0 to +6, in environmental systems it predominantly exists as U(IV) and U(VI) as can be seen from a predominance diagram (Figure 1.1). Uranium(IV) is primarily found in reducing environments as the mineral uraninite $UO_{2(s)}$ that can be oxidized to U(VI) species under oxic conditions (Langmuir 1997). In oxic conditions UO_2^{2+} and associated aqueous complexes are more soluble than U(IV) (Finch and Murakami

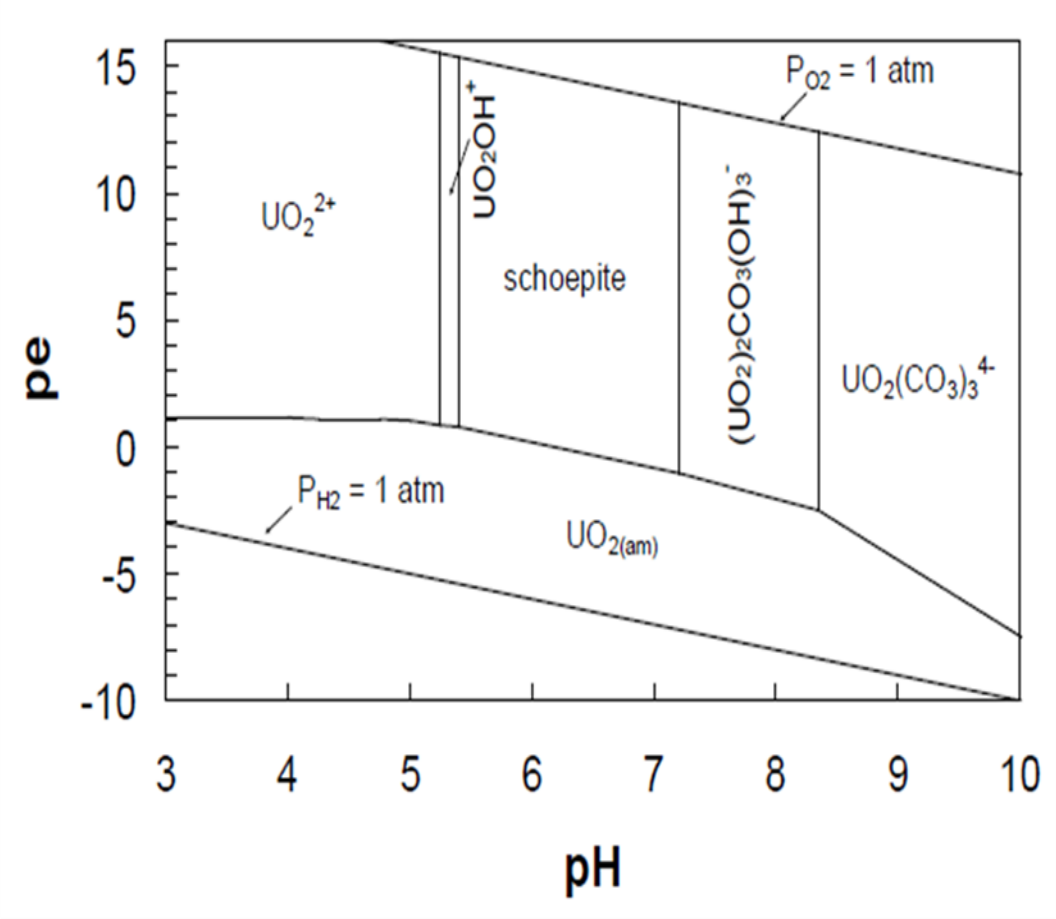

Figure 1.1. pe-pH diagram showing predominant forms for aqueous species and solids in the system U-O_2-CO_2-H_2O at 25 °C, 1 bar total pressure for $[U]_{tot}$ = 5 µM and $P_{CO2}=10^{-3.5}$ atm (Singh 2010).

1999). Figure 1.2 represents a simplified overview of uranium aqueous biogeochemistry. The aqueous solubility of uranium is mainly controlled by pH, dissolved inorganic carbon, and oxidation-reduction potential (Burns et al. 1999). Figure 1.3 illustrates the different U(VI) hydroxide and carbonate complexes that are present over a range of pH values in a system with inorganic carbon. The uranyl ion preferentially interacts with naturally abundant anions to form complexes, the significant ones being complexes with carbonate [$UO_2CO_{3(aq)}$, $UO_2(CO_3)_3^{4-}$ and $UO_2(CO_3)_2^{2-}$], hydroxide [$(UO_2)_3(OH)_4^{2+}$ and $(UO_2)_2OH^{3+}$] and phosphate [($UO_2PO_4^-$

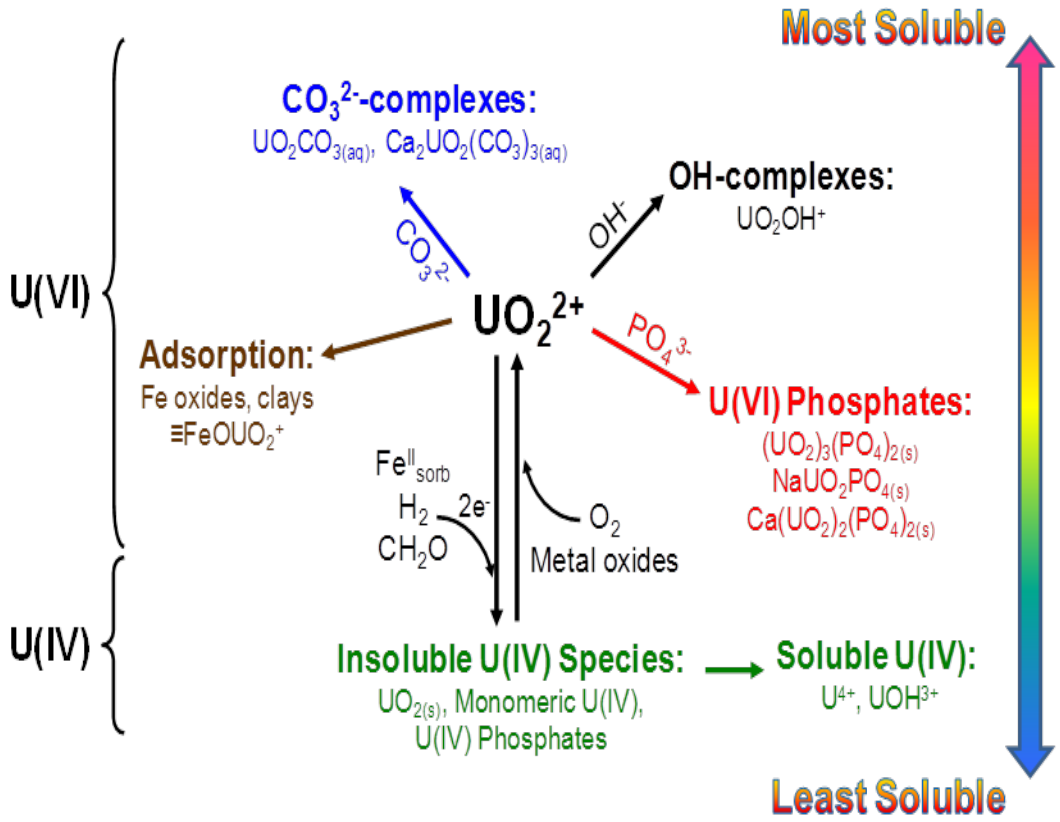

Figure 1.2. Simplified overview of uranium aqueous biogeochemistry.

and $UO_2HPO_{4(aq)}$)] which can be the dominant species over different pH ranges. The complexes with multidentate ligands such as carbonate tend to have greater stability than those with monodentate ligands (Stumm and Morgan 1996). Uranyl carbonates play a critical role in the migration of uranium in alkaline groundwater (Finch and Murakami 1999). These complexes also affect the strength and capacity of U(VI) adsorption to mineral surfaces. In the presence of calcium, which is typically found in significant concentrations in groundwater, complexes of Ca-U(VI)-CO_3^{2-} have been reported that can further influence the solubility of uranium (Dong and Brooks 2006, Kelly et al. 2007).

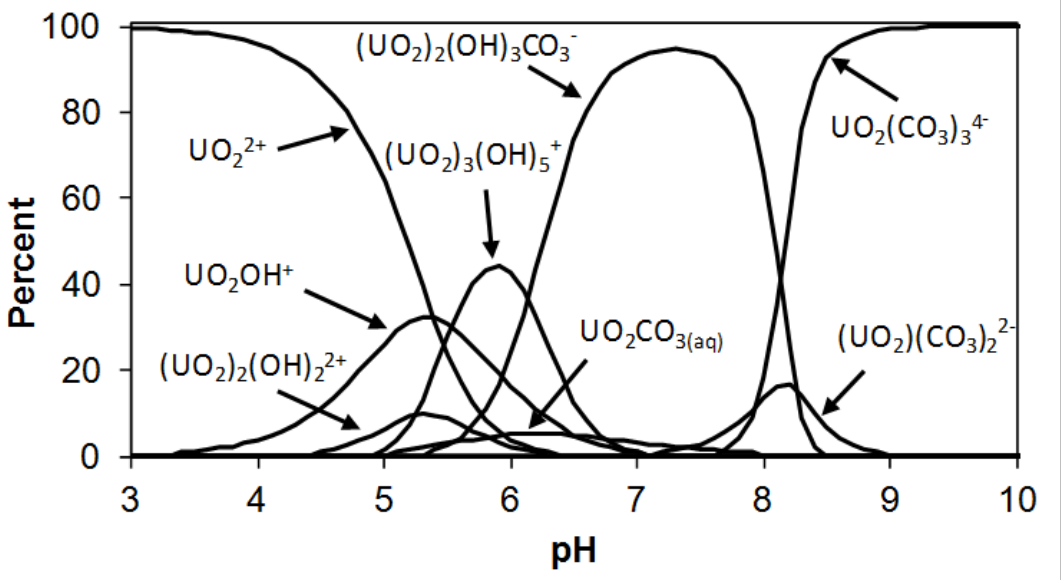

Figure 1.3. Distribution of uranium species for TotU=5 µM, P_{CO2} = $10^{-3.5}$ atm, and 0.01 M ionic strength as predicted using the equilibrium modeling system MINEQL+, v 4.6 (Schecher and McAvoy 2007) with the thermodynamic constants listed in Appendix A, Table A.1. Calculations were made without considering precipitation of any solids.

1.1.2 Phosphate Geochemistry

For many metals, phosphate solids are among the lowest solubility precipitates that can form, and these properties have led to applications of phosphates in different fields. Hence the promotion of phosphate mineral precipitation to sequester inorganic contaminants like lead, cadmium, selenium and strontium has been studied in recent years (Wright et al. 2011, Xie and Giammar 2007). The range of solubility of most of the phosphate minerals varies from slightly soluble to relatively insoluble. The solubility minimum for most of these minerals is observed at circumneutral pH with the majority of minerals being more insoluble under slightly acidic conditions. Along with precipitation, the presence of phosphates can

also play an important role in immobilizing contaminants by adsorption to a phosphate mineral (Arey et al. 1999, Cheng et al. 2004, Fuller et al. 2002, Miretzky and Fernandez-Cirelli 2008, Payne et al. 1996) as well as the enhancement of metal adsorption to other minerals such as iron oxides (Cornell and Schwertmann 2003, Singh et al. 2010).

1.1.3 Uranium – Phosphate Geochemistry and Associated Remediation Strategies

Addition of phosphate amendments can be a useful method to promote the precipitation of low solubility U(VI) phosphates (Beazley et al. 2009, Fuller et al. 2002, Wellman et al. 2005, Wellman et al. 2008) that can remain stable on time scales of years even in the presence of 1 mM bicarbonate (Sowder et al. 2001). Uranyl phosphates have been observed in contaminated soils and sediments at the Oak Ridge reservation (Stubbs et al. 2009) and at the Fernald site (Morris et al. 1996). In natural oxidizing conditions with sites containing uranium ore deposits, phosphate has been found to be primarily associated with U(VI) via formation of uranyl phosphates (Jerden et al. 2003). Phosphate addition can thus be an ideal option for immobilizing uranium *in situ* without sustaining reducing conditions, and phosphate addition can be implemented along with bioremediation especially for sites with naturally oxic conditions.

A diverse group (approximately 40 minerals known) of uranyl phosphates have been identified in the literature. They can be divided into at least three

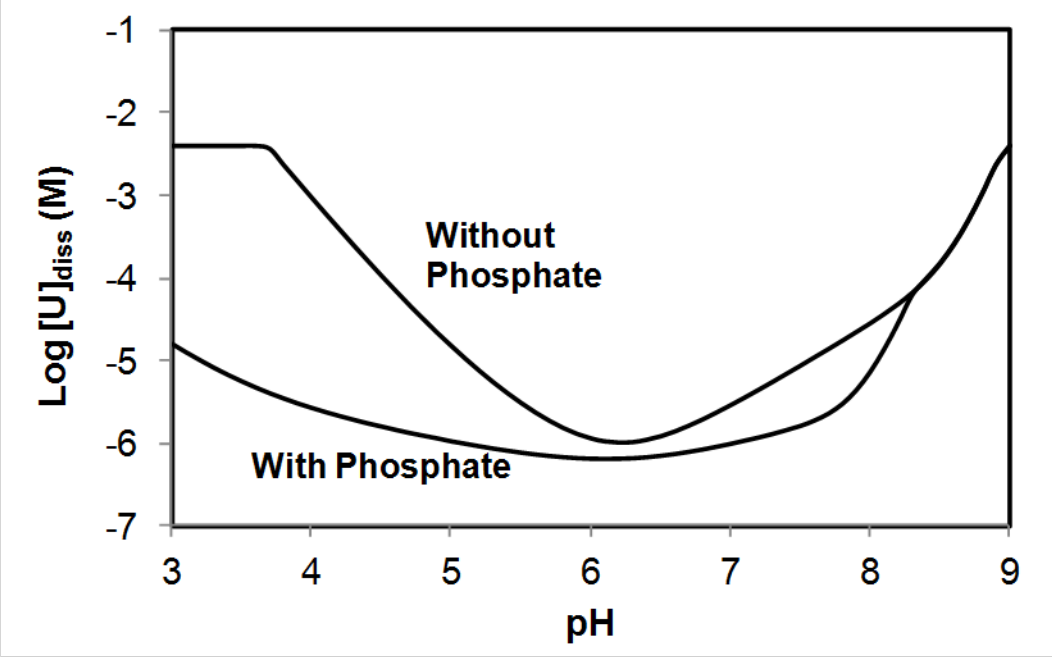

Figure 1.4. Solubility diagram of an open system (in equilibrium with air) with TotU = $10^{-2.4}$ M and Total P = $10^{-2.4}$ M as predicted using the equilibrium modeling system MINEQL with the thermodynamic constants listed in Table A.1. Calculations made with the possibility of precipitation of uranyl orthophosphate [$(UO_2)_3(PO_4)_{2(s)}$] or schoepite [$(UO_3{\cdot}2H_2O_{(s)}$] solids.

structurally and chemically related groups: 1) the autunite and meta-autunite groups which are tetragonal with sheet structures and U:P ratios of 1:1; 2) the phosphuranylite group based on a structural sheet with U:P of 3:2; and 3) the walpurgite group that are triclinic with U:P of 1:2. A list of some relevant minerals is given in Table A.2 in Appendix A.

In the presence of phosphate, the solubility of uranium is controlled at lower values than without phosphate by the formation of uranyl phosphate solids. The benefit of phosphate on decreasing U(VI) solubility is most significant below pH 8, because above this pH U(VI) oxides and oxyhydroxides such as schoepite can control the solubility. The effect of phosphate can be clearly seen in Figure 1.4, especially for the acidic pH range where the solubility is greatly reduced due to

precipitation of uranyl phosphate solids (uranyl orthophosphate in this case). It is to be noted that a wide range of uranyl phosphate solids can exist in the environment based on the presence of cations (different autunites containing $H^+/Ca^{2+}/Na^+/Mg^{2+}/Cu^{2+}$) that are preferentially taken up from the solution. This makes it necessary to understand the different types of uranyl phosphate solids that can form under given conditions.

For homogenous systems with only dissolved species and no minerals, precipitation can be the primary mode of immobilization due to the U(VI)-phosphate interactions. In the case of heterogeneous systems, adsorption of phosphate onto a substrate can prevent the precipitation of the uranyl phosphate solids by lowering the saturation ratios of the potential solids that otherwise would have precipitated (Fuller et al. 2002). Since phosphate is not found in sufficient abundance in most soils and aquatic systems to produce uranyl phosphate solids, an external dose of phosphate has to be added to the subsurface. Direct addition of high concentrations of soluble inorganic phosphate can lead to immediate precipitation of different calcium phosphates that may clog injection wells (Wellman et al. 2006). Precipitation and adsorption can also prevent phosphate from getting transported to the location of U(VI) contamination. To avoid such complications, different methods for releasing phosphate to the subsurface have been suggested; these include injection of polyphosphates that would then disperse and decay to orthophosphate through hydrolysis (Langmuir 1997, Wellman et al. 2008) and biodegradation of injected organophosphate compounds that release orthophosphate as they are metabolized

(Beazley et al. 2009). The occurrence of uranyl phosphates observed in natural as well as contaminated settings reiterates the importance of phosphate and its effects on the fate and transport of uranium in the environment. Although recent studies have reported phosphate-induced precipitation of U(VI) phosphates under laboratory controlled and field scale systems, the fundamental mechanisms controlling U(VI) immobilization are not fully understood. Hence understanding the mechanisms at the microscopic and molecular levels is imperative to successfully implementing phosphate-based *in situ* uranium immobilization while developing a predictive understanding of these complex systems.

1.2 Research Objectives

The overall objective of this project was to determine the dominant mechanisms of U(VI)-phosphate interactions in subsurface environments, especially from an *in situ* remediation perspective. The presence of different constituents (anions and cations) can complicate the interactions by a series of competitive, cooperative (incorporation) and/or non-competitive (interaction between different ions without involvement of uranium) processes. These include precipitation of various uranyl phosphates, precipitation of calcium phosphates that may incorporate U(VI) as a substituting cation, adsorb U(VI) or enhance nucleation of uranyl phosphate solids. By virtue of each of these processes, the reaction pathways can get altered. The solids formed during the reactions might not be the ones that are predicted when the systems have reached equilibrium. Rather the first solid formed

might be a metastable phase that can persist for considerable durations, thus controlling the dissolved uranium concentrations. Improved understanding of these reactions is therefore needed to determine which solids form at which conditions and to understand the dominant mechanisms responsible for controlling uranium fate in phosphate bearing systems with multiple processes operating in parallel. To improve our understanding of the products and mechanisms of phosphate-induced immobilization, two specific research objectives were pursued.

Objective 1: To identify the solid-associated uranium species that result from mixing of uranium and phosphate solutions in simple systems.

Objective 2: To assess the equilibrium solubility of U(VI) for the different species that formed as a result of uranium-phosphate reaction.

Unfortunately, the information obtained through batch systems does not completely provide the capability of predicting U(VI) transport through subsurface media. Batch experiments are often conducted over long enough time frames to reach equilibrium while neglecting the influence of the reaction kinetics. In actual contaminated subsurface environments, however, the reactions (adsorption-desorption as well as precipitation-dissolution) are often rate-limited and controlled by both thermodynamics and kinetics of reaction. The other major difference is the poor mixing conditions in the case of actual porous media which have advective flow and have solute transport affected by various mass transfer processes. Thus understanding transport processes is crucial to avoiding instances where a plume of injected phosphate pushes the U(VI) contamination further downgradient instead of

retarding its mobility. This understanding can then be integrated with the information obtained from the batch systems and incorporated in methods designed to deliver phosphate to locations of U(VI) contamination and then predict the resulting fate and transport of the U(VI). To facilitate this understanding, two additional objectives were pursued.

Objective 3: To investigate the effect of phosphate on U(VI) transport through field sediments at relevant conditions and develop a predictive model for the same.

Objective 4: To identify the dominant forms of uranium in the sediments that resulted from phosphate addition.

1.3 Research Approach and Overview of Dissertation

To address the objectives outlined above, a series of laboratory experiments were designed and conducted. Batch experiments allowed understanding the fundamental equilibrium processes involved in uranium-phosphate interactions through well defined systems. Additionally, controlled laboratory column experiments enabled evaluation of various physical-chemical processes that might occur in subsurface environment. Equilibrium speciation calculations were used to develop a predictive understanding of equilibrium dissolved uranium concentrations.

Initial efforts at developing an equilibrium model that included dissolution-precipitation reactions as well as surface complexation for adsorption reactions were made. In all experiments, an approach was followed that integrated aqueous phase analysis with solid phase characterization. Table 1.1 lists the techniques used in this study.

The overall research approach for the dissertation (Figure 1.5) is divided into two main tasks where each task corresponds to a specific objective. Task 1 is subdivided into Subtasks 1A and 1B. In Subtask 1A, the formation of specific uranyl phosphate solids in homogeneous batch systems were evaluated for a wide range of conditions. Chapter 2 focuses specifically on the effect of pH, DIC and cations (H^+, Na^+ and Ca^{2+}) on the uranium-phosphate reactions. Homogeneous precipitation was thoroughly examined in these experiments to characterize the products of uranium and phosphate reactions, the conditions under which these products form, and the stability of the solids that form. Equilibrium speciation calculations were performed and compared with the observed solubility results to select the most appropriate thermodynamic data for several relevant solids and aqueous complexation reactions. Appendix B includes some additional batch experiments that were performed using synthetic groundwater representative of field sites in Rifle, Colorado and Hanford, Washington.

Subtask 1B involved batch experiments to identify different uranium removal mechanisms like adsorption, incorporation, and precipitation for a uranium-calcium-phosphate system. Chapter 3 specifically examined the effects and dependence of

starting forms of calcium and phosphate on uranium removal through a set of batch experiments. Different analytical techniques were used to investigate, quantify and distinguish the contributions of different uranium uptake mechanisms.

In Task 2, column experiments were used to simulate groundwater flow and investigate formation of products of phosphate injection into uranium-containing sediments. These experiments examined the combined effects of reactions and transport on the products of the reactions and their locations within the columns. Chapters 4 and 5 present an investigation of the transport of U(VI) through sediments obtained from Rifle, Colorado upon addition of phosphate amendment to induce *in situ* uranium immobilization. In Chapter 4, the column experiments conducted represent a scenario of phosphate addition to a site with most of the uranium hosted within the sediments and not dissolved in the groundwater. Batch sorption experiments using Rifle sediments were performed to obtain the uranium partitioning coefficient in the absence and presene of phosphate. A reactive transport model based on the one dimensional non-equilibrium convection-dispersion equation was used to fit uranium and bromide profiles and calculate various transport parameters. LIFS measurements and sequential extractions were used to identify the dominant mode of immoblization. In Chapter 5, the column experiments mimicked treatment of a uranium-contaminated site using phosphate addition to uranium-rich solutions upgradient of the site. In addition to LIFS measurements and sequential extractions, EXAFS was used to quantify and distinguish the specific uranium removal mechanisms on application of phosphate amendment.

Table 1.1. Aqueous and solid phase analytical techniques used in this study

Technique	Phase	Information obtained	Relevance to research investigation
Inductively Coupled Plasma Mass Spectroscopy **(ICP-MS)**	Aqueous	Dissolved elemental concentrations	Quantify the rate and extent of different reactions including those between uranium and phosphorus
Total Organic Carbon **(TOC)** Analyzer		Dissolved inorganic carbon concentration	Confirm the presence of inorganic carbon concentrations and while determining its uptake
Extended X-ray Absorption Fine Structure **(EXAFS)** Spectroscopy	Solid	Atomic coordination environments	Probe molecular-scale coordination environment of uranium
X-Ray Diffraction **(XRD)**		Identity of crystalline phases	Identify the mineralogy of formed/existing solids
Scanning Electron Microscopy **(SEM)** with Energy Dispersive X-ray Analysis **(EDX)**		Imaging at the Nano/Micro meter scale with elemental analysis of spots and regions	Determine shape and size of the formed solids, changes in particle morphology of existing solids and identify spatial distribution of solids
Sequential Extractions		Solid phase speciation	Evaluate the speciation of uranium to help identify the dominant mode of uranium uptake
Laser Induced Fluorescence Spectroscopy **(LIFS)**	Solid/Aqueous	Identity of compounds	Validate the presence of different uranium containing compounds

Chapter 6 summarizes the results of the present work. Recommendations for future work are also included.

Appendix C contains the work done for the auxiliary objective of developing an equilibrium-based model that accounts for both adsorption and precipitation for the uranium-phosphate-goethite system. Goethite was used as a model substrate mineral to simplify the model development owing to the well defined

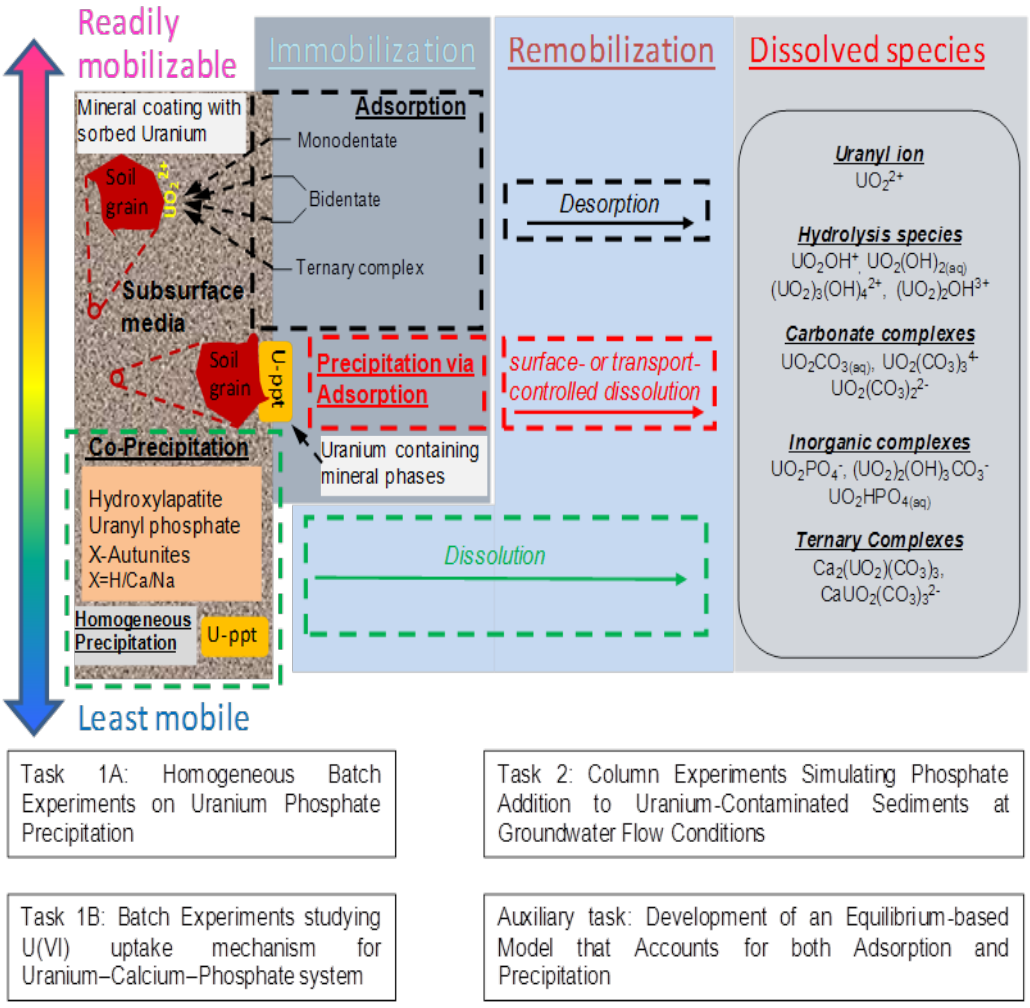

Figure 1.5. Overview of immobilization and remobilization processes involved in uranium-phosphate-porous media systems that are investigated in the dissertation.

characterization of the material. The appropriate reaction constants for precipitation reactions were obtained from the batch experiments in Subtask 1A. The model predictions were compared with the batch sorption experiments to estimate the critical supersaturation ratios for nucleation.

Chapter 2. Effect of co-solutes on the products and solubility of uranium(VI) precipitated with phosphate

Results of this chapter have been published in Chemical Geology **2014**, 364: 66 – 75.

Graphical abstract

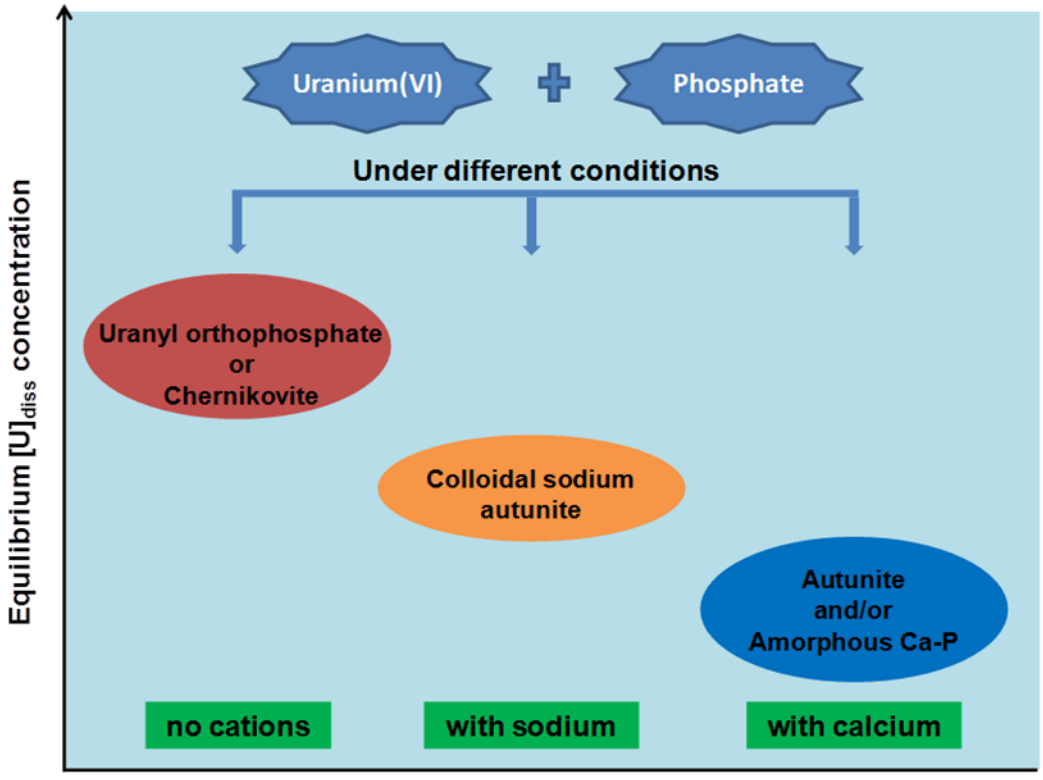

Abstract

Uranyl phosphate solids are often found with uranium ores, and their low solubility makes them promising target phases for *in situ* remediation of uranium-contaminated subsurface environments. The products and solubility of uranium(VI) precipitated with phosphate can be affected by the pH, dissolved inorganic carbon (DIC) concentration, and co-solute composition (e.g. Na^+/Ca^{2+}) of the groundwater. Batch experiments were performed to study the effect of these parameters on the products and extent of uranium precipitation induced by phosphate addition. In the absence of co-solute cations, chernikovite [$H_3O(UO_2)(PO_4)\cdot 3H_2O$] precipitated despite uranyl orthophosphate [$(UO_2)_3(PO_4)_2\cdot 4H_2O$] being thermodynamically more favorable under certain conditions. As determined using X-ray diffraction, electron microscopy, and laser induced fluorescence spectroscopy, the presence of Na^+ or Ca^{2+} as a co-solute led to the precipitation of sodium autunite ([$Na_2(UO_2)_2(PO_4)_2$] and autunite [$Ca(UO_2)_2(PO_4)_2$]), which are structurally similar to chernikovite. In the presence of sodium, the dissolved U(VI) concentrations were generally in agreement with equilibrium predictions of sodium autunite solubility. However, in the calcium-containing systems, the observed concentrations were below the predicted solubility of autunite, suggesting the possibility of uranium adsorption to or incorporation in a calcium phosphate precipitate in addition to the precipitation of autunite.

2.1 Introduction

Programs associated with the production of nuclear materials have led to the generation of uranium-containing wastes at many locations. In the United States the Department of Energy has reported the contamination of over 6.4 trillion liters of groundwater, 40 million cubic meters of soil and debris, and 3 million cubic meters of radioactive waste buried in landfills, trenches and spill areas at more than 120 sites across 36 states (DOE 1997, McCullough et al. 1999). The contamination of groundwater and soil at these sites occurred as a result of direct injection of mixed waste into the subsurface, leakage from storage tanks, and infiltration from unlined storage ponds. Owing to uranium's carcinogenic and other toxic effects and its potential migration into surface water or groundwater sources used for water supplies, uranium contamination poses a significant risk to the environment and human health (EPA 2001). The distributed nature of the contamination at many sites makes it economically challenging to use pump-and-treat or excavation methods for remediation. *In situ* immobilization is an attractive approach (NRC 1993) in which chemical or physical modifications of the subsurface environment promote the formation of the most stable and least mobile solid forms of uranium.

In environmental systems, uranium predominantly exists in the +IV and +VI oxidation states. U(IV) is primarily found in reducing environments as the mineral uraninite [$UO_{2(s)}$], which is one of the most stable forms of uranium. In addition to uraninite, other U(IV) species have also been reported to exist in reducing

environments (Bernier-Latmani et al. 2010, Fletcher et al. 2010, Sharp et al. 2011). Owing to the low solubility of uraninite, many remediation strategies have focused on biologically-mediated reduction of U(VI) to U(IV). However, sparingly soluble U(IV) solids can be oxidized back to highly mobile U(VI) species under oxic conditions (Cerrato et al. 2013, Langmuir 1997, Liu et al. 2005, Moon et al. 2007, Sani et al. 2005, Senko et al. 2007, Wang et al. 2013, Wang et al. 2014, Wu et al. 2007). Naturally oxic conditions found at many contaminated sites can limit the long-term feasibility of bioreduction-based remediation methods.

Addition of phosphate amendments can be used as a stand-alone process to promote *in situ* immobilization or as a complementary process to increase the effectiveness of reduction-based uranium remediation methods (Beazley et al. 2009, Fuller et al. 2002, Simon et al. 2008, Sowder et al. 2001, Wellman et al. 2005, Wellman et al. 2008). Of the potential U(VI) solids that can be precipitated for *in situ* immobilization, U(VI) phosphates have the lowest solubility over a broad range of conditions (Finch and Murakami 1999). There is evidence for formation of uranyl phosphates following oxidation of uranium in ore deposits (Jerden and Sinha 2003, Jerden et al. 2003). Uranium removal via adsorption to phosphate solids has also been evaluated after addition of phosphate amendments to sediments or soils (Arey et al. 1999, Fuller et al. 2003, Fuller et al. 2002).

A diverse group (approximately 40 minerals known) of uranyl phosphates have been identified (Burns et al. 1999, Guillaumont et al. 2003). In the absence of cations, formation of the tetragonal sheet-structured solid chernikovite [$H_3OUO_2PO_4 \cdot 3H_2O$] has been reported to form instead of the thermodynamically

more favorable solid uranyl orthophosphate [$(UO_2)_3(PO_4)_2 \cdot 4H_2O$], which has a tetragonal prism structure (Singh et al. 2010). The presence of common groundwater cations (Na^+, Ca^{2+}) can lead to the formation of sodium autunite [$Na_2(UO_2)_2(PO_4)_2$] or autunite [$Ca(UO_2)_2(PO_4)_2$], respectively. These minerals, which have sheet structures similar to those of chernikovite, have been observed in uranium-contaminated sediments at different field sites which had phosphate present by virtue of mining and processing activities (Buck et al. 1996, Jones et al. 2001). In natural uranium ores (Jerden et al. 2003) reported the presence of the barium end member of the autunite mineral group. Various other uranyl phosphate solids have also been observed in contaminated soils and sediments at the Hanford 300 Area, Oak Ridge Reservation and Fernald Site (Arai et al. 2007, Catalano et al. 2006, Morris et al. 1996, Singer et al. 2009, Stubbs et al. 2009).

The aqueous speciation of U(VI) can include many different species. The uranyl ion (UO_2^{2+}) forms soluble complexes with naturally abundant groundwater anions (Finch and Murakami 1999, Guillaumont et al. 2003, Langmuir 1997). Under neutral conditions, for a typical oxic system that contains phosphate, the most significant dissolved complexes are with carbonate [e.g., $UO_2CO_{3(aq)}$, $UO_2(CO_3)_3^{4-}$, $(UO_2)_2(OH)_3CO_3^-$ and $UO_2(CO_3)_2^{2-}$], hydroxide [e.g., $(UO_2)_3(OH)_4^{2+}$ and $(UO_2)_2OH^{3+}$] and phosphate [e.g., $UO_2PO_4^-$ and $UO_2HPO_{4(aq)}$]. In the presence of calcium, uranium can also form strong ternary complexes with carbonate [$Ca_2UO_2(CO_3)_3$ and $CaUO_2(CO_3)_3^{2-}$]. In addition, phosphate can both enhance and inhibit U(VI) solubility depending on the pH and relative concentrations of total U(VI) and phosphate. Similarly, the addition of calcium can increase U(VI)

solubility, but it may also limit dissolved U(VI) concentrations by forming a calcium phosphate solid to which U(VI) may adsorb or become structurally incorporated. With multiple processes operating in parallel, it is important to understand and differentiate among the dominant mechanisms of uranium-phosphate reactions in subsurface environments.

The objectives of this study were to 1) determine the individual effects of pH, dissolved inorganic carbon (DIC), and cations (H^+, Na^+ and Ca^{2+}) on uranium precipitation with phosphate, 2) identify the products of uranium phosphate interactions, and 3) compare measured and predicted dissolved uranium concentrations in equilibrium with the precipitates that formed. This systematic examination of the impacts of cations on the formation of uranium phosphate solids can provide insights into the processes occurring in ore bodies and during *in situ* remediation.

2.2 Materials and Methods

2.2.1 Materials

The chemicals used in this study were ACS grade or better. A 5 mM uranyl nitrate [$UO_2(NO_3)_2$] stock solution was prepared in ultrapure water (> 18.2 MΩ.cm resistivity). A 100 mM phosphate stock solution was prepared in ultrapure water using phosphoric acid. Dilute tetrabutylammonium hydroxide (TBAOH) solution and/or nitric acid solutions were used to adjust the pH of the solutions to the target values. TBAOH was used because, unlike the Na^+ that comes from NaOH, the

tetrabutylammonium ion is unlikely to be structurally incorporated into the uranium phosphate precipitates because of its large size. For investigation of the effects of Na^+ and Ca^{2+} on U(VI) phosphate precipitation, the sources of the cations were a $NaNO_3$/$NaHCO_3$ mixture and $Ca(NO_3)_2$ solution, respectively.

Three different U(VI) phosphate solids were synthesized to serve as reference materials for comparison with solids generated in subsequent batch experiments. Chernikovite was synthesized as per the method described in Vesely et al. (1965) with some modifications. Briefly, phosphate and uranium were added in a stoichiometric molar ratio of 2:1 in the presence of nitric acid and ultrapure water and allowed to react at 22°C for 1 week. Unlike in the method of Vesely et al. (1965) $NaNO_3$ was not added to the mixture, which avoided the possibility of forming sodium autunite. Uranyl orthophosphate was synthesized as per the hydrothermal method described in Gorman-Lewis et al. (2009). Briefly, 0.28 g of Na_2HPO_4, 6 mL of 0.5 M $UO_2(NO_3)_2$, and 4 mL of H_2O were combined and then heated for 7 d at 150°C in a sealed PTFE reactor enclosed within a stainless steel reactor; the molar ratio of uranium and phosphate in the synthesis product is 1.52:1. The resulting solid was rinsed three times with 25 mL volumes of boiling H_2O and then air-dried prior to characterization. Sodium autunite was synthesized as per the indirect precipitation method described in Wellman et al. (2005). Solutions of 110 mM uranyl nitrate and 1.1 M phosphoric acid were combined in a 1:1 volumetric ratio (phosphate to uranium molar ratio of 10:1) with continuous stirring and then reacted for 30 minutes at 22 °C to first yield chernikovite. The settled chernikovite was then separated from the supernatant and reacted in 200 mL of 2 M NaCl solution for two days at the

ambient laboratory temperature. The intermediate chernikovite synthesis step in the sodium autunite synthesis was performed at a higher initial supersaturation ratio than in the synthesis of the chernikovite reference material. The greater initial supersaturation enabled faster precipitation of the chernikovite needed as the starting material for sodium autunite formation.

2.2.2 Methods

2.2.2.1 Batch experiments

Batch experiments were performed at room temperature (22±0.5 °C) to study the effect of co-solutes (DIC/ Ca^{2+}/ Na^{+}) and pH (4.0-7.5) on uranium immobilization induced by addition of phosphate amendments (Table 2.1). The pH range was chosen to encompass the most relevant environmental conditions. For example, pH 4.0 has been reported at many uranium-contaminated waste sites due to acidic uranium waste disposal (Barnett et al. 2000, Bostick et al. 2002), whereas groundwater at the 300 Area of the Hanford Site approaches pH 8.0 (Zachara et al. 2005). While almost all natural environments will contain appreciable concentrations of Na^{+} and Ca^{2+}, cation-free experiments provide important end member cases for evaluating the impacts of cation concentrations on the identity and equilibrium solubility of the precipitates that form. Additionally, these cation-free experiments helped to explore the issue of metastability in the case of chernikovite versus uranyl orthophosphate formation. The concentrations of Na^{+} and Ca^{2+} were selected based

Table 2.1. Conditions for batch experiments conducted for starting pH values of 4.0, 6.0 and 7.5.

Set No	Tot U(VI) (μM)	Tot PO_4^{3-} (μM)	DIC (mM)		Cations (mM)	Sampling Time (Days)
			Target	Actual		
1–15[a,b]	100	1000	Air equilibrated[c]		--	0, 1, 4, 10
	100	--				
16–30[a]	100	1000	0	BDL	--	0, 1, 4, 10
	100	--				
31–45[a]	100	1000	1	0.01-0.79[d]	--	0, 10
	100	--				
46–60[a]	100	1000	1	0.77-1.10	Na^+ (1 mM)[f]	0, 10
	100	--				
61–75[a]	100	1000	1	0.77-1.00	Na^+ (7.44 mM)[f]	0, 10
	100	--				
76-78[b]	100	1000	1	0.61-1.03	Na^+ (5 mM)	0, 10
79-81[b]	100	1000	1	0.10-0.83[e]	Ca^{2+} (5 mM)	0, 10

[a] Experiments were performed in duplicate with U(VI) and PO_4^{3-} together as well as duplicate PO_4^{3-}-free control along with a single U(VI)-free control.

[b] Experiments were performed in scaled up 2 L batches to provide enough material for solid characterization.

[c] Predicted DIC concentrations in equilibrium at pH 4.0, 6.0 and 7.5 are 10.9 μM, 15.6 μM and 163 μM, respectively.

[d] Measured DIC concentrations at pH 4.0 (10 μM) and pH 6.0 (90 μM) were close to those predicted for air equilibrated conditions.

[e] Measured DIC concentrations at pH 4.0 (10 μM) and pH 6.0 (150 μM) were low.

[f] The concentrations based on reported values for the Hanford 300 Area (Zachara et al. 2005) and a site in Rifle, Colorado (Campbell et al. 2011, DOE 1999).

BDL – Below detection limit, detection limit: 1.5 μM

on reported values for the Hanford 300 Area (Zachara et al. 2005) and a site in Rifle, Colorado (Campbell et al. 2011, DOE 1999).

All experiments were performed in stirred glass reactors (250 mL unless otherwise mentioned). Depending on the specific conditions that were being probed, the respective solutions were added to set the solution composition to desired values (Table 2.1). Duplicate experiments were performed, and both uranium-free and phosphate-free control experiments were conducted to assess any removal of uranium or phosphate in the absence of the other. Uranium concentrations of 100 µM were selected to provide sufficient solid mass for performing solids characterization at the end of the experiment. Excess phosphate (1000 µM to provide a molar ratio of P:U of 10:1) was added to solutions. The high P:U ratio provided favorable conditions for the solutions to be supersaturated with respect to uranyl phosphate solids. Excess phosphate relative to uranium would also be used in remediation strategies to promote precipitation and overcome other pathways for phosphate removal such as adsorption to sediment minerals. Experiments were conducted at fixed DIC concentrations as well as in the absence of DIC. Experiments in the absence of DIC served as an important bounding case for evaluating the effects of DIC on uranyl phosphate solubility.

Samples were collected from the batch reactors at the intervals noted in Table 2.1. Samples for measurement of dissolved U, P, Na, and Ca were filtered using both 0.22 µm (polycarbonate membrane filters, Millipore) and 0.05 µm (polyethersulfone syringe filters, Tisch scientific) filters, and the filtrates were acidified to provide a 1 % nitric acid matrix to preserve the samples prior to analysis. For a limited set of conditions, samples were centrifuged instead of filtered; as will be discussed later the centrifugation was performed at conditions that would remove

particles smaller than 0.05 μm. Separate 0.22 μm-filtered samples were collected, not acidified, and used immediately after collection for DIC measurements.

2.2.2.2 Solid phase analysis

Solids for X-ray diffraction (XRD) analysis were collected on 47-mm diameter mixed cellulose ester filter membranes having 0.45 μm pore size (Millipore). XRD analysis was performed on a Rigaku Geigerflex D-MAX/A diffractometer using Cu-Kα radiation at a power of 35 kV and 35 mA. The diffractometer has a fixed sample holder that accepts horizontal mounts of powders and dried materials contained on filter membranes, and it is controlled by PC-based Datascan software by Materials Data, Inc. (MDI). MDI's Jade software was used to analyze mineral diffraction patterns. Samples for scanning electron microscopy (SEM) were collected on 25-mm diameter polycarbonate membranes (Millipore) of 0.22 μm pore size. The solids were then viewed with a JEOL 7001FLV field emission (FE) scanning electron microscope equipped with an energy dispersive X-ray elemental analysis system (EDS). The use of different pore size (0.45 μm and 0.22 μm) filters for XRD and SEM did not result in differences in the structure and composition of solids collected since they are expected to have similar characteristics. However, as will be discussed later, the inability to collect particles smaller than the pore sizes can have significant implications with respect to the measured equilibrium solubility.

For laser induced fluorescence spectroscopy (LIFS) analysis, the samples were obtained at the end of the experiment through a series of steps. First, the batch reactors were kept still without any mixing to concentrate the suspension by gravitational settling. The concentrated suspensions and aliquots of carefully removed supernatants were loaded into 2 mm × 4 mm x 25 mm (ID) quartz cuvettes for analysis. For sodium-containing experiments, concentrated suspensions were centrifuged followed by freeze drying before being loaded into quartz cuvettes for the LIFS analysis. Instrumentation and experimental procedures for LIFS analysis have been described previously (Wang et al. 2005, Wang et al. 2004). The quartz cuvettes were attached to the cold finger of a CRYO Industries RC152 cryostat with liquid helium vaporizing beneath the sample to reach a sample temperature of 8 ± 2 K. The samples were excited with a Spectra-Physics Nd:YAG laser-pumped Lasertechnik-GWU MOPO laser at 415 nm, and the emitted light was collected at 85° to the excitation beam and detected with a thermoelectrically cooled Princeton Instruments PIMAX intensified CCD camera after spectral dispersion through an Acton SpectroPro 300i double monochromator spectrograph. The spectra were analyzed using the commercial software application IGOR (Wavematrix, Inc).

2.2.2.3 Dissolved phase analysis

Dissolved elemental concentrations using inductively coupled plasma-mass spectrometry (ICP-MS, Agilent Technologies 7500ce) in the presence of an internal standard solution. A set of 8-10 calibration standards made from certified standards

(Fisher Scientific) was used for obtaining the calibration curves and calculating the concentrations. Calibration curves were generated using a weighted linear regression. The detection limit was 0.2 µg/L for uranium, 10 µg/L for phosphorus, and 50 µg/L for calcium and sodium. The 0.05 µm filters were used to remove any nanoparticles that formed during the reaction and that passed through the 0.22 µm filters. Control filtration tests with known aqueous uranium concentrations and conditions confirmed that the filters themselves did not remove any dissolved uranium (e.g., by adsorption to the filter material). DIC was measured using a TOC analyzer (Shimadzu, TOC-$L_{CPH/CPN}$ PC-controlled model) installed with a high sensitivity catalyst (detection limit of 10 µg/L) and an auto sampler. The DIC concentration sometimes drifted down from its initial value during the run of an experiment (Table 2.1). Observed drift, especially at low pH (pH 4.0) was consistent with the loss of inorganic carbon to the headspace of the reactors as CO_2 and to the laboratory atmosphere during sampling and pH measurement activities. However, the change in DIC concentrations would not lead to changes in uranyl phosphate solubility at the lower pH values studied (pH 4.0 and pH 6.0) due to the limited contributions of uranyl carbonate complexes to overall U(VI) speciation at those conditions. The maximum contributions of uranyl carbonate complexes to dissolved uranium at pH 4.0 and pH 6.0 are less than 10 % in the absence of phosphate and less than 5 % in the presence of phosphate.

2.2.2.4 Equilibrium speciation calculations

Equilibrium calculations were performed using MINEQL+ v 4.6 (Schecher and McAvoy 2007) with the thermodynamic database customized to use the aqueous reactions and thermodynamic constants listed in Table A.1 in the appendix. Potentially relevant solids include metaschoepite [$UO_3 \cdot 2H_2O$], chernikovite, sodium autunite, uranyl orthophosphate, autunite, and various calcium phosphates. The dissolution reactions and associated equilibrium constants are listed in Table A.2 of the appendix. The log K_{sp} values of several of the relevant uranium-containing minerals were included from a recent publication (Singh et al. 2010) wherein the compilation of these constants was based on earlier reviews of solubility studies (Gorman-Lewis et al. 2008a, Gorman-Lewis et al. 2008b, Gorman-Lewis et al. 2009).

2.3 Results and Discussion

2.3.1 Effect of pH, phosphate and dissolved inorganic carbon without Na^+ or Ca^{2+}

2.3.1.1 Solid characterization

In the absence of Na^+ or Ca^{2+}, PO_4^{3-} addition led to formation of chernikovite as suggested by XRD (Figure 2.1). The precipitates were thin square plates (Figure 2.2), a morphology characteristic of chernikovite but not uranyl orthophosphate (Finch and Murakami 1999). Digestion of the precipitates formed in the presence of phosphate using concentrated nitric acid followed by ICP-MS analysis confirmed the expected U:P stoichiometry of 1:1. The solids formed during the batch experiments

were much smaller than those formed in the synthesis of the reference material. This could be due to the different P:U ratio used in the batch experiments (10:1) than during the reference material synthesis (2:1). In phosphate-free control experiments, uranium remained very soluble at pH 4.0 and 6.0 and precipitated only at the highest pH (7.5) studied; the precipitate in that case was confirmed to be metaschoepite. Analysis of selected samples using LIFS (Figure 2.3) confirmed that the solids formed in the presence and absence of phosphate has spectra dominated by chernikovite and metaschoepite, respectively.

2.3.1.2 Solubility of uranium

Measurements of the dissolved concentrations of uranium and phosphate were useful for tracking the progress of the precipitation reaction. They also facilitated comparisons of the observed and predicted solubility of the precipitated solids that provide complementary information to the characterization of precipitated solids. The majority of the precipitation reaction had already occurred within 1 day, and dissolved uranium concentrations were stable by 10 days in the absence of DIC. Samples were thus collected only at the end of the experiment (10 days) for fixed DIC experiments to minimize any losses of DIC that would occur during opening of the reactors for sampling and pH measurement. Because the reactors remained sealed over this 10-day period, the pH drifted with the reaction progress and was not readjusted to the target value; however, because of the inherent buffering capacity of both carbonate and phosphate species at pH 6.0 and 7.5, the final pH values were

generally within 0.3 pH units of the target value. Both in the absence and presence of DIC, the measured solubility agrees well with the predicted solubility of chernikovite at pH 4.0 and 6.0 (Figure 2.4). At pH 7.5 in the absence of DIC, the measured solubility is also in good agreement with chernikovite solubility; with DIC present at pH 7.5, equilibrium calculations predict no precipitation of chernikovite, but a small amount of precipitation is observed.

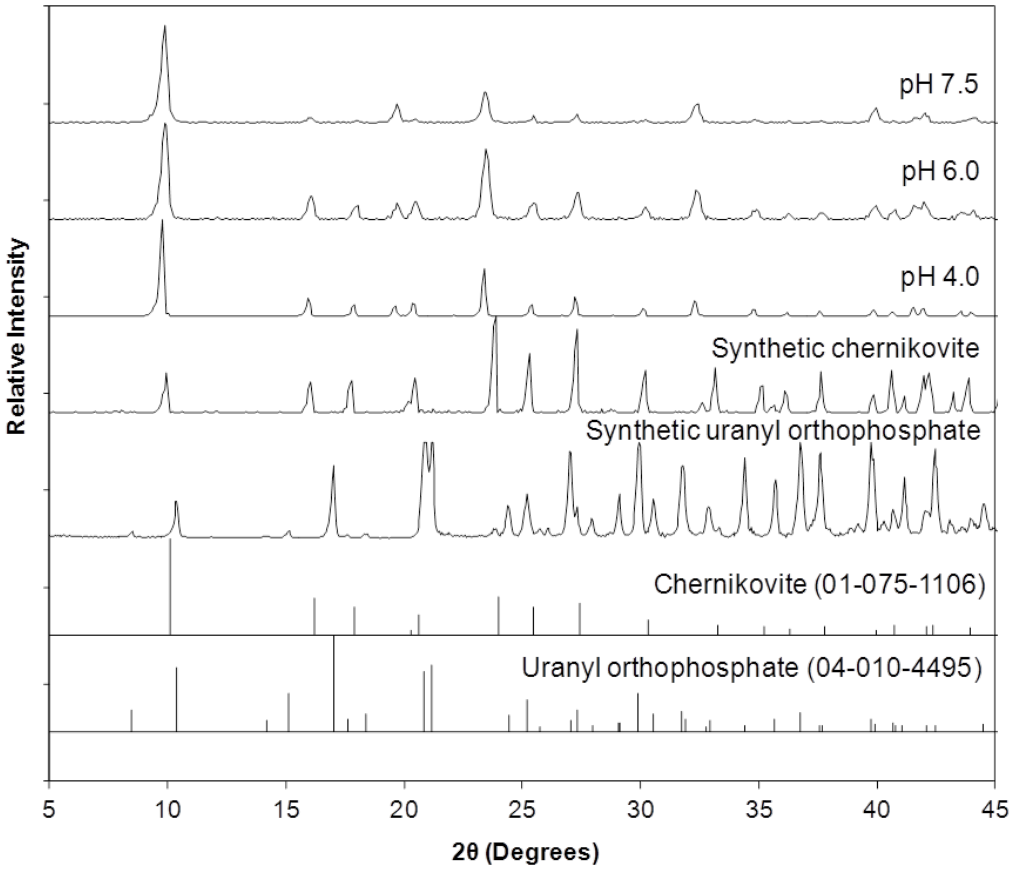

Figure 2.1. X-ray diffraction patterns of the synthesized solids (synthetic chernikovite and synthetic uranyl orthophosphate) and solids from experiments without added sodium or calcium. Solids included were obtained from the set of experiments with 100 µM U, 1000 µM P and no DIC. For reference, the standard patterns obtained from the International Crystal Diffraction Database with the respective PDF card numbers are included. The synthetic uranyl orthophosphate pattern represents the solid synthesized and characterized by (Catalano and Brown Jr. 2004).

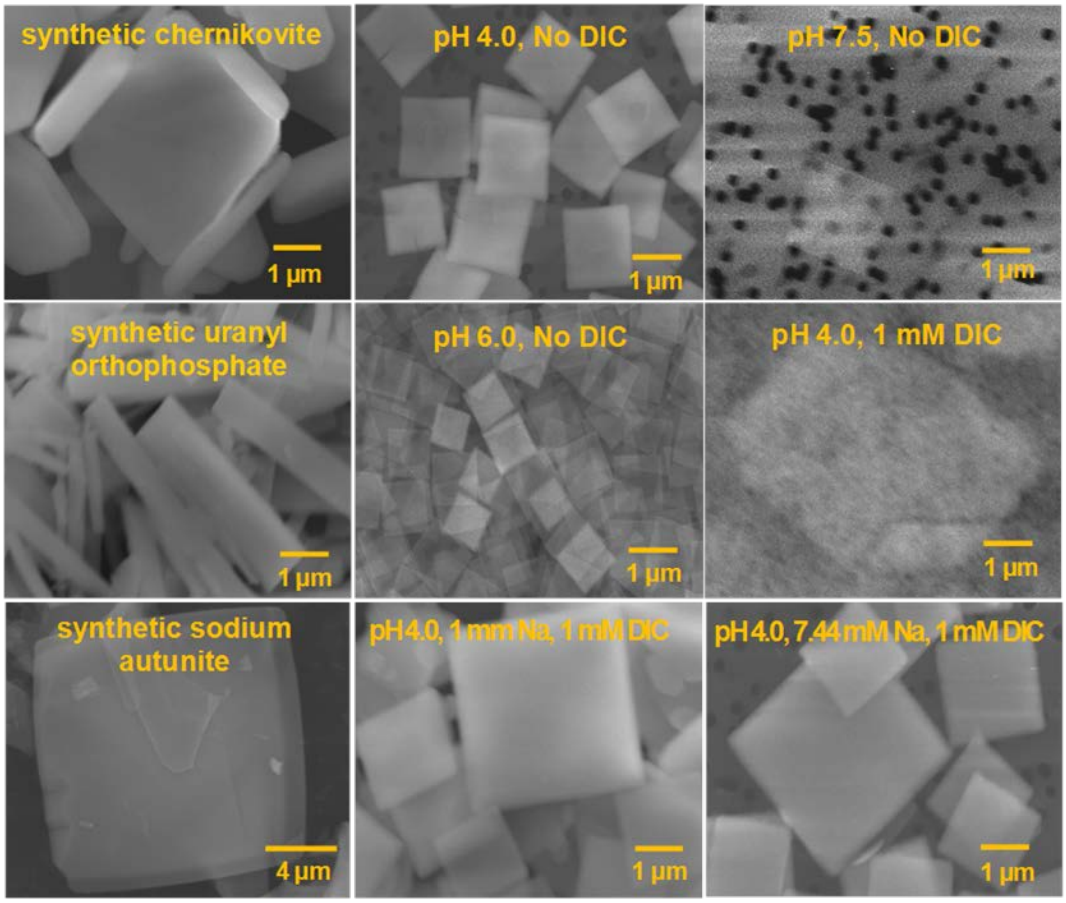

Figure 2.2. Scanning electron microscopy (SEM) images of the synthesized solids and selected precipitates (obtained for experiments containing 100 µM U and 1000 µM P in the absence or presence of DIC and sodium) collected on 0.22 µm filter membranes.

Use of different pore size filters to measure dissolved uranium was critical to identifying the presence of particles smaller than 0.22 µm that formed during precipitation experiments. By comparison of the dissolved uranium concentrations measured after filtration through 0.22 µm and 0.05 µm membranes (Figure 2.4), the contribution of colloidal particles smaller than 0.22 µm to the overall amount of precipitate can be assessed. The percentage of the precipitate present in the sub-0.22 µm fraction was largest at pH 6.0, smaller at pH 7.5, and negligible at pH 4.0. This trend is consistent with nucleation theory; the size of the initially precipitated

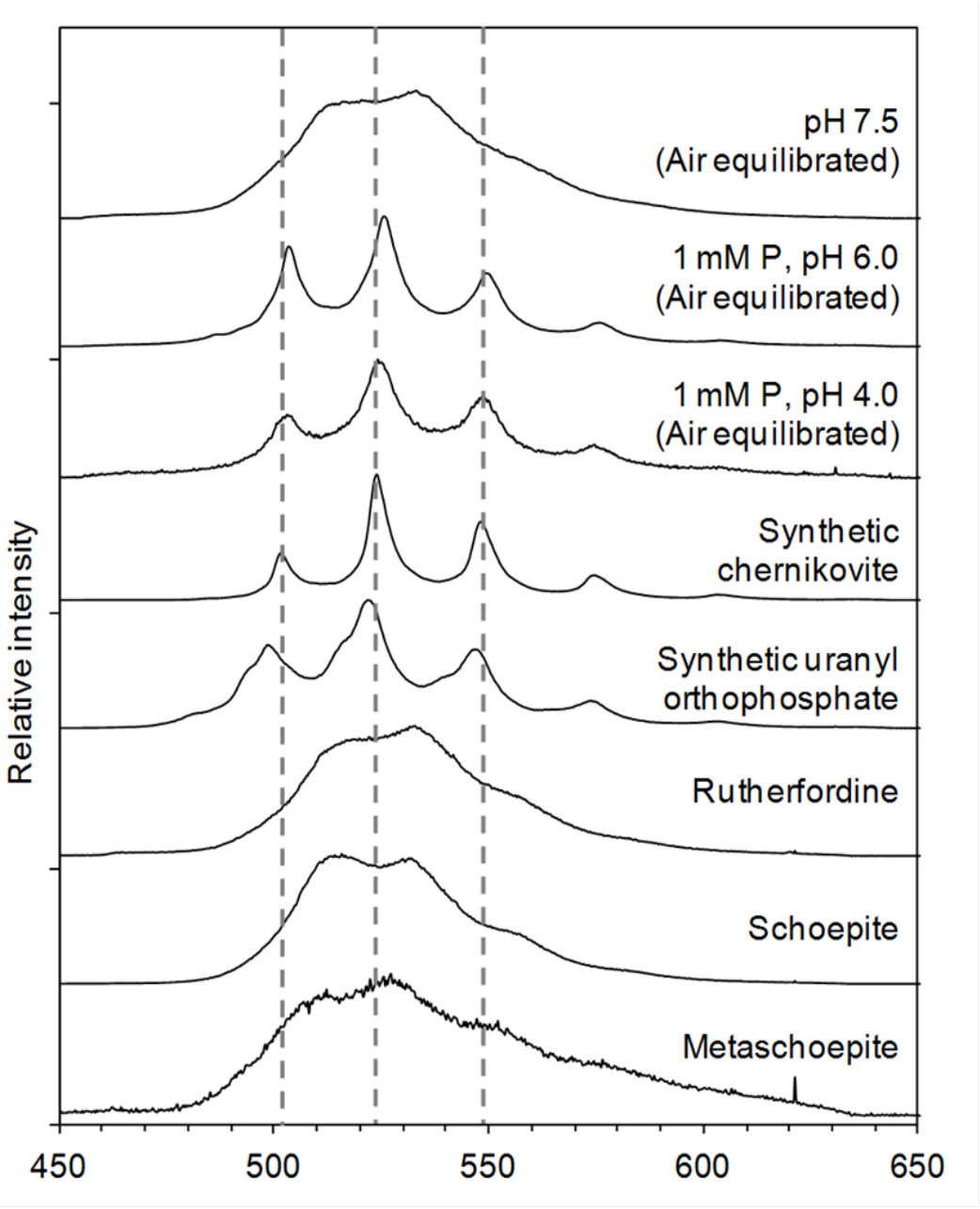

Figure 2.3. Laser induced fluorescence spectra of selected precipitates obtained from a set of experiments containing 100 µM U under varying conditions and collected at λ_{ex} = 415 nm. Spectra of synthetic chernikovite, synthetic uranyl orthophosphate, rutherfordine, schoepite and metaschoepite are included for comparison. For clarity, the spectra were normalized and plotted with offsets along the y-axis.

particles is inversely proportional to the initial degree of solution supersaturation (Lasaga 1998). The initial solution was maximally supersaturated with respect to

chernikovite at pH 6.0, and this is the pH with the largest percentage of the precipitate in the sub-0.22 µm fraction.

Comparison of observed versus predicted solubility indicates the formation of chernikovite as a metastable phase at some conditions. For pH 6.0 and 7.5 with and without DIC, the dissolved uranium concentrations were in good agreement with the predicted solubility of chernikovite despite uranyl orthophosphate being the thermodynamically most favorable phase. At pH 4.0 the predicted solubility of chernikovite and uranyl orthophosphate are very similar, and the measured uranium concentrations were close to both values; as noted above, solid phase characterization identified chernikovite as the only solid present.

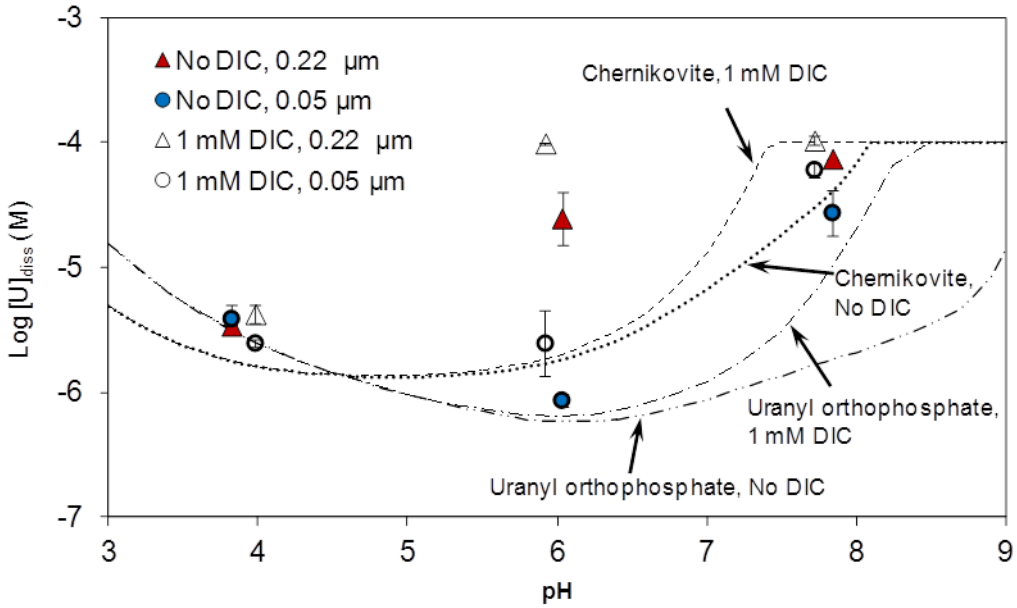

Figure 2.4. Comparison of observed concentrations after 10 days with predicted equilibrium solubility. Lines represent the predicted concentrations of dissolved uranium in equilibrium with the respective solid. Data points represent mean final dissolved uranium concentrations observed through duplicates with the starting concentrations of 100 µM U, 1000 µM P and 0 or 1 mM DIC. Error bars are the standard error.

The predictions made using the currently available database of equilibrium constants are very sensitive to the values of the thermodynamic constants for precipitation and complexation reactions of U(VI) with phosphate. The formation constant (K_{sp}) used for calculating chernikovite solubility could affect the match between the predicted and measured equilibrium solubility; however, any changes to this value would affect the predicted solubility at all three pH values studied. The log K_{sp} value for the chernikovite solubility recommended in a critical review (Grenthe et al. 1992) was -24.20, and other studies have used a relatively narrow range of -24.12 to -25.50 (Gorman-Lewis et al. 2009, Tripathi 1984, Vesely et al. 1965). In our calculations we used the value of -25.50 since the study that yielded this value approached equilibrium from both directions (dissolution and precipitation) and included solid characterization and calorimetric data (Gorman-Lewis et al. 2009). Chernikovite solubility predicted using the value of -24.20 was more than an order of magnitude higher at pH 4.0 and 6.0 as compared to those predicted using the value of -25.50. The results suggest that the log K_{sp} value of chernikovite of -25.50 does a better job predicting uranium concentrations and should be adopted over earlier reported values. The results of these cation-free experiments demonstrate the formation of chernikovite as a metastable phase instead of uranyl orthophosphate and illustrate the variation in equilibrium uranium solubility with pH and DIC concentration.

2.3.2 Effect of Na^+ on the solids formed

2.3.2.1 Solid characterization

In solutions with sodium, the addition of phosphate induced the precipitation of sodium autunite for all the pH conditions studied (Figure 2.5). While XRD patterns are only shown for 5 mM sodium concentrations, sodium autunite was also the product at other sodium concentrations. The solids formed in the presence of sodium and phosphate have morphologies consistent with autunite-type sheet structured minerals (Figure 2.2). EDS analysis of the solids obtained from experiments with all three sodium concentrations (1, 5 and 7.44 mM) confirmed the presence of sodium in the solid with a molar Na:U:P ratio of 1:1:1 at pH 6.0 and 7.5 conditions, which is indicative of sodium autunite and rules out the presence of chernikovite, which has a similar morphology and a similar XRD pattern to sodium autunite. EDS analysis of solids formed at pH 4.0 found less sodium in the solids (Na:U:P ratio of 0.3:1:1 and 0.35:1:1 for 5 mM and 7.44 mM sodium concentrations respectively). LIFS spectra of solids obtained from experiments with 5 mM Na (Figure 2.6) provide further evidence of predominantly sodium autunite at pH 6.0 and 7.5 and a mixture of solids at pH 4.0. Under these conditions, chernikovite and sodium autunite are predicted to be supersaturated to similar extents (Figure 2.7 [b] and 2.7 [c]). The lower sodium content of the solids precipitated at pH 4.0 suggests that these are either a mixture of sodium autunite and chernikovite or a solid solution having a composition intermediate between these two phases. Previous studies (Butt and Graham 1981, Locock et al. 2004) also reported the formation of solid solutions of autunite-group minerals with various monovalent cations. A lower molar ratio

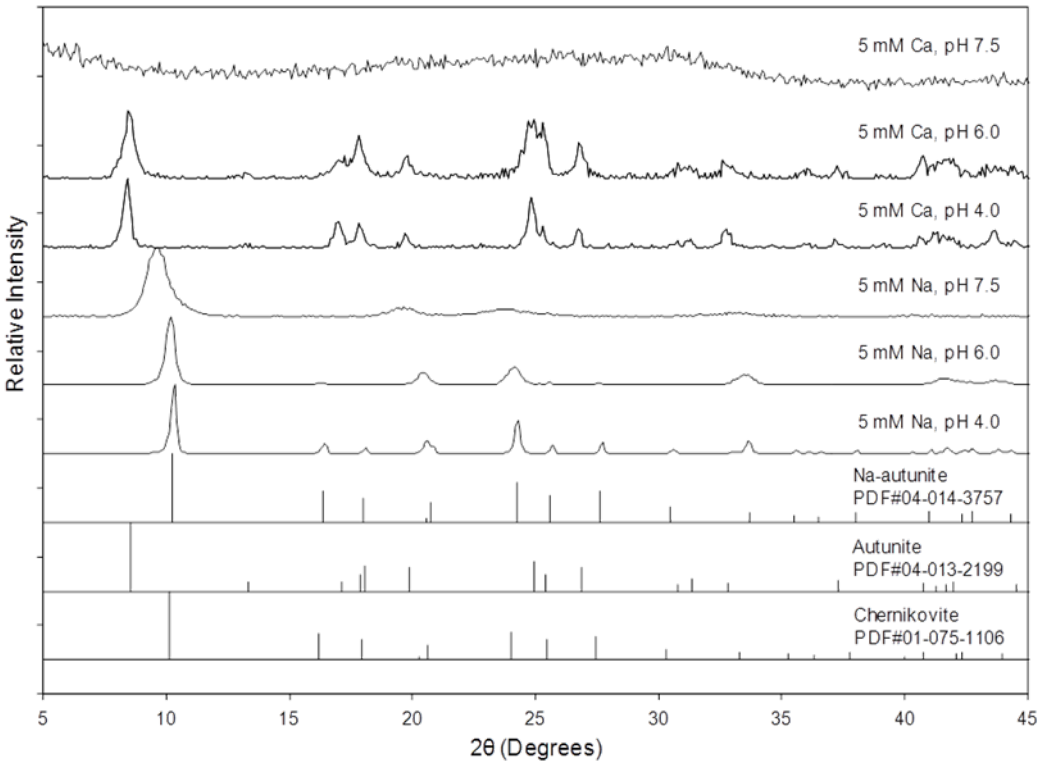

Figure 2.5. X-ray diffraction patterns of selected precipitates obtained for the experiments containing 100 µM U, 1000 µM P and 1 mM DIC added with Na or Ca. Solids were also identified as sodium autunite at sodium concentrations of 1 mM and 7.44 mM concentrations. For reference, the standard patterns (sodium autunite and autunite) obtained from the International Crystal Diffraction Database with the respective PDF card numbers are included.

(Na:U:P ratio of 0.1:1:1) at pH 4.0 conditions was observed for the experiments with the lowest sodium concentration (1 mM), which indicates that the solid in this case was predominantly chernikovite. At pH 4.0 chernikovite is clearly a lower solubility phase than sodium autunite at 1 mM sodium (Figure 2.7 [a]), whereas the difference in equilibrium solubility between the two phases is much smaller at the higher sodium concentrations (Figure 2.7[b-c]).

2.3.2.2 Solubility of uranium

The dissolved uranium concentrations observed in the presence of sodium follow a trend similar to the predicted solubility of sodium autunite (Figure 2.7). The dissolved uranium concentrations observed for the systems in the presence of 5 mM and 7.44 mM sodium were lower than those seen in the absence of sodium by a factor of 100 or more at pH 6.0 and 7.5. With 1 mM sodium concentrations at pH 6.0

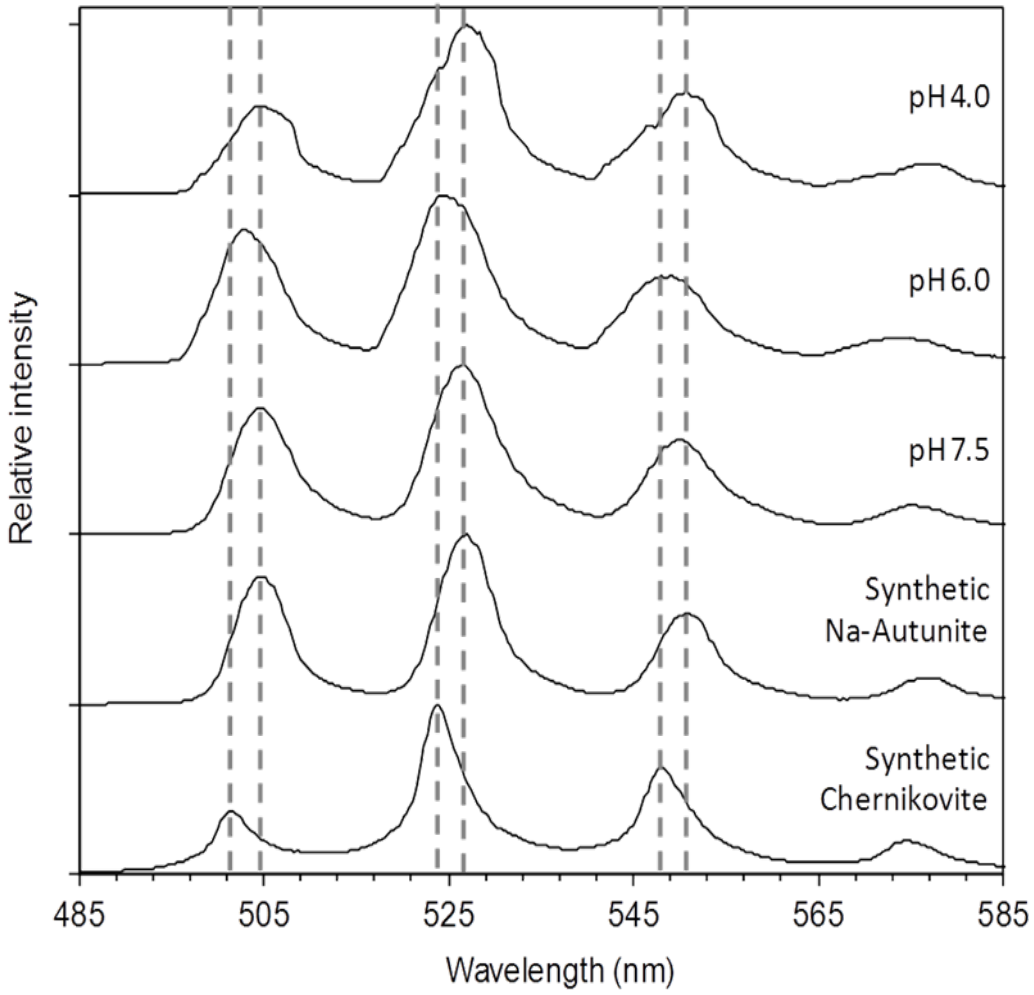

Figure 2.6. Laser induced fluorescence spectra of precipitates containing 100 µM U, 1 mM P, 5 mM Na and 1mM DIC at pH 4.0, 6.0 and 7.5 collected at λ_{ex} = 415 nm. Spectra of synthetic Na-autunite and synthetic chernikovite are included for comparison. For clarity, the spectra were normalized and plotted with offsets along the y-axis.

and 7.5, the concentrations were at least one order of magnitude lower than those observed in the absence of sodium. As discussed in the preceding section, at pH 4 the predicted equilibrium solubility of sodium autunite and chernikovite are more similar and the precipitated solids may be a mixture of chernikovite and sodium autunite.

Dissolved uranium concentrations measured after 0.22 μm filtration were consistently higher than after 0.05 μm filtration (Figure 2.7[a] and 7[c]). The difference in dissolved uranium concentrations in the filtrates obtained through 0.22 μm and 0.05 μm filters increases with increasing sodium concentration from 1 mM to 7.44 mM. This observation agrees with the nucleation theory discussed earlier for chernikovite precipitation that solutions with greater initial extents of supersaturation yield precipitated solids that have the smallest initial particle sizes. For 5 mM sodium concentrations, solids were removed from suspension by centrifugation and not filtration; settling velocity calculations suggest that particles larger than 0.05 μm should have been removed during the 35 minutes of centrifugation. Formation of sodium autunite nanoparticles has also been reported previously (Zheng et al. 2006).

2.3.3 Effect of Ca^{2+} on the solids formed

2.3.3.1 Solid characterization

The presence of calcium resulted in formation of both autunite and a poorly crystalline calcium phosphate solid. Greater losses of calcium and phosphate from solution than could be accounted for by autunite precipitation were observed at pH

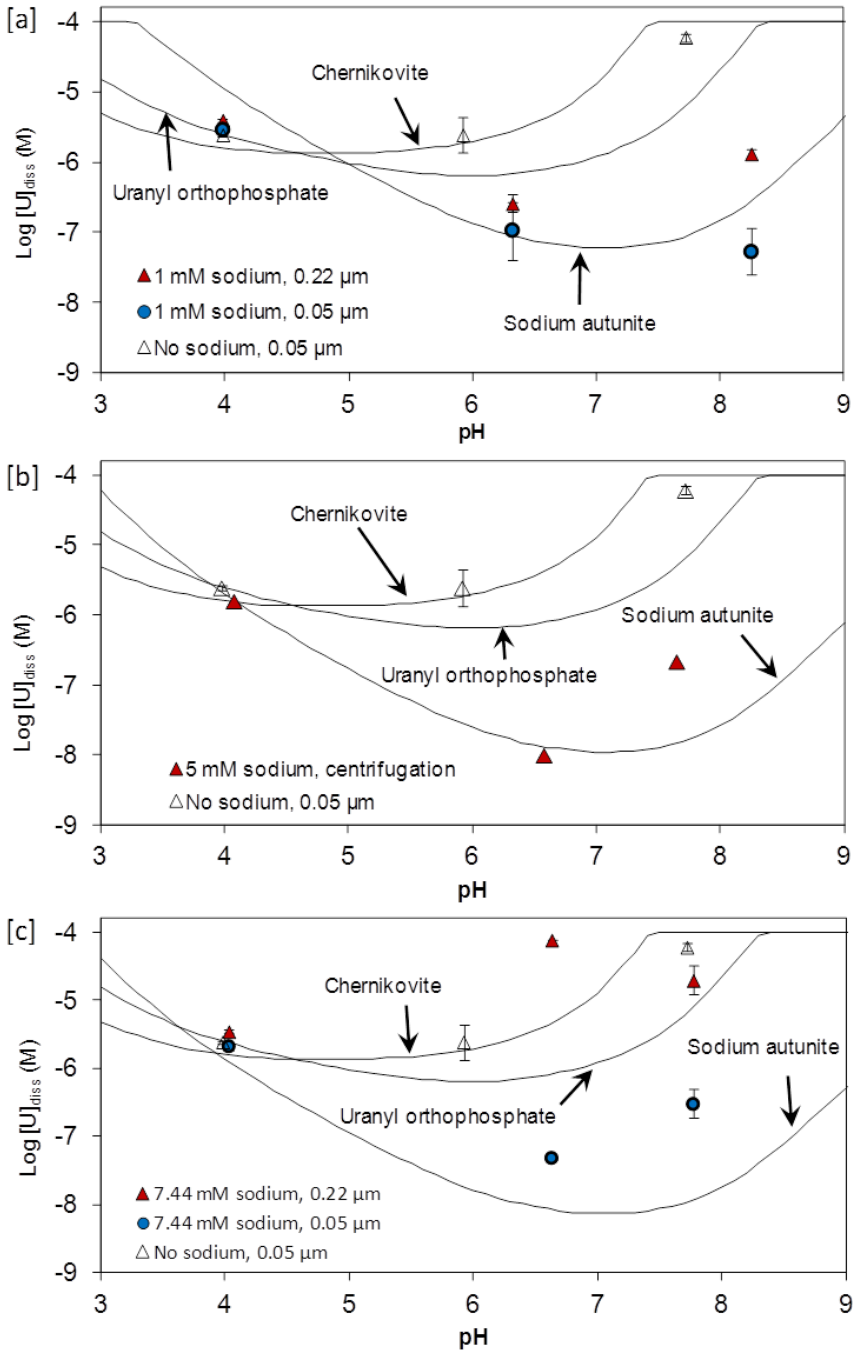

Figure 2.7. Observed uranium concentrations after 10 days versus predicted solubility for systems containing 100 µM U, 1 mM P and 1 mM DIC in the absence (open triangles) or presence of sodium (closed triangles and closed circles) concentrations of [a] 1 mM Na^+, [b] 5 mM Na^+ and [c] 7.44 mM Na^+. The data points represent mean values from duplicate studies with the error bars representing standard error. Data points (closed triangles) in [b] represent the concentrations observed from 2L scaled up batch reactors used to generate solids for characterization purposes.

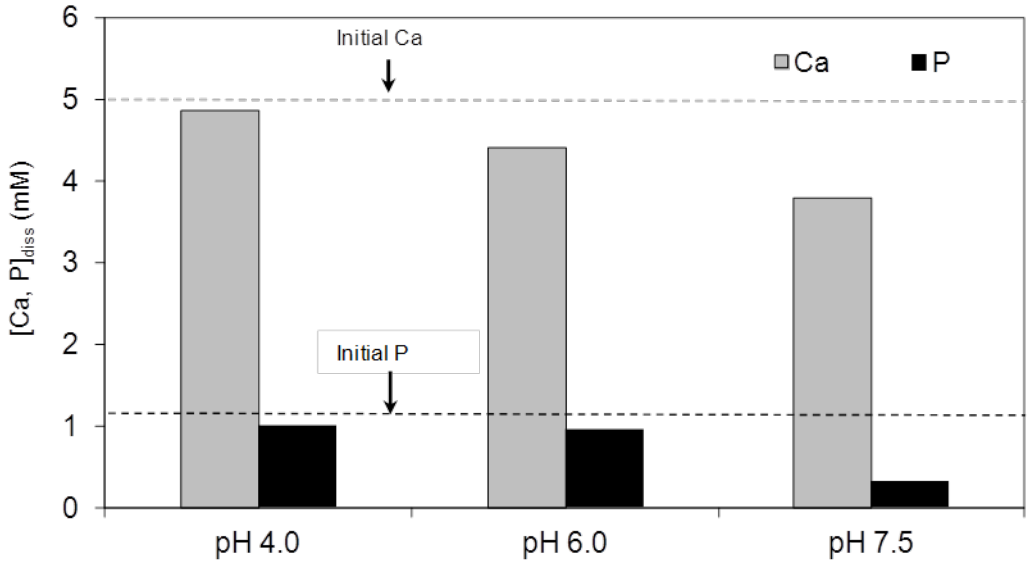

Figure 2.8. Dissolved calcium and phosphorus concentrations after 10 days for systems initially containing 100 µM U, 5 mM Ca, 1.1 mM P and 1 mM DIC.

4.0 and 6.0 (Figure 2.8). At pH 7.5much more calcium and phosphate were lost from solution (Figure 2.8), and the mass of solids collected from the reactors was significantly more than what would have been expected based simply on autunite precipitation. XRD analysis identified at pH 4.0 and 6.0 (Figure 2.5). A recent study (Fanizza et al. 2013) reported formation of chernikovite in the presence of calcium under acidic (pH 4.1) conditions; however, that study was conducted under flowing conditions and at lower calcium concentrations that could have kinetically limited the formation of autunite. Unlike the solids formed at pH 4.0 and 6.0, those obtained at pH 7.5 did not have detectable diffraction peaks of autunite or any other phases (Figure 2.5). The non-uranium-containing solids for which the solutions were supersaturated included hydroxylapatite [$(Ca_5(PO_4)_3(OH)$] and calcium phosphate [$Ca_3(PO_4)_2$]. SEM analysis for all the samples (including those obtained at pH 7.5) did not provide any information pertaining to the identity of the solids based on the

shape and morphology of the solid phase. EDS analysis suggested a calcium phosphate at pH 7.5 with a Ca:P ratio of 1.35:1. Similar ratios have been reported by (Christoffersen et al. 1990) for octacalcium phosphate [$Ca(PO_4)_{0.74}H_{0.22}$] which was found to be a precursor to hydroxylapatite.

2.3.3.2 Solubility of uranium

The predicted solubility of uranium for systems with calcium is higher than with sodium, especially at the higher pH conditions, due to the formation of calcium-uranyl-carbonate complexes. The log K_{sp} value of -48.36 for autunite as suggested by

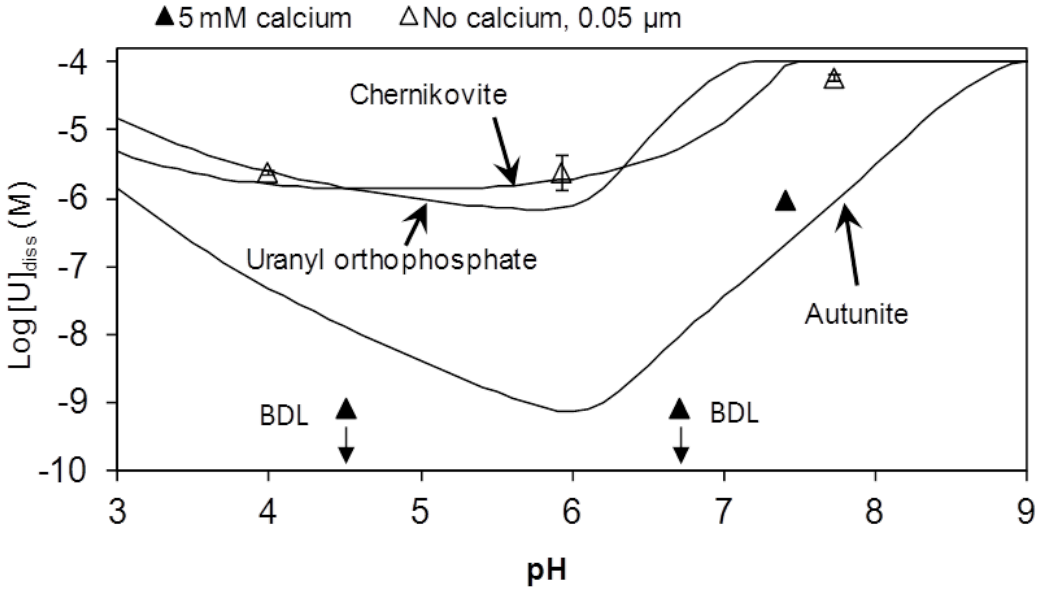

Figure 2.9. Observed uranium concentrations after 10 days versus predicted solubility for systems containing 100 µM U, 1 mM P and 1 mM DIC in the absence (open triangles) or presence of 5 mM calcium (closed triangles). The data points (open triangles) represent mean values from duplicate studies with the error bars representing standard error. Data points (closed triangles) represent the concentrations observed from 2L scaled up batch reactors used to generate solids for characterization purposes (BDL-Below detection limit (8.4×10^{-10} M).

Gorman-Lewis et al. (2009) was used in this study to calculate the predicted solubility. This value was selected because it was determined by approaching equilibrium from both the directions (i.e. dissolution and precipitation) and had confirmation that autunite was the only solid present. The observed uranium concentrations (Figure 2.9) were below the predicted solubility of autunite at pH 4.0 and 6.0 and slightly higher than the predicted solubility at pH 7.5. The concentrations were also lower than those observed for the sodium-containing or cation-free systems at pH 4.0 and 6.0. The observation of autunite at pH 4.0 and 6.0 despite the final solution being undersaturated with respect to autunite suggests that multiple mechanisms of uranium loss from solution were occurring. The initial solutions were supersaturated with respect to autunite as well as calcium phosphate solids, and it is likely that the autunite precipitated quickly and then persisted even as dissolved uranium concentrations dropped to lower values as uranium was taken up with calcium phosphate solids. The autunite may persist given its slow dissolution relative to the timescales of the experiments. Low dissolution rates for autunite (3.13×10^{-14} mol/m^2/s) at pH 5 have been reported previously (Wellman et al. 2007).

In addition to autunite precipitation, there is evidence that the removal of uranium from solution involves adsorption onto or incorporation in calcium phosphate solids formed during the reaction. The decrease in calcium and phosphate concentrations, especially at pH 7.5, demonstrates the formation of calcium phosphate solids (Figure 2.8). Calculations using the observed final dissolved calcium and phosphate concentrations determined saturation indices of -0.87, 2.39 and 2.62 with respect to octacalcium phosphate and -6.94, 11.3 and 13.5 with respect

to hydroxylapatite at pH 4.0, 6.0 and 7.5 respectively. The complete absence of autunite peaks in the XRD pattern of solids from the reaction at pH 7.5 suggests that adsorption and structural incorporation may be the sole removal mechanisms at this pH and that combinations of mechanisms prevail at pH 4.0 and 6.0.

Several previous investigations have shown high uranium uptake on phosphate minerals through adsorption. Phosphate minerals investigated included reagent grade synthetic hydroxylapatite and apatite-containing bone meal and bone charcoal materials. Studies were performed in the pH range of 6.3 – 9.3 (Fuller et al. 2003, Fuller et al. 2002, Wellman et al. 2008). For studies done in the presence of carbonate, uranium uptake of up to 11,200 μg U(VI)/g of solid occurred and resulted in final dissolved U(VI) concentrations as low as 0.71 μM (Fuller et al. 2003). X-ray absorption spectroscopic measurements showed that U(VI) was removed from solution through adsorption via the formation of inner sphere surface complexes (Cheng et al. 2004, Payne et al. 1996, Singh et al. 2012). Hence, a similar phenomenon may be occurring at pH 7.5 in the calcium-containing experiments with the formation of calcium phosphate solids (possibly amorphous or nanocrystalline octacalcium phosphate) on which uranium adsorbs.

In addition to adsorption to phosphate minerals, uranium removal in the presence of calcium phosphate minerals can occur through structural incorporation and by precipitation at the calcium phosphate surface. Uranium(VI) can substitute for calcium in the structure of apatite minerals, and phosphate minerals are often found with structurally incorporated uranium (Finch and Murakami 1999). Uranium

concentrations in natural apatites have been observed in the parts per million range (Altschuler et al. 1958) and can reach a few weight percent (2.3 %) in synthetic apatites (Rakovan et al. 2002). U(VI) phosphates may also precipitate at apatite surfaces. The magnesium uranyl phosphate saleeite formed on the surface of apatite despite the solution being undersaturated. The authors attributed this uranium mineralization to local solution supersaturation (Murakami et al. 1997). For a uranium- fluorapatite system studied at acidic pH conditions, autunite formed at the fluorapatite surface (Ohnuki et al. 2004). While the current results are suggestive of adsorption and structural incorporation of uranium into calcium phosphate solids in addition to autunite precipitation, a more detailed molecular-scale characterization of the solids would be necessary to definitively establish the mechanisms of uranium removal from solution.

2.4 Conclusions

In the absence of cations, chernikovite precipitated despite uranyl orthophosphate being the most thermodynamically favorable solid at pH 6.0 and 7.5 conditions. In the presence of sodium (Na^+), sodium autunite was observed at all the pH conditions studied; however, at pH 4.0 a mixture of chernikovite and sodium autunite or a H-/Na-autunite solid solution formed. In the presence of calcium (Ca^{2+}), uranium removal occurred through different processes at different pH values. At pH 7.5, uranium was predominantly removed by adsorption onto or incorporation into a poorly crystalline calcium phosphate solid. At pH 4.0 and 6.0, uranium was removed

primarily through precipitation of autunite with possible contributions from uptake with calcium phosphate.

The exact composition of sodium and calcium in uranium-contaminated environments that are remediated by phosphate addition will strongly affect the products of remediation and the extent of decrease in soluble uranium concentrations. The presence of co-solutes, especially sodium, can be beneficial for successful *in situ* uranium immobilization. In the case of calcium, additional possibilities of uranium adsorption to or structural incorporation into calcium phosphates exist. Adsorption might not be an ideal scenario from the perspective of long term immobilization since uranium uptake through adsorption is more vulnerable to mobilization in response to changes in subsurface conditions.

Acknowledgements

We are grateful to the McDonnell International Scholars Academy at Washington University for providing the Ameren corporate fellowship for Vrajesh Mehta. This work was supported by the U.S. Department of Energy (DOE) Subsurface Biogeochemical Research program (Award No. DE-SC0006857). LIFS measurements were performed at the Environmental Molecular Sciences Laboratory (EMSL), a national scientific user facility sponsored by the DOE Office of Biological and Environmental Research and located at the Pacific Northwest National Laboratory. PNNL is operated for DOE by Battelle Memorial Institute under Contract # DE-AC06-76RLO-1830.

Chapter 3. Uranium uptake with solid phases: Dependence on starting forms of calcium and phosphate

Results of this Chapter are being prepared for a manuscript to be submitted to *Environmental Science & Technology*.

.

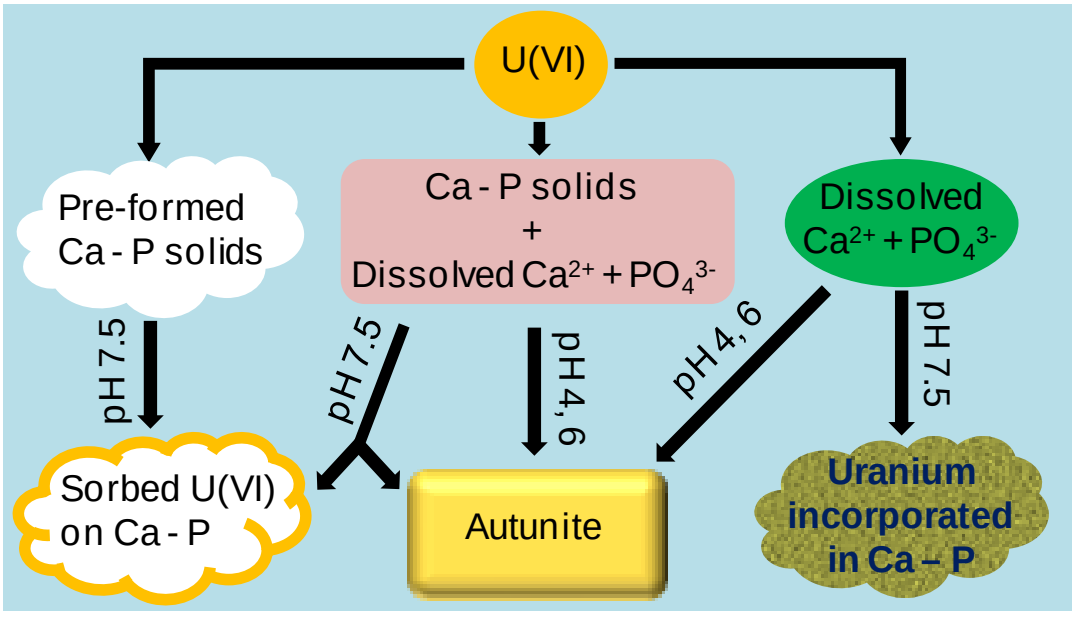

Abstract

Addition of phosphate amendments to subsurface environments contaminated with uranium can be used as an *in situ* remediation approach. Batch experiments were conducted to evaluate the dependence of U(VI) uptake mechanisms on the starting forms of calcium and phosphate at concentrations relevant to field sites. Aqueous samples were analyzed and considered in the context of equilibrium speciation, and solid phases were characterized by X-ray absorption spectroscopy and laser induced fluorescence spectroscopy. When U(VI) was reacted with dissolved calcium and phosphate at pH 4 and 6, uranium uptake occurred via precipitation of autunite ($Ca(UO_2)(PO_4)_3$) irrespective of the starting forms of calcium and phosphate. At pH 7.5 the uptake mechanisms depended on the nature of the calcium and phosphate with which U(VI) reacted. When dissolved uranium, calcium, and phosphate were simultaneously added to a reactor, uranium was incorporated into an amorphous calcium phosphate structure. When dissolved uranium was contacted with pre-formed amorphous calcium phosphate solids, adsorption was dominant. When U(VI) was added to a suspension containing amorphous calcium phosphate solids as well as dissolved calcium and phosphate, then uptake occurred through precipitation (57±4 %) of autunite and adsorption (43±4 %) onto calcium phosphate.

3.1 Introduction

Past programs associated with nuclear materials production has left a legacy of uranium contamination (DOE 1997, McCullough et al. 1999). Cost-effective remediation strategies are required to address the widespread nature of the contamination. *In situ* remediation has received significant attention in recent years as an attractive solution to this problem (EPA 2001, NRC 1993). Addition of phosphate amendments has been proposed for *in situ* uranium immobilization, usually because of the low solubility of U(VI) phosphate solids,(Beazley et al. 2009, Newsome et al. 2014, Singh et al. 2010, Sowder et al. 2001, Wellman et al. 2008, Wellman et al. 2006) but addition or formation of phosphate solids can also immobilize uranium via adsorption (Arey et al. 1999, Fuller et al. 2003, Fuller et al. 2002). Phosphate-based approaches can be used as a standalone remediation strategy or as a complementary process to other remediation approaches. A wide range of uranyl phosphates can form and many have been observed in natural ores as well as contaminated sediments (Buck et al. 1996, Finch and Murakami 1999, Jerden and Sinha 2003, Jones et al. 2001).

The influence of solution composition on uranium immobilization from phosphate addition has been evaluated in laboratory studies. Systematic evaluation of co-solute effects showed that presence of sodium led to formation of sodium autunite [$Na_2(UO_2)_2(PO_4)_2$] with U(VI) concentrations matching well with equilibrium predictions. However, in the case of calcium, U(VI) concentrations were below the

predicted solubility of autunite, which suggested that additional uptake processes were occurring (Mehta et al. 2014). Calcium can also react with phosphate to form calcium phosphate solids that are good sorbents for uranium (Arey et al. 1999, Fuller et al. 2003, Fuller et al. 2002). Additionally, surface mineralization has been reported as a plausible uranium uptake pathway on the calcium phosphate mineral apatite in which a leached layer of autunite formed on the apatite (Ohnuki et al. 2004). Moreover, calcium can form strong ternary complexes with uranium and carbonate that increase uranium solubility (Dong and Brooks 2006). Some field-scale studies of phosphate addition resulted in limited formation of calcium-phosphate solids and were not fully successful because of incomplete mixing of calcium and phosphate-bearing fluids (Vermeul et al. 2009). However, it is likely that calcium phosphate precipitation will occur at the field scale under favorable mixing conditions.

The objective of this study was to identify the dominant U(VI) uptake mechanisms responsible for U(VI) immobilization in systems with calcium and phosphate. A set of batch experiments were performed in which the order of reactant addition was varied to simulate different possible scenarios of uranium-calcium-phosphate interactions. Solid phase characterization was combined with aqueous phase analysis to identify and quantify the dominant uptake mechanisms for each experiment. Assessment of dominant pathway is important to evaluating the long term fate and transport of sequestered uranium. Insights into the effects of the starting forms of calcium and phosphate on U(VI) uptake can aid in designing efficient remediation strategies.

3.2 Materials and Methods

3.2.1 Materials

The chemicals used in this study were ACS grade or better. A 5 mM uranyl nitrate ($UO_2(NO_3)_2$) stock solution was prepared in ultrapure water (> 18.2 MΩ·cm resistivity). A 100 mM phosphate stock solution was prepared in ultrapure water using phosphoric acid. Dilute tetrabutylammonium hydroxide (TBAOH) solution and/or nitric acid solutions were used to adjust the pH of the solutions to the target values. TBAOH was used because, unlike the Na^+ that comes from NaOH, the tetrabutylammonium ion is unlikely to be structurally incorporated into uranium phosphate precipitates because of its large size. An air-equilibrated TBAOH solution was used as a stock for adding dissolved inorganic carbon (DIC). A $Ca(NO_3)_2$ solution was used as the source of calcium.

3.2.2 Batch experiments

Experiments were performed to delineate the effects of the calcium and phosphate forms added (Table 3.1) on U(VI) uptake. The pH range of 4.0 – 7.5 was selected because it encompasses the conditions at many uranium-contaminated sites, and previous results suggested that different mechanisms might be responsible for U(VI) immobilization at pH 4.0 versus pH 7.5 (Mehta et al. 2014).

All experiments were performed in capped and stirred glass reactors at room temperature (22 ± 0.5 °C). Both uranium-free and phosphate-free control

experiments were conducted to assess removal of uranium or phosphate in the absence of the other. Uranium concentrations were selected to provide sufficient solid mass for characterizing solids at the end of the experiment. Calcium

Table 3.1. Conditions of batch experiments conducted

Batch ID	Tot U(VI) (μM)	Tot PO_4^{3-} (mM)	Tot Ca^{2+} (mM)	Starting pH	Sampling time
Pre-formed[a] (Time study)	20	31.5	41	7.5	0, 2 min, 10 min, 30 min, 1 h, 4 h, 12 h, 1 d, 6 d
Pre-reacted[b]	100	1.0	5	4., 6, 7.5	0, 4 d, 10 d
All added together[c]	100	1.0	5	4, 6, 7.5	0, 10 d

[a] Calcium phosphate precipitation was initiated by 24 h reaction of a solution that contained dissolved calcium (250 mM) and phosphate (50 mM). Following the reaction, the excess dissolved calcium and phosphate was discarded and the dry solids obtained by centrifugation and freeze-drying were added to 250 mL bottles that contained dissolved uranium at pH 7.5. The calcium: phosphate ratio of the freeze-dried solids was determined by digestion of a portion of the solids followed by ICP-MS analysis. Reactors were stopped at different time intervals and sampled for liquid and solid analyses.

[b] Calcium and phosphate were allowed to react for 4 days at different starting pH conditions. After this 4-day pre-reaction period, uranium was added and allowed to react for 6 more days.

[c] A solution containing dissolved uranium and calcium was added to a solution containing dissolved phosphate and allowed to react for 10 days.

concentrations were similar to those at uranium-contaminated sites (Campbell et al. 2011, DOE 1999). Excess phosphate (P:U molar ratio) addition made the solutions supersaturated with respect to uranyl phosphate solids. Excess phosphate relative to uranium would also be used in remediation strategies to promote precipitation and

overcome other pathways for phosphate removal such as adsorption to sediment minerals. Samples were collected from the batch reactors at time intervals noted in Table 3.1. Samples for measurement of dissolved U, P and Ca were filtered using 0.05 µm filters (polyethersulfone syringe filters, Tisch Scientific), and the filtrates were acidified to provide a 1 % nitric acid matrix to preserve the samples prior to analysis.

Three different approaches were pursued in reacting U(VI), calcium, and phosphate (Table 3.1). In the first approach (pre-formed/time study), calcium and phosphate were reacted for 24 h in 2-L glass bottles. The excess dissolved calcium and phosphate was discarded and the precipitated solids (Ca-P) were centrifuged and freeze-dried to obtain dry Ca-P solids. Fixed quantities of these solids were then added to 250 ml glass bottles that contained 20 µM dissolved uranium at pH 7.5. The final pH of the solutions was within 0.4 units of the target pH (7.5). The pre-formed experiments were done only at pH 7.5 since no collectible solids were obtained at pH 4 and 6 from calcium and phosphate reactions. In the second approach (pre-reacted), calcium and phosphate were allowed to react for 4 days at different starting pH conditions. After this 4-day pre-reaction period, uranium was added and the contents reacted for 6 more days. The pH during this study was within 0.3 units of the target values. For the third approach (all added together), a solution containing calcium and uranium was quickly added to a solution containing dissolved phosphate and DIC with pH adjusted to desired values in 2-L glass bottles. Final pH adjustment was done using 0.1 M TBAOH solution and the solution was allowed to react for 10 days.

Reactors were stopped at different times (Table 3.1) and sampled for liquid and solid analyses.

The total ratios of U, Ca, and P were the same in the pre-reacted and all added together experiments, which enabled an examination of the order of addition on U(VI) uptake from solution and are analogous to the situation in which phosphate amendments might be injected into Ca-containing and U-contaminated groundwater. The experiments with pre-formed calcium phosphate solids had a much lower ratio of U to Ca and P. Although these experiments do not allow a direct comparison with respect to the order of reactant addition, they enabled the generation of an end-member solid phase most likely to have uranium uptake dominated by adsorption. This experiment is also most analogous to a field-scale situation involving a calcium phosphate permeable reactive barrier.

3.2.3 Analytical methods

Dissolved concentrations were determined using inductively coupled plasma-mass spectrometry (ICP-MS, Perkin Elmer ELAN DRC II system). A set of 8–10 calibration standards made from certified standards (Fisher Scientific) was used. The detection limit was 0.2 μg/L for uranium, 10 μg/L for phosphorus, and 50 μg/L for calcium. DIC was measured using a TOC analyzer (Shimadzu, TOC-$L_{CPH/CPN}$ PC controlled model) installed with a high sensitivity catalyst (detection limit of 10 μg/L) and an autosampler. Solids from different reactors were obtained at the end of the experiment by centrifugation followed by freeze-drying. Freeze-dried solids were

used for solid phase analysis using X-ray diffraction (XRD, Rigaku Geigerflex D MAX/A), scanning electron microscopy (SEM, JEOL 7001FLV FE) with energy dispersive X-ray analysis (EDS), laser induced fluorescence spectroscopy (LIFS), and extended X-ray absorption fine structure (EXAFS) spectroscopy. XRD, SEM EDS and LIFS measurements were done using methods previously reported (Mehta et al. 2014).

3.2.4 EXAFS analysis

Samples for EXAFS were sealed in polycarbonate sample holders with Kapton tape and then heat-sealed in polyethylene bags for secondary containment. U L_{III}-edge EXAFS spectra were collected at room temperature on beamline 20-BM-B at the Advanced Photon Source at Argonne National Laboratory. The beamline employed a Si(111) fixed-offset, double-crystal monochromator and a torroidal focusing mirror to increase usable flux on the sample (Heald 2011, Heald et al. 1999). Fluorescence-yield data were collected using a 12-element solid-state Ge energy dispersive detector. Energy calibration was performed before the measurements using a Y metal foil, with the first inflection point of the Y K-edge set to 17038 eV.

Data were processed using the Athena interface (Ravel and Newville 2005) to the IFEFFIT software package (Newville 2001); linear-combination fitting was also performed in Athena. Fitting of structural models to the EXAFS spectra were performed in SIXPack (Webb 2005) using backscattering phase and amplitude functions generated in FEFF 7.02 (Ankudinov and Rehr 1997) with the program set

to automatically overlap muffin tin potentials, using the crystal structure of autunite (Locock and Burns 2003). The three multiple scattering paths associated with the axial oxygen atoms of the uranyl moiety (Hudson et al. 1996) were included in all fits. Sodium meta-autunite was synthesized for use as a standard following a previously described procedure (Wellman et al. 2005).

3.2.5 Geochemical equilibrium calculations

MINEQL + v 4.6 was used to perform equilibrium calculations that evaluated the saturation state of solutions (Schecher and McAvoy 2007). The solubility products of the relevant solids used for calculating saturation indices are noted in Table S3.1 in the supporting information.

3.3 Results and Discussion

3.3.1 Solubility of uranium

When calcium and phosphate were first reacted together at pH 7.5 without U(VI), the solids that formed after 24 h were amorphous or poorly crystalline. Acid digestion of dry solids resulted in Ca:P molar ratios of 1.30:1, very similar to the ratio in octacalcium phosphate (1.35:1), a precursor to crystalline hydroxylapatite (Christoffersen et al. 1990). When these pre-formed calcium phosphate solids were added to solutions of U(VI) (i.e. pre-formed study), 95% of the uranium uptake occurred within the first 2 minutes; 99.9 % of the uranium was removed from

solution over the remaining 6 days of reaction (Figure 3.1 (a)). While U(VI) uptake occurred, the solids released up to 1.4 mM calcium and 0.8 mM phosphate to the aqueous phase during the 6 days of reaction. For the experimental conditions (pH 7.5)

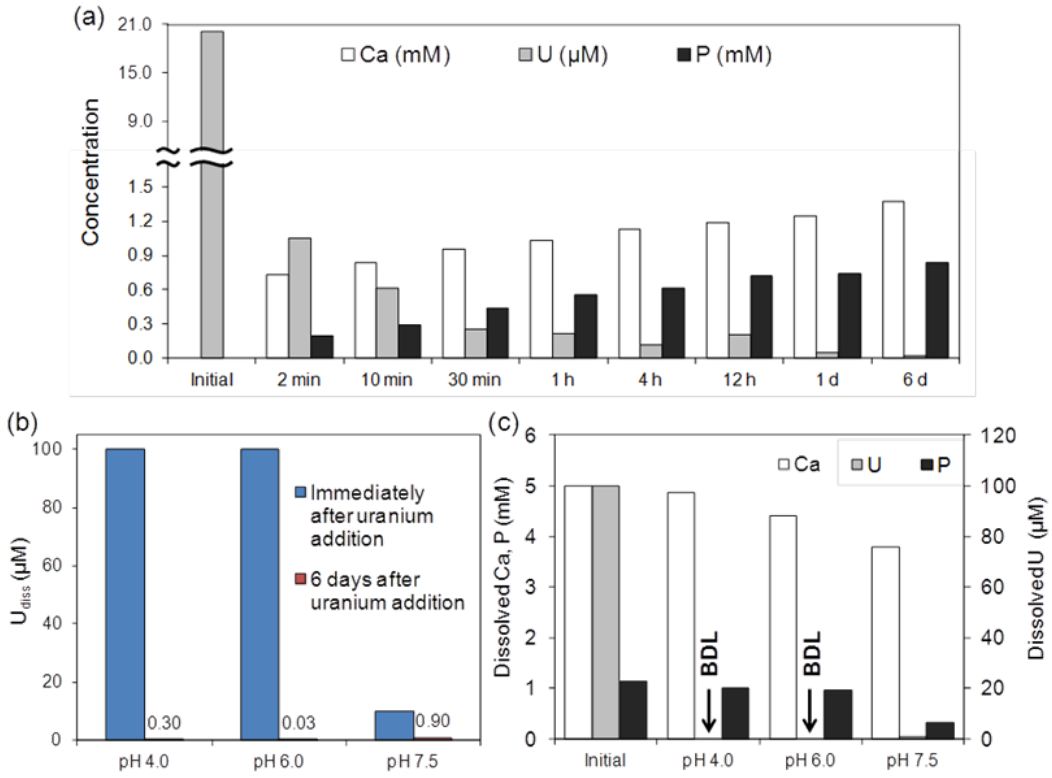

Figure 3.1. Observed concentrations of uranium, calcium and phosphate under different experimental conditions. (a) Uranium (20 μM) solution reacted with pre-formed calcium phosphate solids at a starting pH of 7.5 with samples collected at different reaction times. (b) Uranium (100 μM) added to a pre-reacted Ca-P suspension (containing Ca-P solids and excess dissolved calcium and phosphate after 4 days of reaction). (c) Dissolved concentrations of uranium, calcium and phosphate after 10 days of reaction at varying pH conditions when all three were added together. At pH 4 and 6, the uranium concentrations were below the detection limit of 0.00084 μM.

at these concentrations after 6 days of reaction, the solution was highly supersaturated with respect to various calcium phosphates with a saturation index of 2.7 for octacalcium phosphate. Dissolution of the solid to concentrations exceeding the predicted equilibrium solubility of octacalcium phosphate, the most soluble of

the calcium phosphates considered, may be due to the poorly crystalline nature of the octacalcium phosphate solids used in this study as compared to those used by Christoffersen et al. (1990). Saturation index values with respect to potential uranium-containing solids suggested that the solution was undersaturated with respect to autunite (-2.19). The solids attained uranium concentrations of ~ 1475 µg/g of octacalcium phosphate or ~ 0.1 µmol/m^2 under the assumption of a previously reported specific surface area of 65 m^2/g for octacalcium phosphate (Yang et al. 2012). A high ratio of Ca and P to U and the trend of decreasing uranium concentrations from a solution that is undersaturated with respect to uranium-containing solids suggest that uranium uptake occurred via adsorption. A previous study of U(VI) sorption to powdered bone charcoal obtained adsorbed uranium at loadings of 2960 µg/g (~ 0.19 µmol/m^2) (Fuller et al. 2003).

In the experiments with uranium addition to pre-reacted calcium phosphate suspensions, the 4-day pre-reaction resulted in varying amounts of Ca-P precipitation for different pH conditions with the maximum precipitation observed at pH 7.5 (Figure S3.1). The solutions still had significant amounts of dissolved calcium and phosphate in the aqueous phase. Immediately following uranium addition (within 2 minutes of reaction), samples were collected and analyzed for aqueous phase concentrations. The analysis suggested that essentially all of the U(VI) added was still in solution immediately following the addition at pH 4 and 6 whereas rapid uptake was observed at pH 7.5 (Figure 3.1 (b)). Furthermore, the calcium and phosphate concentrations further decreased at pH 4 and 6 in small amounts that

would be expected for uranium uptake via formation of a uranyl phosphate precipitate.

Table 3.2. Saturation index calculations for the final concentrations in experiments in which dissolved Ca, P and U were added together.

pH[#]	Concentration[#] (mM)				Saturation Index (SI)		
	U(VI)	Ca^{2+}	PO_4^{3-}	DIC	Autunite	OCP	HAP
4.50	$8.4\times10^{-7*}$	4.86	0.998	0.09	-2.37	-0.24	-3.43
6.70	$8.4\times10^{-7*}$	4.41	0.966	0.15	0.97	2.39	11.36
7.40	9.65×10^{-4}	3.79	0.331	0.83	1.27	2.62	13.55

[*] Below detection limit of 8.4×10-10 M
[#] Measured values at the end of experiment (10 days)
OCP: Octacalcium phosphate

In the experiments in which all the solutes (calcium, uranium and phosphate) were initially mixed from dissolved forms, uranium concentrations were found to be below detection levels (8.4×10^{-4} µM) at pH 4 and 6 as compared to 0.97 µM at pH 7.5 (Figure 3.1 (c)). At pH 4 and 6, there is limited evidence for calcium and phosphate precipitation in excess of that involved in precipitation of a uranyl phosphate solid. At pH 7.5, much more calcium and phosphate precipitation was observed than would be expected for stoichiometric removal via formation of autunite. The calcium and phosphate behaviors suggest different uranium uptake mechanisms at different pH conditions. To determine what uranium solids may have precipitated the saturation indices were calculated for the final concentrations in the experiments (Table 3.2); since uranium concentrations were below the detection

limit at pH 4.0 and 6.0, the detection limit was used as the input for the uranium concentration in these calculations. At pH 4.0 and 6.0, the saturation indices for autunite were -2.37 and 0.97 respectively; because characterization of the solids identified autunite as the only detectable solid in these samples, the deviation of the saturation indices from zero (i.e., the value if the solutions were in equilibrium with autunite) may be due to variations in the degree of crystalline of the solids or uncertainty in equilibrium constants used for predicting solubility. At pH 7.5, the initial solutions and the final solutions were supersaturated with respect to autunite as well as calcium-phosphates. It is possible that autunite and calcium phosphate precipitated initially and then additional uranium was taken up by calcium phosphate solids while the precipitated autunite slowly dissolved (Mehta et al. 2014, Wellman et al. 2007).

3.3.2 Solids characterization

3.3.2.1 XRD and SEM-EDXS analysis

XRD analysis of solids obtained when U(VI) was added to a solution of Ca and P that had been pre-reacted identified autunite at pH 4.0 and 6.0. Slight differences in diffraction patterns for the samples as compared to a standard reference pattern of autunite could be a result of preferred orientation due to its sheet structure. Additional broad features were observed for the pH 7.5 sample (Figure 3.2) indicative of poorly-crystalline or amorphous materials. Similar observations were made for samples that were obtained from the study when Ca, P and U(VI) were all

added together. However, the XRD pattern for pH 7.5 had no detectable autunite nor any other crystalline solid (Mehta et al. 2014). SEM-EDXS analysis of the all added together samples did not provide any information (data not shown) pertaining to the identity of the solids based on shape and morphology of the solid phase.

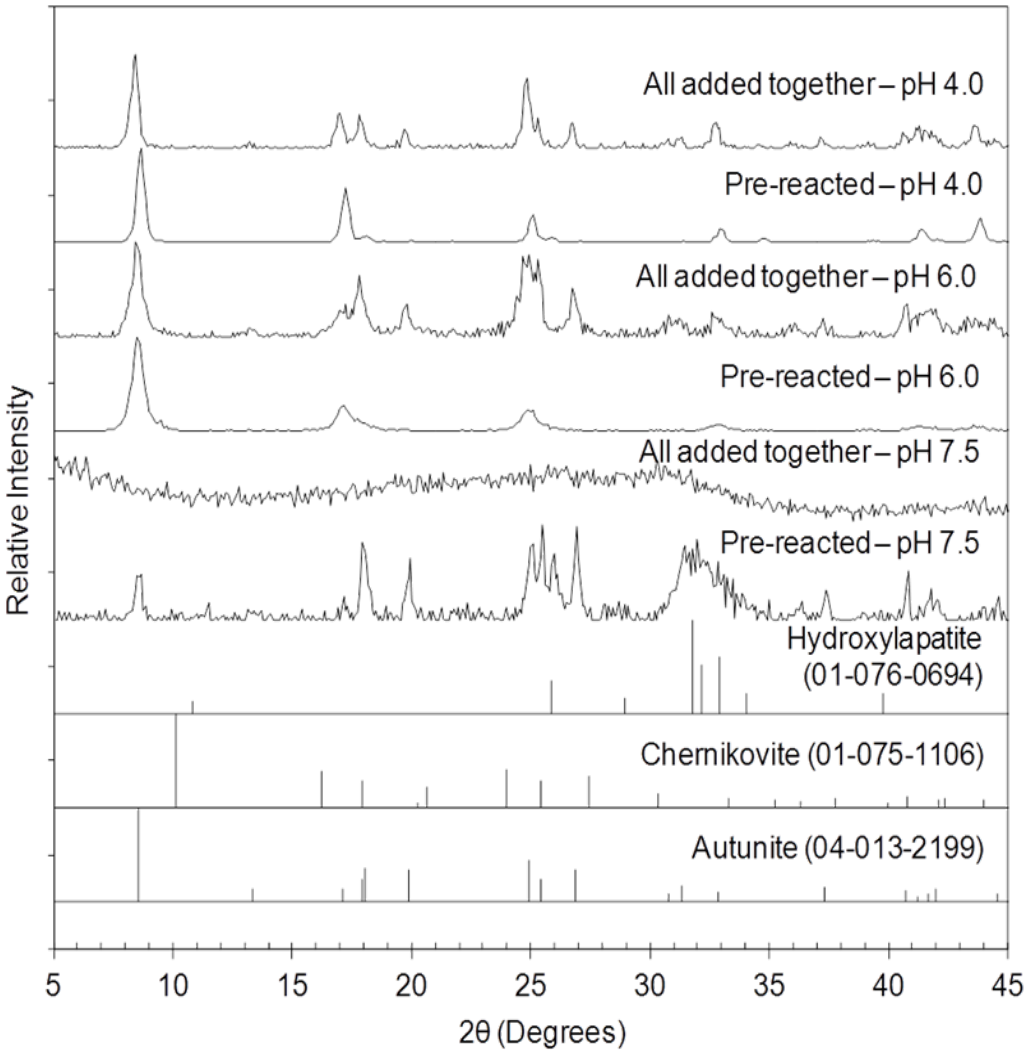

Figure 3.2. X-ray diffraction patterns of the solids obtained from experiments in which dissolved U, phosphate, and Ca were added simultaneously (all added together) and when the U(VI) was added 4 days after the Ca and phosphate had been pre-reacted. For reference, the standard patterns obtained from the International Crystal Diffraction Database with the respective PDF card numbers are included.

3.3.2.2 Laser induced fluorescence spectroscopy analysis

Solids obtained at pH 4 and 6 when Ca, U and P were added together or when uranium was added to pre-reacted Ca-P solution had similar fluorescence spectra to that of synthetic sodium autunite (Figure S3.2 (a)). The emission bands observed for synthetic sodium autunite at approximately 504.0, 526.5, and 550.0 nm are similar to those observed for natural autunite (504.0, 524.2, and 548.0) or metaautunite (501.8, 522.9, and 546.9) (Baumann et al. 2006) which suggest that using sodium autunite's spectrum as a proxy for autunite is reasonable. The minor shifts in sample spectra could be due to the presence of some other species with autunite being the dominant phase or to different extents of hydration for autunite (Baumann et al. 2006). The solids obtained at pH 7.5 for both the studies (when Ca, P and U were all added together or when U was added to pre-reacted Ca-P suspension) had emission maxima at wavelengths similar to those for the solids obtained at pH 4 and 6 conditions. However, the fluorescence intensity was lower for both the pH 7.5 samples as compared to those with pH 4 and 6 samples. Moreover, the peaks were broader when Ca, U and P were all added together as compared to when U was added to pre-reacted Ca-P suspension. This peak broadening could be due to the presence of different U(VI) species, uptake mechanisms other than precipitation, or a mixture of multiple species. The aqueous phase analysis and solids characterization results indicate that the uptake mechanism at pH 7.5 was different than at pH 4 and 6 and

that it depended on the order in which uranium was reacted with calcium and phosphate.

The spectra of the samples when uranium was reacted with pre-formed Ca-P solids were all similar suggesting that a single uranium species that formed within 2 minutes of reaction existed for the remainder of the reaction (6 days). The spectra were different than the reference spectrum of sodium autunite and had emission maxima blue shifted by about 4 nm (Figure S3.2 (b)). Moreover, the spectra were also different from those observed for pH 7.5 samples from the pre-reacted and all added together studies. Spectra of U(VI) adsorbed onto Hanford 300 Area sediments also displayed strong bands at 498.6, 519.7, 542.1 and 564.5 nm, and this spectrum motif was attributed to be a characteristic of low concentration adsorbed U(VI) (Wang et al. 2011). These observations along with aqueous analysis suggest adsorption as the dominant uranium uptake mechanism for reaction with pre-formed Ca-P solids.

3.3.2.3 Uranium speciation via EXAFS spectroscopy

EXAFS spectra of U(VI) reacted with dissolved calcium and phosphate at pH 4 and 6 are consistent with the formation of autunite (Figure S3.3), regardless of the order of addition. In contrast, the three reaction conditions investigated at pH 7.5 each yielded distinct EXAFS spectra (Figure 3.3 and 3.4). Principal component analysis (PCA) (Malinowski 1977, 2002, Manceau et al. 2002, Wasserman et al. 1999) on the collection of spectra required three spectral components for adequate

sample reconstruction, suggesting that three distinct U species occur. Target transformation analysis (Malinowski 1978) showed that an autunite-group mineral was likely one real component, but only when the spectrum of U(VI) contacted with the pre-reacted suspension of calcium and phosphate was included in the PCA calculation. These observations indicate that this sample was the only one to contain

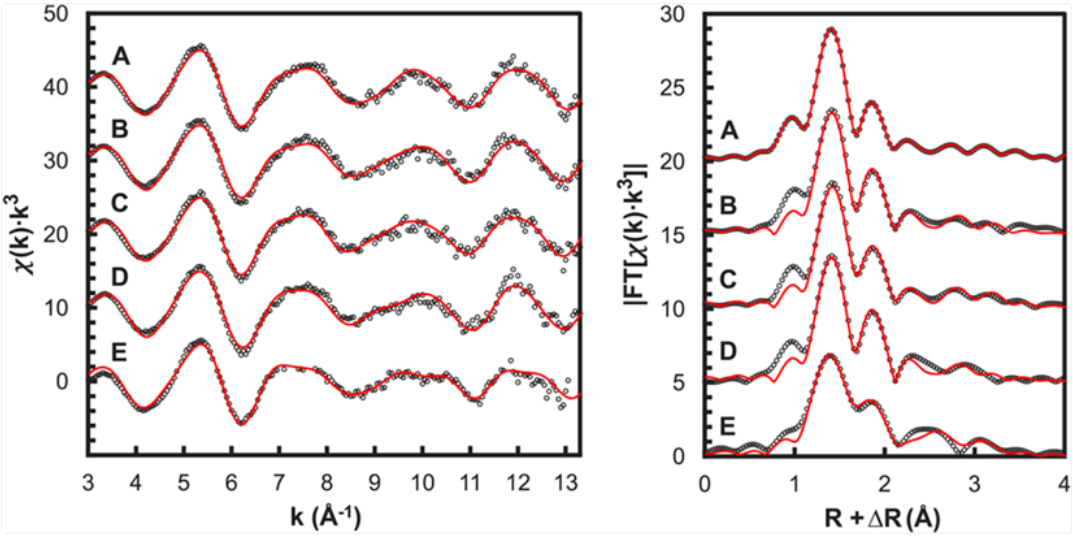

Figure 3.3. Data (dotted) and structural model fits (solid) to the U L_{III}-edge EXAFS spectra (left) and corresponding Fourier transform magnitudes (right) of U(VI) sorbed to amorphous calcium phosphate after reaction times of (A) 2 minutes, (B) 30 minutes, (C) 1 day, and (D) 6 days and (E) of U(VI) coprecipitated with calcium and phosphate (all added together) at pH 7.5.

an autunite precipitate as a substantial U species, i.e., less than 5 mol% of the total uranium in other samples were contained in such a phase.

Based on this initial analysis the spectra were analyzed in two distinct ways. Spectra of samples from the time series of U(VI) adsorbed to amorphous calcium phosphate and when U, Ca and P were all added together were fit with a structural model consisting of the first oxygen coordination shell as well as phosphorus shells

at distances corresponding to edge-sharing bidentate (~3.1 Å) and bridging bidentate (~3.6 Å) phosphate neighbors. These two types of coordination motifs to phosphate groups have been identified in previous studies (Fuller et al. 2003, Fuller et al. 2002). The time series samples of U(VI) adsorbed to amorphous calcium phosphate are spectrally similar and this is reflected in the fitting results (Table S3.2), which show no systematic trends in interatomic distances or coordination numbers and the same overall local structural environment. The total P coordination number for these samples is consistent with uranium existing solely as surface complexes.

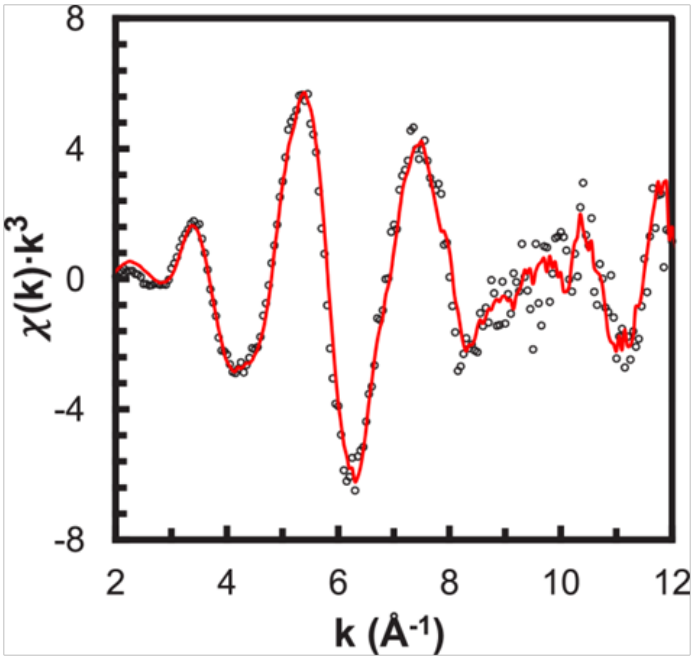

Figure 3.4. Data (dotted) and the 2-component linear combination fit (solid) to the U L_{III}-edge EXAFS spectrum of solids 6 days after U(VI) addition to a pre-reacted suspension of calcium phosphate at pH 7.5.

The spectrum of U(VI) when added together with calcium and phosphate has a substantially greater number of P neighbors at both ~3.1 and ~3.6 Å. This sample

also shows shorter bond lengths between uranium and equatorial oxygens, indicating that it exists in a distinct coordination environment. The observed spectrum is distinct from that of U(VI) phosphate minerals (Catalano and Brown Jr. 2004, Fuller et al. 2003, Fuller et al. 2002). Moreover, the digestion of freeze dried solids resulted in Ca:U molar ratio of 10.64:1. These observations suggest that U(VI) in this sample is incorporated in the amorphous calcium phosphate structure. U(VI) can substitute for calcium in the structure of apatite minerals, and phosphate minerals are often found with structurally incorporated uranium (Finch and Murakami 1999). Previous studies have also shown that U(VI) uptake can occur through surface mineralization in addition to adsorption and precipitation (Murakami et al. 1997, Ohnuki et al. 2004). The spectrum of U(VI) reacted with the pre-reacted solution of calcium and phosphate was analyzed differently because PCA and target transform analysis suggest that this sample contained an autunite phase. However, the spectrum is not identical to spectra of autunite group minerals, which are largely indistinguishable from one another (Catalano and Brown Jr. 2004), indicating that the sample contains multiple U(VI) species. The spectrum was thus fit as a linear combination of the spectrum of an autunite, U(VI) sorbed to calcium phosphate for 6 days (adsorbed U), and U(VI) coprecipitated with calcium phosphate (incorporated U). The incorporated uranium component refined to within error of zero in initial fitting and was excluded from the final fit (Figure 3.4), which determined that 57±4% of the uranium in the sample occurs as an autunite and 43±4% adsorbed to calcium phosphate.

3.4 Environmental Implications

Uranium uptake from solution in the presence of calcium and phosphate can occur through 1) adsorption onto calcium phosphate (Arey et al. 1999, Fuller et al. 2003), 2) incorporation in the amorphous calcium phosphate structure (Ohnuki et al. 2004), and 3) precipitation via formation of an insoluble uranyl phosphate like autunite (Mehta et al. 2014) as well as combinations of these processes (Fuller et al. 2003, Fuller et al. 2002). This study revealed that the dominant uptake mechanism depends on the starting forms of calcium and phosphate and the order in which uranium is reacted with these. The study in which Ca, U and P were all reacted together from dissolved forms closely mimics a real world scenario in which phosphate is added to groundwater that initially has calcium as well as uranium. At pH 4 and 6 uranium uptake would occur primarily through precipitation of autunite. At pH 7.5 conditions that are commonly observed in groundwater, uranium uptake might occur via incorporation into a Ca-P solid.

The removal of uranium through adsorption to or incorporation into calcium phosphates that was observed in the present study demonstrates that uranyl phosphate precipitation is not required for successful *in situ* immobilization of U(VI) by phosphate addition. Uranium reactions with pre-formed calcium phosphate solids could occur in phosphate-containing permeable reactive barriers (Fuller et al. 2003) or when a U(VI) plume flows into a downgradient zone that was treated with phosphate to produce calcium phosphate minerals *in situ* that effectively act as a permeable reactive barrier. For these scenarios the dominant immobilization

mechanism would be adsorption, although depending on the ratios of uranium to calcium and phosphate some autunite could also precipitate.

Phosphate-based remediation strategies will also need consider how precipitation reactions influence porosity and permeability since these flow properties can affect the long term fate and transport of uranium mobility in subsurface environments. The extent of mixing of injected phosphate solutions is also important, and some field-scale studies were not been fully successful due to limited mixing of calcium and phosphate bearing fluids (Vermeul et al. 2009).

Acknowledgements

We are grateful to the McDonnell International Scholars Academy at Washington University for providing the Ameren corporate fellowship for Vrajesh Mehta. This work was supported by the U.S. Department of Energy (DOE) Subsurface Biogeochemical Research program (Award No. DE-SC0006857). ICP-MS analysis was performed in the Nano Research Facility (NRF), a member of the National Nanotechnology Infrastructure Network (NNIN), which was supported by the National Science Foundation under Grant No. ECS-0335765. LIFS measurements were performed at the Environmental Molecular Sciences Laboratory (EMSL), a national scientific user facility sponsored by the DOE Office of Biological and Environmental Research and located at the Pacific Northwest National Laboratory (PNNL). PNNL is operated for DOE by Battelle Memorial Institute under Contract # DE-AC06-76RLO-1830.

Chapter 3. Supporting Information

Supplementary data associated with this article includes two tables (1 - Relevant reactions and their solubility products and 2 - EXAFS fitting summary) and three figures (1 - Dissolved calcium and phosphate concentrations for pre-reacted study, 2 - LIFS spectra and 3 - U(VI) EXAFS spectra for solids formed at pH 4 and 6 conditions when Ca, U and P were all added together and when uranium was added to pre-reacted calcium-phosphate solution).

Table S3.1. Relevant solids and their solubility products at 298 K and I = 0 M

Uranium solids:	**Log K**	**Mineral name**
$UO_3 \cdot 2H_2O_{(s)} + 2H^+ = UO_2^{2+} + 3H_2O$	5.60	Metaschoepite
$UO_3 \cdot 2H_2O_{(s)} + 2H^+ = UO_2^{2+} + 3H_2O$	4.81	Schoepite
$UO_2HPO_4 \cdot 4H_2O_{(s)} = UO_2^{2+} + H^+ + PO_4^{3-} + 4H_2O$	-25.50	Chernikovite
$(UO_2)_3(PO_4)_2 \cdot 4H_2O_{(s)} = 3UO_2^{2+} + 2PO_4^{3-} + 4H_2O$	-49.36	Uranyl orthophosphate
$UO_2(H_2PO_4)_2 \cdot 3H_2O_{(s)} = UO_2^{2+} + 4H^+ + 2PO_4^{3-} + 3H_2O$	-45.10	Uranyl phosphate
$Ca(UO_2)_2(PO_4)_{2(s)} = 2UO_2^{2+} + Ca^{2+} + 2PO_4^{3-}$	-48.36	Autunite
$Na_2(UO_2)_2(PO_4)_{2(s)} = 2UO_2^{2+} + 2Na^+ + 2PO_4^{3-}$	-47.41	Sodium autunite
$UO_2CO_{3(s)} = UO_2^{2+} + CO_3^{2-}$	-14.76	Rutherfordine
$Ca(PO_4)_{0.74}H_{0.22(s)} = Ca^{2+} + 0.22H^+ + 0.74PO_4^{3-}$	-13.102	Octacalcium phosphate
$Ca_5(PO_4)_3OH + H^+ = 5\,Ca^{2+} + 3PO_4^{3-} + H_2O$	-44.33	Hydroxylapatite

Log K values for different solids were selected from different literature and is noted previously (Mehta et al. 2014).

TABLE S3.2. Summary of U L_{III}-edge EXAFS fitting results for U(VI) adsorbed to Ca-PO_4 (time study) at different time points (A-D) and U(VI) when added together with Ca^{2+} and PO_4^{3-} (E).

Sample		$U\text{-}O_{ax}$	$U\text{-}O_{eq1}$	$U\text{-}O_{eq2}$	$U\text{-}P_1$	$U\text{-}P_2$	ΔE_0 (eV)[d]	χ_v^{2}[e]	R factor[e]
A) 2 minutes	N[a]	2.0	3.3(4)	2.5(5)	1.0(4)	0.9(6)	8(1)	14.50	0.012
	R (Å) [b]	1.794(5)[f]	2.30(2)	2.46(2)	3.11(2)	3.60(4)			
	σ^2 ($Å^2$) [c]	0.0012(3)	0.005	0.005	0.005	0.005			
B) 30 minutes	N	2.0	3.7(5)	2.2(6)	1.1(4)	0.6(7)	11(2)	17.30	0.019
	R (Å)	1.803(6)	2.34(1)	2.52(3)	3.13(3)	3.62(7)			
	σ^2 ($Å^2$)	0.0017(4)	0.005	0.005	0.005	0.005			
C) 1 day	N	2.0	3.7(4)	2.1(5)	1.1(3)	1.1(5)	10(1)	8.76	0.012
	R (Å)	1.808(5)	2.32(1)	2.48(2)	3.13(2)	3.62(3)			
	σ^2 ($Å^2$)	0.0016(3)	0.005	0.005	0.005	0.005			
D) 6 days	N	2.0	4.3(5)	2.0(6)	1.0(4)	0.7(6)	10(1)	16.05	0.016
	R (Å)	1.799(5)	2.33(1)	2.52(2)	3.11(3)	3.57(5)			
	σ^2 ($Å^2$)	0.0016(4)	0.005	0.005	0.005	0.005			
E) Coprecipitate (all added together)	N	2.0	4.2(5)	2.7(6)	1.6(4)	1.4(7)	6(2)	34.00	0.017
	R (Å)	1.79(1)	2.28(2)	2.44(4)	3.07(2)	3.59(3)			
	σ^2 ($Å^2$)	0.0028(5)	0.005	0.005	0.005	0.005			

[a] Coordination number. [b] Interatomic distance. [c] Debye-Waller factor. [d] Difference in the threshold Fermi level between the data and theory. [e] Goodness of fit parameters (Kelly et al. 2008). [f] Value in parentheses represents the 1σ uncertainty in the last digit; parameters without specified uncertainties were held constant during fitting.

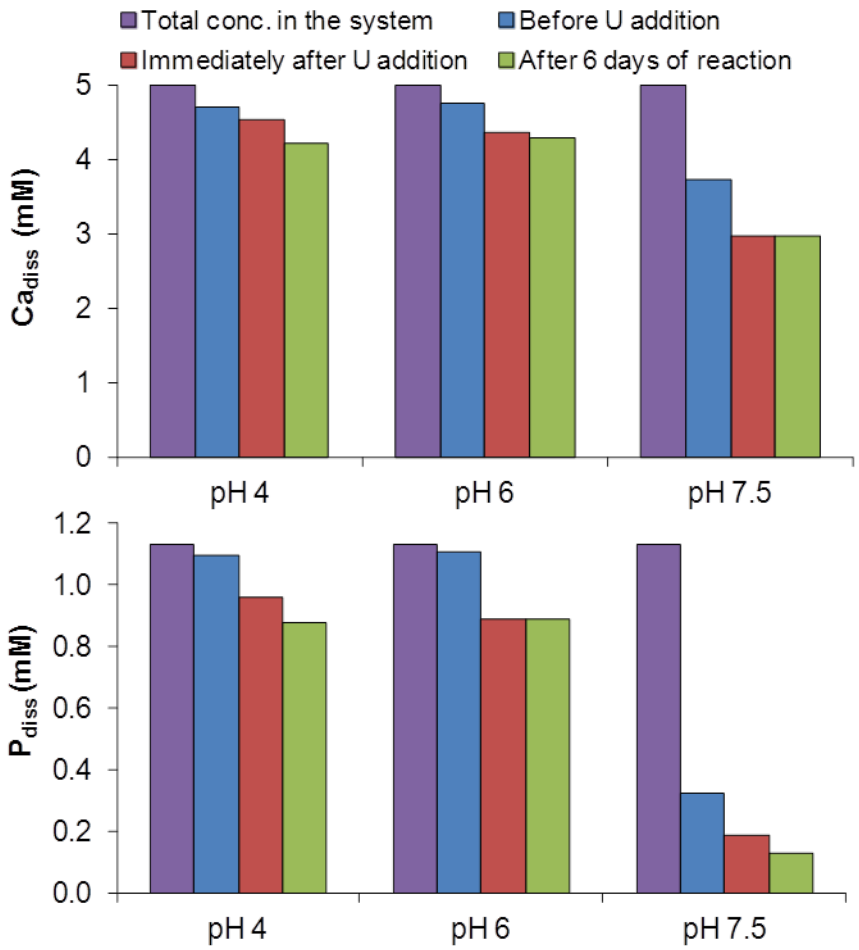

Figure S3.1. Dissolved calcium and phosphate concentrations in response to addition of uranium to the pre-reacted solutions. The bars represent the total concentration added at the start of experiment, concentrations after 4 days of Ca-P reaction (before U addition), concentrations immediately (within 2 minutes) after U addition, and concentrations 6 days after U addition.

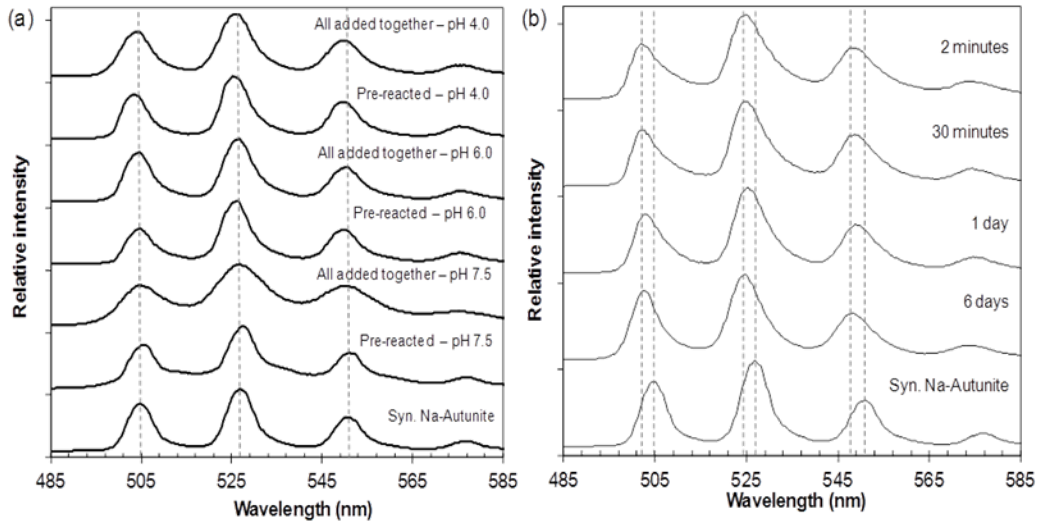

Figure S3.2. LIFS spectra of samples obtained from different experimental conditions. Samples obtained from "all added together" and "pre-reacted" sets of experiment at starting pH conditions of 4, 6 and 7.5 are included in (a). Samples for the Ca-P time series i.e., "pre-formed study" experiment at pH 7.5 condition are included in (b). A spectrum of synthetic sodium autunite is included in both figures as a reference.

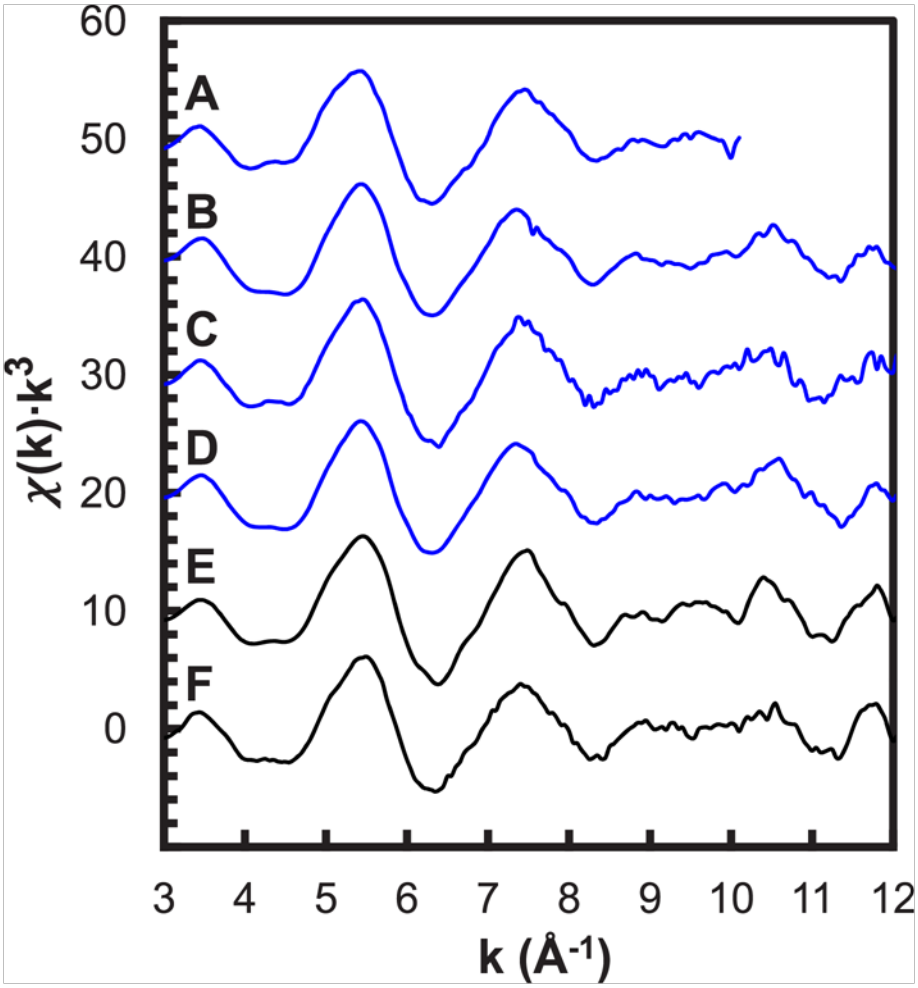

Figure S3.3. U L_{III}-edge EXAFS spectra of the solids formed from (A) the "all added together" study at pH 4, (B) adding U(VI) to pre-reacted calcium and phosphate at pH 4, (C) "all added together" study at pH 6, and (D) adding U(VI) to pre-reacted calcium and phosphate at pH 6. The spectra of two autunite-group minerals, (E) chernikovite and (F) sodium meta-autunite, are shown for comparison. Autunite-group minerals have generally indistinguishable EXAFS spectra (Catalano and Brown Jr. 2004).

Chapter 4 Transport of U(VI) through sediments amended with phosphate to induce *in situ* uranium immobilization

Results of this Chapter are being prepared for a manuscript to be submitted to *Water Research.*

Abstract

Phosphate amendments can be added to U(VI)-contaminated subsurface environments to promote *in situ* remediation. The primary objective of this study was to evaluate the impacts of phosphate addition on the transport of U(VI) through contaminated sediments. In batch experiments using sediments (<2 mm size fraction) from a site in Rifle, Colorado, U(VI) only weakly adsorbed due to the dominance of the aqueous speciation by Ca-U(VI)-carbonate complexes. Column experiments with these sediments were performed with flow rates that correspond to a groundwater velocity of 1.1 m/day. In the absence of phosphate, the sediments took up 1.68 – 1.98 µg U/g of sediments when the synthetic groundwater influent contained 4 µM U(VI). When U(VI)-free influents were then introduced with and without phosphate,

substantially more uranium was retained within the column when phosphate was present in the influent. Sequential extractions of sediments from the columns revealed that uranium was uniformly distributed along the length of the columns and was primarily in forms that could be extracted by ion exchange and contact with a weak acid. Laser induced fluorescence spectroscopy (LIFS) analysis along with sequential extraction results suggest adsorption as the dominant uranium uptake mechanism. The response of dissolved uranium concentrations to stopped-flow events and the comparison of experimental data with simulations from a simple reactive transport model indicated that uranium adsorption to and desorption from the sediments was not always at local equilibrium.

4.1 Introduction

Uranium contamination of soil and groundwater at more than 120 sites across 36 states in the United States has occurred as a result of activities associated with production of nuclear materials (Palmisano and Hazen 2003). The widespread contamination at many sites makes it economically challenging to use pump-and-treat or excavation methods for remediation. An alternative approach is to manipulate the chemical or physical conditions of the subsurface environment to promote *in situ* immobilization of uranium via formation of stable solid forms of uranium (Ahmed et al. 2012, Crane et al. 2011, Sharp et al. 2011). Addition of phosphate amendments to U(VI)-contaminated subsurface environments has been evaluated in laboratory and field studies as a potential *in situ* remediation method

(Arey et al. 1999, Beazley et al. 2011, Fuller et al. 2002, Mehta et al. 2014, Wellman et al. 2008). Phosphate addition can immobilize uranium by inducing the precipitation of low solubility U(VI) phosphate solids (Jensen et al. 1996, Singh et al. 2010). Various U(VI) phosphates have been observed at uranium-contaminated field sites (Arai et al. 2007, Buck et al. 1996, Catalano et al. 2006, Jones et al. 2001, Singer et al. 2009) and are also found in some ore settings without external addition of phosphate (Jerden et al. 2003).

In addition to helping to precipitate U(VI) solids, phosphate can influence U(VI) adsorption to mineral surfaces. Uranium sorption by ferrihydrite and goethite was enhanced in the presence of phosphate at weakly acidic pH because of the strong surface binding of phosphate and subsequent formation of ternary surface complexes (Cheng et al. 2004, Payne et al. 1996, Singh et al. 2012). The presence of reactive mineral surfaces, like those of iron oxides and clays, can potentially limit the precipitation of U(VI) phosphate solids by adsorbing dissolved U(VI) and phosphate to make the solution less saturated with respect to potential precipitates or may facilitate heterogeneous nucleation of precipitates (Singh et al. 2010). Even U(VI) adsorption to calcium phosphate mineral surfaces can decrease the dissolved concentration of U(VI) to prevent U(VI) phosphate precipitation (Fuller et al. 2002).

The primary objective of this study was to determine the impacts of phosphate addition on the transport of U(VI) through columns loaded with sediments from an environmentally relevant field site in Rifle, Colorado. Batch and column experiments were performed using these sediments with solutions that simulated the groundwater composition at the field site. Batch experiments were used to calculate

the equilibrium uranium sorption capacity of Rifle sediments with synthetic groundwater in the absence and presence of added phosphate. Column experiments involved analysis of the influent and effluent solutions, reactive transport modeling, and characterization of the reacted sediments by sequential extractions and fluorescence spectroscopy. Insight into the processes controlling the impact of phosphate on U(VI) transport can help identify conditions that lead to the greatest reductions in U(VI) mobility.

4.2 Materials and Methods

4.2.1 Materials

All chemicals used in this study were ACS grade or better. Stock solutions were prepared in ultrapure water (>18.2 MΩ-cm resistivity). Background sediments (<2 mm size fraction) from a uranium-contaminated site in Rifle, Colorado were used as the porous medium. Detailed characterization of these sediments has been reported previously (Campbell et al. 2012, Komlos et al. 2008), with the background sediment samples having up to 1.7 µg U/g of sediments as determined from nitric acid extraction. XRD analysis of the sediments revealed the presence of quartz (52 %) and plagioclase (23 %) and potassium feldspars (15 %), with lesser amounts of amphibole (2 %), calcite (2 %), and clays. The clay size fraction is dominated by illite and smectite with minor amounts of chlorite and kaolinite. Mössbauer spectroscopy shows that iron is predominantly hosted in silicates and Al-rich

goethite; the iron oxides hematite, magnetite, and ferrihydrite are also present but at lesser abundance.

4.2.2 Batch sorption experiments

The sediments were pre-equilibrated with synthetic Rifle groundwater (SRGW) (Table 4.1) under a 2.7 % CO_2 environment for 2 days under well-mixed conditions at a solids loading of 250 g/L. This step was included to remove any labile background uranium. After pre-equilibration the sediments were separated from the solution and contacted with freshly prepared SRGW, spiked with varying

Table 4.1. Composition of the Synthetic Rifle Ground Water

Analyte	Concentration (mM)
Na	11.00
Ca	5.00
Mg	4.94
K	0.33
U(VI)[a]	$0/4\times10^{-3}$
Li[b]	0.13
DIC[c]	7.44
SO_4	10.78
Cl	3.00
NO_3	0.53
$Si(OH)_4$	0.28
PO_4[a]	0/1.00
Br[b]	0.13
pH	7.10

[a] Concentration of 0 corresponds to experimental conditions without any addition of U(VI) or PO_4^{3-} in the influent feed
[b] Lithium (Li) and bromide (Br) were added as conservative tracers with the influent to aid in the calculation of transport parameters.
[c] DIC stands for dissolved inorganic carbon

concentrations of uranium (0.1 – 100 µM) and phosphate (0 – 1000 µM), and equilibrated for 2 days. Samples were then collected, filtered using 0.22 µm filters, and acidified to 1 % HNO_3 for elemental analysis. SRGW was prepared to simulate the conditions at the field site (Campbell et al. 2011, DOE 1999). For the phosphate-free experiments and the lowest concentrations of U(VI), even after pre-equilibration some of the adsorption experiments resulted in final dissolved U concentrations greater than the initial concentrations. These samples were not included in the linear adsorption isotherm determination.

4.2.3 Column experiments

Column experiments were conducted at room temperature (22±0.5 °C). Sediments were wet-loaded into glass columns (2.5 cm diameter x 15 cm length) and retained using porous plates (20 µm pore size) that also helped to distribute flow evenly to the column cross-section. This method resulted in porosity (θ) of 0.32 – 0.38 as determined from measurements of the sediment mass, total column volume, and volume of water needed to saturate the pore space. Plastic bags that were impermeable to gases (e.g., O_2 and CO_2) were used to store the SRGW, which allowed introduction of solutions with dissolved inorganic carbon concentration and solution pH that mimicked those at the actual site but that would have resulted in CO_2 exsolution to the ambient laboratory atmosphere. The SRGW was introduced into the columns in an upflow mode using a peristaltic pump at a rate (8 mL/h) that

corresponded to a linear velocity of ~1.1 m/d, which was in the range observed at the site (Fang et al. 2009, Moon et al. 2010, Yabusaki et al. 2007).

Experiments were performed in different modes (Figure 4.1) that involved feeding SRGW to the columns with or without uranium and phosphate. A conditioning mode during which SRGW that did not contain uranium and phosphate was included to remove the background labile fraction of uranium from the sediments. Columns were then operated in an uptake mode until with 4 µM U(VI) in the influent until uranium breakthrough occurred. Finally a release mode was performed with uranium-free influents both with and without added phosphate. Bromide was included as a conservative tracer for calculating hydrodynamic

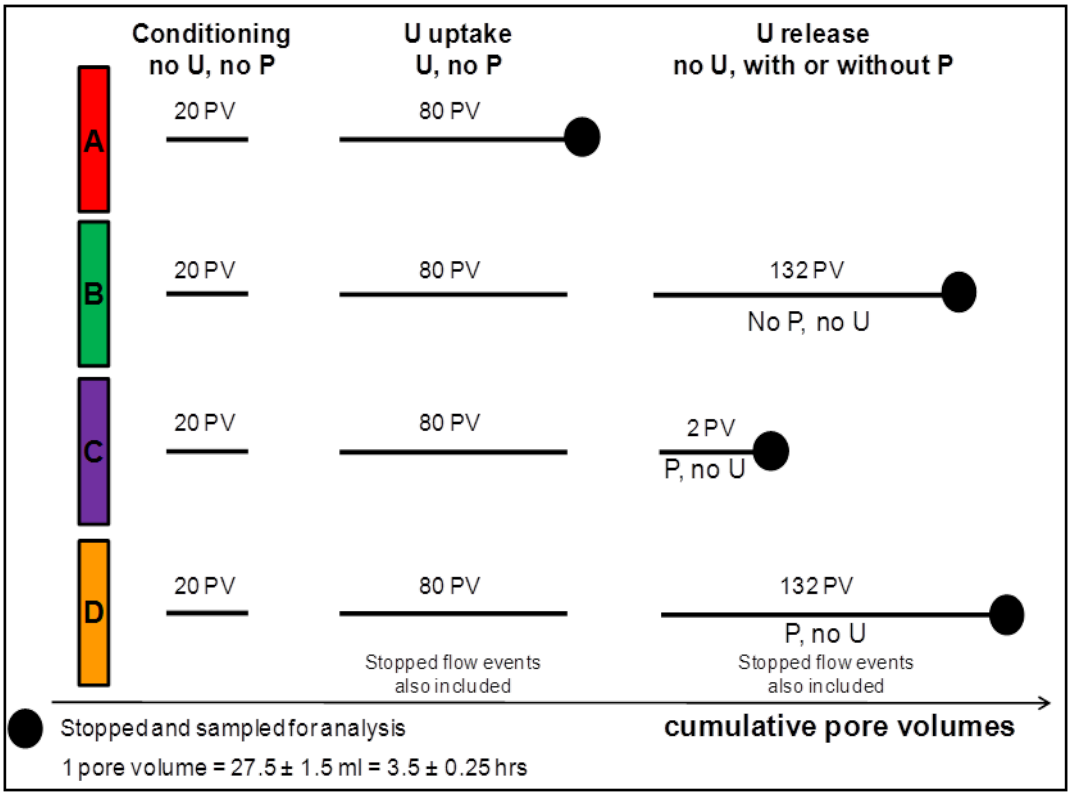

Figure 4.1. Experimental modes of operation to study the transport of U(VI) through sediments amended with phosphate to induce *in situ* uranium immobilization.

transport parameters. A stopped flow technique described by Brusseau et al. (1997) was used to observe the effects of non-equilibrium processes on uranium uptake and release. Column experiments were terminated at different times, and sediment samples were collected in increments from various depths (roughly 5 cm each) to study the speciation and spatial distribution of uranium along the length of the column. The current study represents a scenario of a site with a relatively stable plume of uranium-contaminated groundwater into which phosphate solution is introduced.

Thermodynamic calculations using the latest critically reviewed database for uranium and relevant reactions (Mehta et al. 2014) determined that the SRGW solution was undersaturated with respect to any uranium solid phase. In the absence of phosphate, the solution was slightly supersaturated (SI = 0.33) with respect to calcite. In the presence of phosphate, the solution was supersaturated with calcium phosphates that included hydroxylapatite and octacalcium phosphate; however, no precipitates were visibly present in the influent reservoirs and influent samples indicated no loss of calcium or phosphate from the influent solution.

4.2.4 Chemical analysis of influent and effluent

Samples (influent and effluent) were regularly collected, analyzed for pH and bromide concentration, saved for dissolved inorganic carbon (DIC) analysis, and preserved for elemental analysis by acidifying to 1% HNO_3. Dissolved concentrations of U, P, Ca, Na, Mg, K and Si were measured using inductively

coupled plasma-mass spectrometry (ICP-MS, Perkin Elmer Elan DRC II). The ICP-MS detection limit was 0.1 µg/L for uranium, 10 µg/L for phosphorus, and 50 µg/L for other measured elements. DIC was measured using a TOC analyzer (Shimadzu, TOC-$L_{CPH/CPN}$ PC-controlled model). Bromide was measured with an ion selective electrode (Cole-Parmer).

4.2.5 Calculation of transport parameters

Bromide and uranium breakthrough and washout curves were used to calculate various transport parameters using the CXTFIT-Excel tool (Tang et al. 2009) originally based on the FORTRAN version (Parker and Van Genuchten 1984) and modified by Toride et al. (1995) to include the convection dispersion equation (CDE) solving capabilities. Equation 1 represents the generic form of the CDE assuming one-dimensional steady flow in a homogenous, isotropic porous medium.

$$R\frac{\partial C}{\partial t} = D_L\frac{\partial^2 C}{\partial x^2} - v\frac{\partial C}{\partial x} + r \quad (1)$$

where C = concentration in liquid phase [mol/m^3], t = time [s], D_L = longitudinal hydrodynamic dispersion coefficient [m^2/s], x = distance [m], v = average linear velocity [m/s], and r indicates a the rate of a biological or chemical reaction (production/sink) [mol/m^3-s] of the solute other than sorption. R is the retardation factor, which is related to the partition coefficient (K_d) [m^3/kg] as shown in equation 2.

$$R = 1 + \frac{\rho_b K_d}{\theta} \quad (2)$$

where, ρ_b is the bulk density (kg/m^3) and θ is the porosity. As determined from the known column volume and the measured masses of the sediments and the water-saturated column, values of ρ_b ranged from 1740 to 1810 kg/m^3 and values of θ varied from 0.32 – 0.38 for different columns.

Equations 3 and 4 represent the dimensionless non-equilibrium CDE. The model is based on the assumption that the aqueous phase can be partitioned into mobile and immobile regions.

$$\beta R \frac{\partial C_m}{\partial T} = \frac{1}{Pe} \frac{\partial^2 C_m}{\partial X^2} - \frac{\partial C_m}{\partial X} - \omega(C_m - C_{im}) \quad (3)$$

$$(1-\beta) R \frac{\partial C_{im}}{\partial T} = \omega(C_m - C_{im}) \quad (4)$$

where T = νt/L and X = x/L are dimensionless representations of time and distance along the column, and subscripts m and im indicate the mobile and immobilize zones respectively.

Fitting of the model to experimental data was used to calculate the dimensionless parameters ω and β in equations 3 and 4. These parameters from the non-equilibrium CDE are then further based on properties of the columns and the processes indicated in equations 5 and 6.

$$\omega = \frac{\alpha L}{\theta \nu} \quad (5)$$

$$\beta = \frac{\theta_m + f \rho_b K_d}{\theta + \rho_b K_d} \quad (6)$$

where α is the first-order mass transfer coefficient (s^{-1}) governing the rate of solute exchange between the mobile and immobile liquid regions and f is the fraction of adsorption sites that equilibrates with the mobile liquid phase.

As would be expected for a non-reactive solute, bromide transport was not retarded through the column and its R value was set to 1. Effluent bromide and uranium data were simultaneously fit to determine the Peclet number (Pe), mobile water fraction (β), mass transfer coefficient (ω) and uranium retardation factor (R). The dispersivity (λ in cm) was determined using the Peclet number and length (L) of the column (Equation 7).

$$P_e = \frac{L}{\lambda} = \frac{L\,v}{D_L} \quad (7)$$

The retardation coefficient obtained through fitting was used to calculate the value of the partition coefficient K_d.

4.2.6 Sequential extractions

Sediments were collected in roughly three equal sections along the length of the column at the end of each experiment and classified as those from the inlet,

Table 4.2. Steps in the sequential extraction method.

Step	Target phase	Extractant composition	pH	Procedure
1	Water soluble	Ultrapure water	5.5	Shake suspension 16 h.
2	Ion exchangeable	1 M ammonium acetate	7.0	Shake suspension 16 h. Rinse with ultrapure water.
3	Acid soluble/Carbonate	1 M acetic acid	5.0[a]	Shake suspension 16 h. Rinse with ultrapure water.
4	Residual solids	8 mL HNO_3 acid + 2 mL HCl acid + 40 mL DI water	--	Digest in heated block held at 100°C for 4 h.

[a] Sodium hydroxide was added to acetic acid solution to raise the pH levels to 5.0.

midsection, and outlet. Extractions were performed in duplicate for all the column samples. A four step sequential extraction method (Table 4.2) modified from Tessier et al. (1979) with a solid to solution ratio of 40 g/L (34 g dry weight/L based on moisture content measurements) in 50-mL reactors was used to evaluate the solid phase speciation and spatial distribution of uranium. A single step total digestion using a mixture of nitric acid and hydrochloric acid at 100° C for 4 h was also performed to more directly measure the total uranium content for comparison with the total content determined from the sum of the uranium amounts from the four steps of the sequential extraction.

4.2.7 Laser induced fluorescence spectroscopy (LIFS) analysis

Sediment samples from different depths within a column were loaded into 2 mm × 4 mm x 25 mm quartz cuvettes for analysis. Instrumentation and experimental procedures for LIFS analysis have been described previously (Wang et al. 2005, Wang et al. 2004). The quartz cuvettes were attached to the cold finger of a CRYO Industries RC152 cryostat with liquid helium vaporizing beneath the sample to reach a sample temperature of 8 ± 2 K. The samples were excited with a Spectra-Physics Nd:YAG laser-pumped Lasertechnik-GWU MOPO laser at 415 nm, and the emitted light was collected at 85° to the excitation beam and detected with a thermoelectrically cooled Princeton Instruments PIMAX intensified CCD camera after spectral dispersion through an Acton SpectroPro 300i double monochromator

spectrograph. The spectra were analyzed using the commercial software IGOR (Wavematrix, Inc).

4.3 Results and Discussion

4.3.1 Batch sorption experiments

Increasing phosphate concentrations (0 – 1000 µM) resulted in increased uranium uptake for starting uranium concentrations of 0.1 – 100 µM (Figure 4.2). For a linear adsorption isotherm, K_d values of 0.4, 0.6 and 2.2 mL/g are calculated for 0, 100 and 1000 µM phosphate concentrations, respectively. Increased uranium uptake caused by phosphate could be due to the formation of inner-sphere U(VI)-

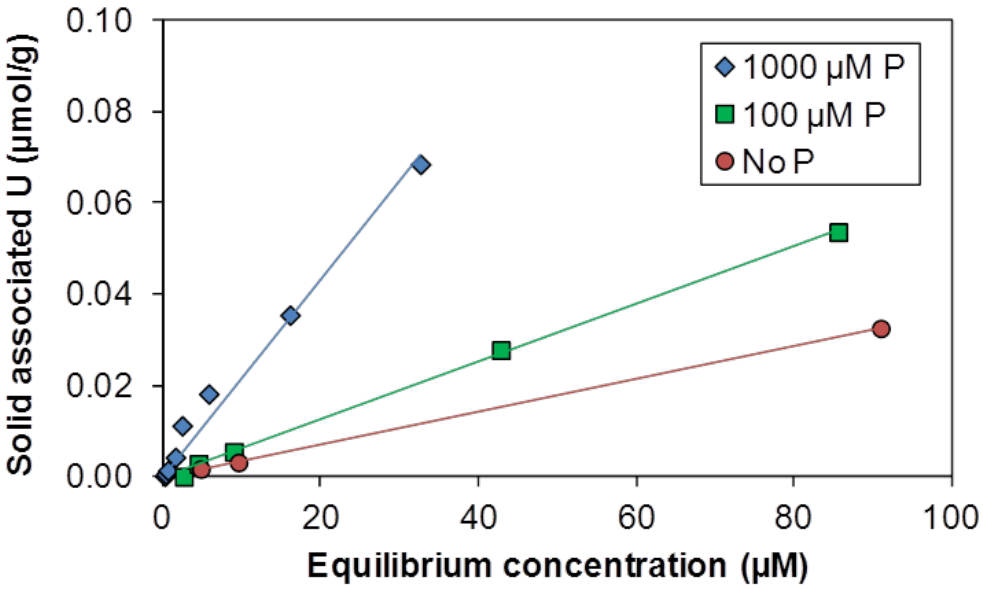

Figure 4.2. Equilibrium uranium sorption on Rifle sediments (250 g/L) after 2 days of reaction with SRGW for three phosphate concentrations. Trendline(s) included for different starting phosphate concentrations were used to determine K_d values of 0.4, 0.6 and 2.2 mL/g for 0, 100, and 1000 µM P respectively. Only data points for which uranium uptake can be unambiguously assigned to adsorption have been included.

phosphate ternary surface complexes that have previously been observed in the presence of phosphate and various iron-oxides (Bostick et al. 2002, Cheng et al. 2004, Payne et al. 1996, Singh et al. 2010). Uranium adsorption onto Rifle sediments could occur through cation exchange to interlayer sites in clays and inner-sphere binding to iron oxide surfaces or to edge sites on clays like montmorillonite. Surface complexes could include binary surface complexes as well as ternary surface complexes with phosphate as noted above as well as ternary surface complexes with carbonate (Bargar et al. 1999, Bernhard et al. 2001, Sherman et al. 2008). Both iron oxides and clays are present in this sediment (Campbell et al. 2012, Komlos et al. 2008).

Previous batch studies on uranium sorption in the absence of phosphate using background sediments from the Rifle site have measured K_d values up to 1.25 mL/g at pH 7.2 and 2.6 % CO_2 conditions (Hyun et al. 2009); the present study had pH 7.1 and ~ 2.7 % CO_2. Adsorption of U(VI) by the Naturita aquifer sediments (another former uranium milling site in Colorado) had K_d values of ~ 3 mL/g at 1.6 % CO_2 (Davis et al. 2004). The lower K_d values under phosphate-free conditions observed in the present study may be due to slight differences in the chemical compositions of the solutions. Several studies have found K_d values to be very sensitive to CO_2 conditions (Hyun et al. 2009, Kohler et al. 1996, Reardon 1981). The higher calcium concentration (5 mM) in this study as compared to the 3 mM in Hyun et al. (2009) could also have inhibited sorption. Higher calcium concentrations decrease U(VI) adsorption due to formation of stable aqueous Ca-UO_2-CO_3 ternary

complexes (Bernhard et al. 1998, Bernhard et al. 2001, Dong and Brooks 2006, Stewart et al. 2010).

The K_d values determined in the present study and previous work for the Rifle site are overall much lower than those determined for sediments from other sites. K_d values of 14 – 22 mL/g, 51 – 95 mL/g and 40 – 30000 mL/g have been determined for sediments from the Hanford site in Washington (Qafoku et al. 2005), Oak Ridge site in Tennessee (Stewart et al. 2010) and F-area Savannah River site in South Carolina (Dong et al. 2011), respectively. Differences in sediment mineralogy and groundwater composition may explain the different adsorption affinities found at various sites.

4.3.2 Uranium uptake and release in the absence of phosphate

4.3.2.1 Aqueous phase analysis

The conditioning mode flushed an appreciable amount (0.2 μg/g) of labile uranium from the initial sediments (Figure 4.3). During the uptake mode similar bromide breakthrough profiles were observed for all columns. As a conservative tracer, bromide concentrations increased rapidly to reach the influent level within 4 pore volumes (PV) as compared to ~ 35 PV required for uranium to achieve complete breakthrough (Figure 4.3). Calculations based on a simple mass balance approach (equation 8) that accounts for the difference in influent and effluent concentrations determined uranium uptake of up to 1.98±0.14 μg/g of sediments (Table 4.3).

$$U_{mass}\ uptaken\ \left(\frac{\mu g}{g}\right) = \frac{\sum[(C_{in} - C_{out}) * Q * t]}{m_{sed}} \quad (8)$$

where C_{in} and C_{out} are the measured uranium concentrations (μg/L), Q is the flow rate (L/h), t is the total time of flow at a given concentration (h), and m_{sed} is the mass of sediments in the column (g).

Uranium release was initiated following the uptake mode by introducing uranium-free SRGW both without (Column B) and with (Columns C and D) phosphate. In the absence of phosphate, all of the uranium that had been taken up during loading was desorbed from the sediments within 100 PV.

Table 4.3. Uranium concentrations in the sediments calculated using mass balance approach.

Mass of U (μg/g)	Col. A	Col. B	Col. C	Col. D
Released during conditioning phase	0.21±0.02	0.20±0.01	0.21±0.01	0.18±0.01
Adsorbed during uptake phase	1.90±0.13	1.68±0.12	1.69±0.12	1.98±0.14
Desorbed during release phase	--	1.95±0.14	--	0.47±0.03
Retained or Accumulated	--	-0.27±0.18*	--	1.51±0.14

* The number (negative concentration) is statistically not significantly different from zero.

The stopped flow events revealed noticeable non-equilibrium sorption behavior for all columns. For these events during the uptake mode, the uranium concentrations were lower when flow was resumed than immediately before it was stopped, which indicates that during stopped flow the uranium was taken up by

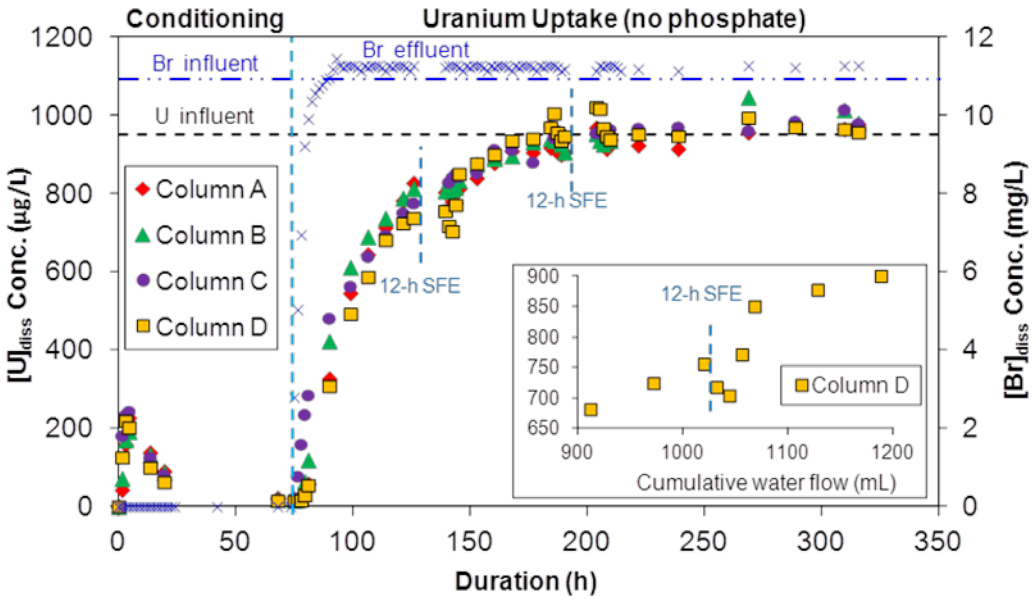

Figure 4.3. Uranium and bromide breakthrough profiles (uptake phase) for columns A-D following the conditioning phase of the experiments. Two 12-hour stopped flow events (SFE) are also included. Representative bromide data for Column A are shown with open cross symbols, and closed symbols represent uranium data for columns A-D (1 pore volume (PV) = 3.50±0.25 h). The inset provides a closer view of a stopped flow event for Column D.

processes that could not reach local equilibrium with flowing water. Uranium release was also influenced by the stopped flow event wherein the uranium concentrations increased when there was no flow. A similar phenomenon was observed for Hanford sediments in column experiments (Qafoku et al. 2005) in which the magnitude of change in concentrations was proportional to the duration of stopped flow. For 24-h stopped flow events with Hanford sediments, the U(VI) concentrations decreased by < 10 % during the adsorption phase. In the current study with only 12 h stopped flow events, the U(VI) concentrations decreased by ~ 10 % during the adsorption phase.

Non-equilibrium uranium adsorption could occur due to chemical (different adsorption kinetics) and/or physical (intraparticle diffusion) processes. Since the adsorption of U(VI) to mineral surfaces is generally fast, typically attaining

equilibrium within few minutes (Giammar and Hering 2001, Hsi and Langmuir 1985), the non-equilibrium U(VI) adsorption behavior is believed to result from physical mass transfer processes. For example, physical non-equilibrium models have been used previously to successfully simulate uranium transport in column and field-scale studies (Fox et al. 2012, Greskowiak et al. 2011, Qafoku et al. 2009). The non-equilibrium behavior of uranium in this study has thus been attributed to the intragrain diffusional mass transfer limitations existing within local micro-environments.

4.3.2.2 Simulating the reactive transport of uranium

Adsorption and release profiles for both uranium and bromide were fitted simultaneously for column B (Figure 4.4(a)), and only the adsorption profiles for uranium were fitted for columns A, C and D (Figure 4.4(b)). The desorption profiles for column C and D were not fitted because CXTFIT can only be used to fit adsorption-desorption modes with the same composition. It was likely that in the presence of phosphate, reactions other than adsorption-desorption of uranium were also occuring, and CXTFIT can only account for processes like adsorption that can be interpreted using a simple partition constant. To be consistent with the stopped flow event observations, which indicated that local equilibrium was not achieved for the mobile fluid residence times of the experiments, a non-equilibrium CDE model using a single set of parameters was used to simulate uranium transport. Values of 4.62 for Pe, 0.55 for β, and 0.98 for ω provided the optimal fits to the data (Figure

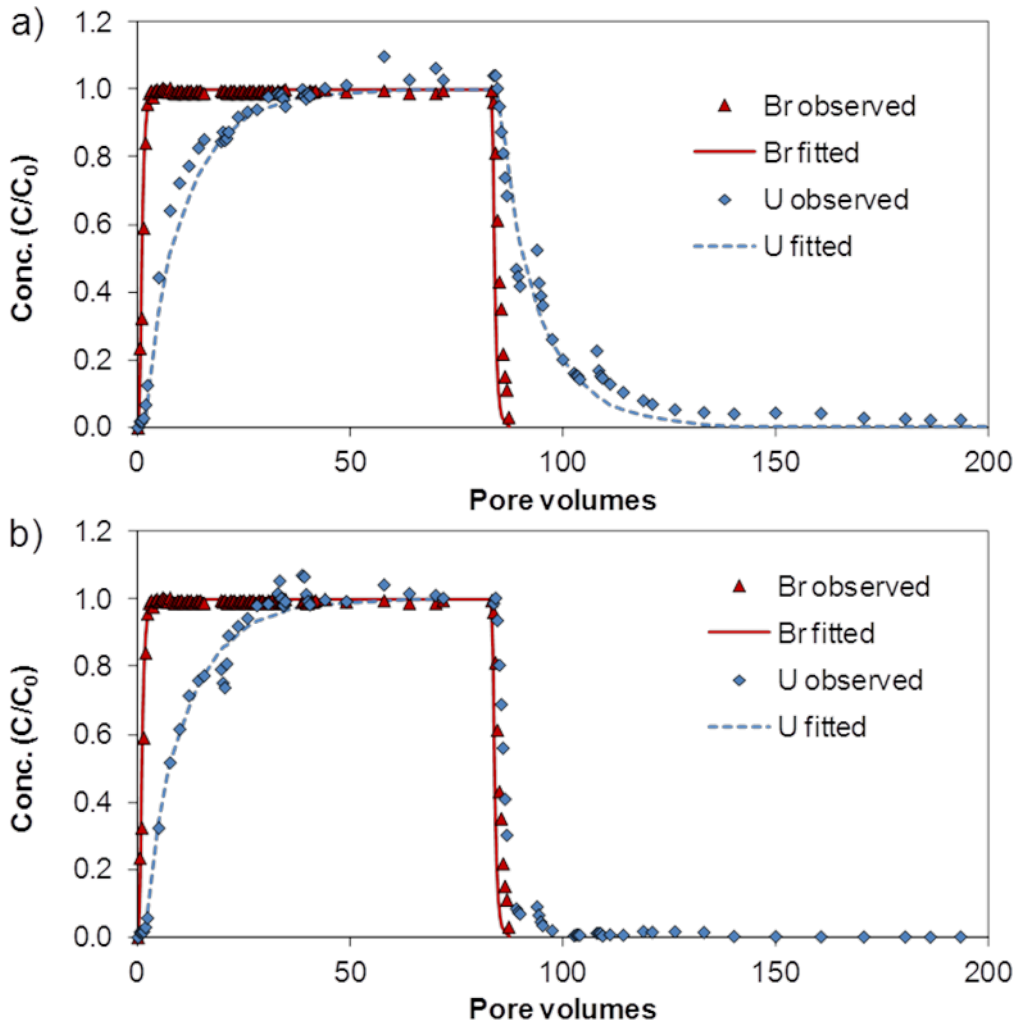

Figure 4.4. Uranium and bromide profiles during both uptake and release phase (observed and fitted using non-equilibrium CDE) for Column B (a) and Column D (b). The release phase of Column D (with phosphate) was not included for uranium fitting because reactions other than adsorption-desorption were likely occurring. Symbols represent the normalized concentrations for bromide and uranium as a function of flow in pore volumes. Dashed and solid lines represent fitted profiles for uranium and bromide respectively.

4.4). These values yielded an f value of 0.50, λ of 3.25 cm and α ranging from 2.6×10^{-5} – 3.1×10^{-5} s^{-1}. The Peclet number is consistent with longitudinal transport being primarily controlled by advection. The value of f indicates that the pore water is evenly distributed (i.e. 50% / 50%) between mobile and immobile phases. The α values are sufficiently large that even with 50% of the surface sites contained in

immobile water the transfer of solutes from the mobile to immobile regions still allows considerable adsorption to intragranular sites to occur during flow. Values ranging from 0.19 – 2.99 and 0.37 – 0.60 have been reported for ω and β, respectively, from similar fitting of column experiments with clayey soils and investigation of tritiated water (^3H_2O) and boron (B) transport (Tang et al. 2009). The fitting exercise involved estimation of multiple parameters (Pe, β, R and ω) simultaneously to yield the optimal fit of the model to the data; however, other combinations of parameters may also be able to provide reasonable fits. So, the exact parameters determined are used primarily to illustrate that non-equilibrium processes are important for U(VI) transport in these sediments.

A retardation factor (R) of 10.85 was obtained through the fitting of uranium profiles which resulted in K_d values in the range of 1.90 – 2.03 mL/g using equation (2) based on linear isotherm assumptions. The range of K_d values obtained is similar to those previously determined for background sediments from Rifle area [up to 1.25 mL/g] (Hyun et al. 2009) and sediments from another former Uranium milling site in Colorado [~ 3 mL/g] (Davis et al. 2004); however, they are somewhat higher than the K_d of 0.4 mL/g determined from the present study's batch experiments. R values of 87 – 127 were obtained by fitting uranium profiles in Hanford column experiments (Qafoku et al. 2005).

4.3.2.3 Sequential extractions

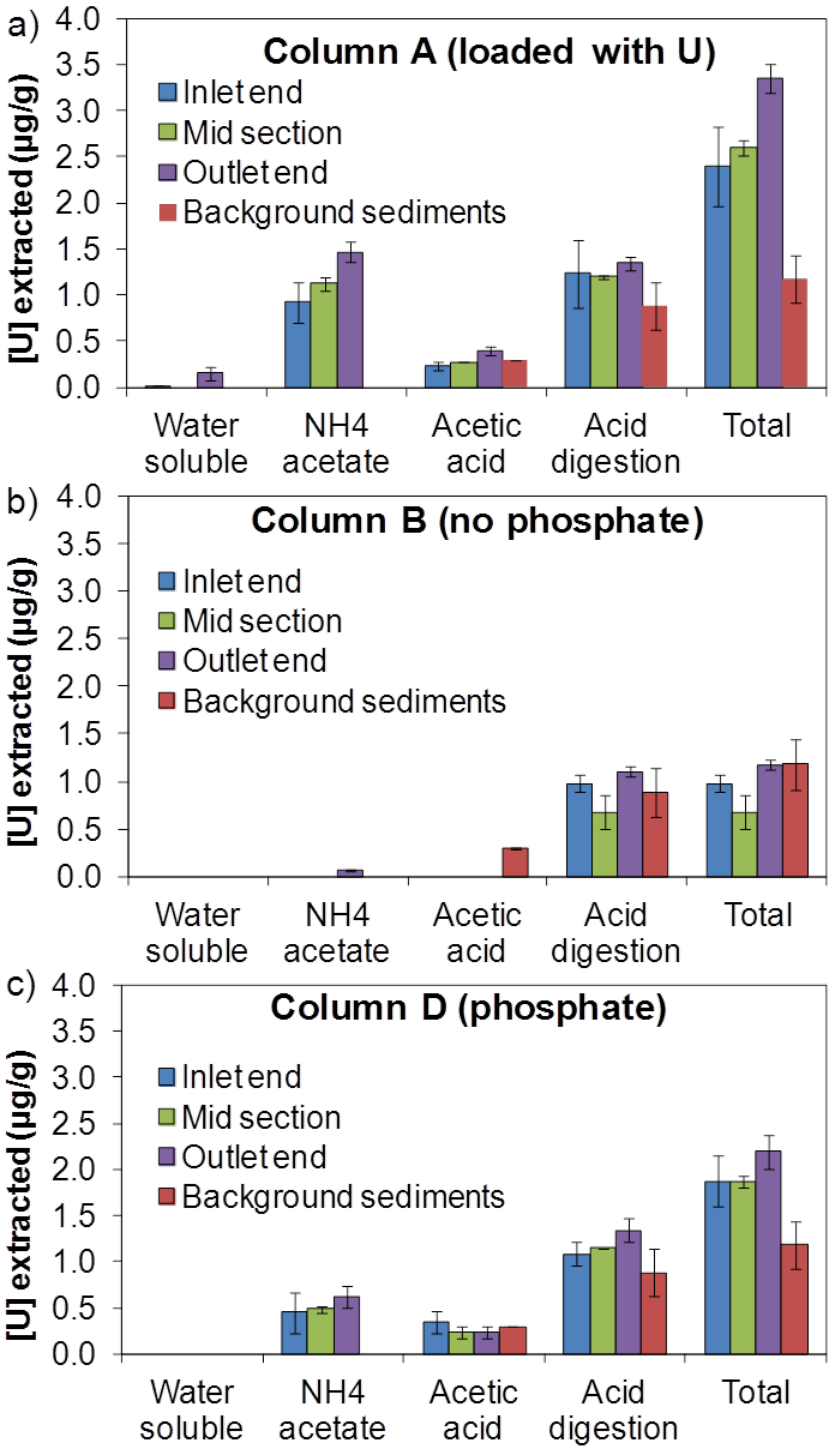

Figure 4.5. Sequential extraction results for uranium extracted from three depth increments of Columns A, B and D. Results of background sediments are shown for reference. Error bars represent standard error for the data obtained from duplicate samples.

Sequential extractions provided important information about the amounts and speciation of uranium in the sediments. Uptake amounts calculated for column A using the influent-effluent mass balance approach (1.9 μg/g) were very similar to those obtained through sequential extractions (2.1 μg/g). Similarly, the uptake amounts calculated for columns B and D using two different methods were within 30 % of each other. Negligible amounts were extracted in the water soluble step. The dominant fractions of labile uranium were extracted in the step targeting ion exchangeable species and then in the weak acid extraction step (Figure 4.5(a)). Up to 1.5 μg/g of U was retrieved in the hot acid digestion step from the sediments both before and after loading of U in the columns. This amount of uranium is consistent with recalcitrant solid forms of uranium in the original Rifle sediments (Campbell et al. 2012) and was not included in the estimates of the amount of uranium taken up during the loading portion of the experiment. The amount of uranium in the background sediments shown in Figure 4.5 is for sediments that had undergone conditioning with SRGW that removed some labile U.

4.3.3 Uranium release in the presence of phosphate

4.3.3.1 Aqueous phase analysis

Uranium concentrations decreased faster for the phosphate-treated columns (Columns C and D) than for the column (Column B) that was not treated with phosphate (Figure 4.6). Although this observation might initially suggest that phosphate's presence resulted in faster uranium desorption, the influent-effluent

mass balance for the column indicated that more than 75 % of the adsorbed uranium (1.51 µg/g) was retained over 100 PV of operation when phosphate was present (Column D) in the influent (Table 4.3). The more rapid decrease to low concentrations when phosphate was present was caused by enhanced retention of uranium by the sediments.

4.3.3.2 Sequential extractions

Sequential extraction results confirmed the observations regarding phosphate's effect on uranium retention. For sediments for which uranium was released after 132 PV of uranium and phosphate-free SRGW was flushed through the

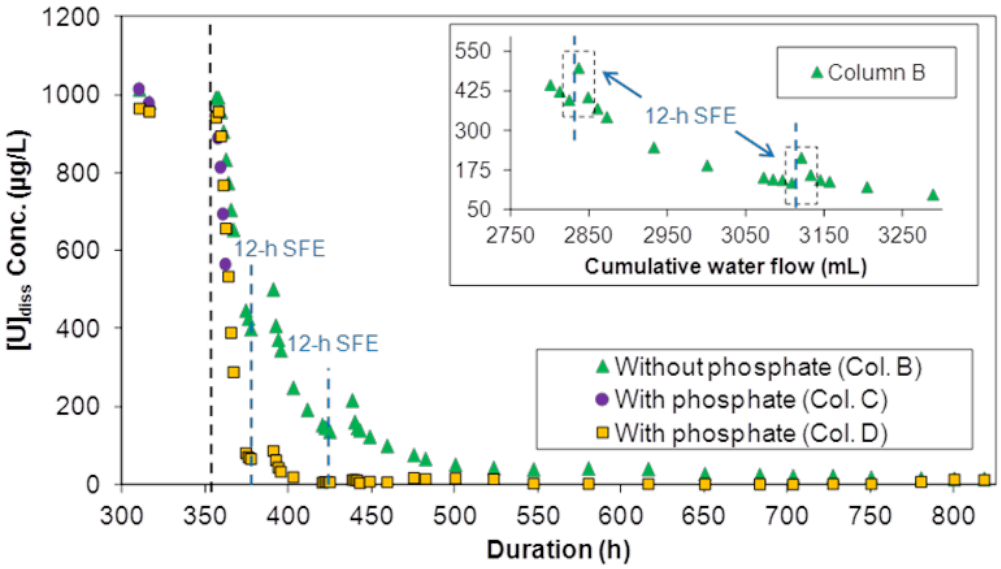

Figure 4.6. Uranium release profiles from Columns B-D following the end of the uptake mode. SRGW with (Columns C-D) or without (Column B) phosphate was started at ~ 353 hours (vertical black dashed line). Stopped flow events (SFE) of 12 hours are also shown. Column C was stopped and sampled after 2 PVs of phosphate-treatment (7.5 h). Closed symbols represent uranium data from different columns (1 PV = 3.5±0.25 h). The inset shows the stopped flow events for Column B.

column (i.e. Column B, following the completion of the release mode), almost no uranium was detectable in the first three extraction steps (Figure 4.5(b)). In contrast, when phosphate was added to the uranium-free influent during the release mode, uranium retained was detectable and primarily in forms that could be mobilized by ammonium acetate and acetic acid (Figure 4.5(c)). The extractions were carried out at pH 7 (ammonium acetate) and pH 5 (acetic acid) and it is likely that not all adsorbed uranium was desorbed or that not all precipitated uranium solids dissolved. Enhanced retention caused by phosphate was probably due to adsorption or precipitation. Uniform distribution of uranium along the length of the column suggests that adsorption was the dominant uranium uptake mechanism. If uranium uptake had occurred through precipitation, then more uranium would have been expected near the inlet where maximum supersaturation would have occurred as the phosphate-containing influent first contacted the uranium-loaded sediments.

4.3.4 LIFS determination of likely U(VI) species present

Fluorescence spectra of samples from Column A showed very little or no discernible fluorescence spectral intensity (Figure 4.7). This behavior could be attributed to multiple reasons. First, a weak broad spectral background could result from surface complexes (Wang et al. 2005). Second, iron oxides in the sediments (Campbell et al. 2012, Komlos et al. 2008) could quench fluorescence at room temperatures and result in poorly resolved spectra (Wang et al. 2011). Finally, multiple quenching mechanisms are exhibited by the uranyl ion that could lead to

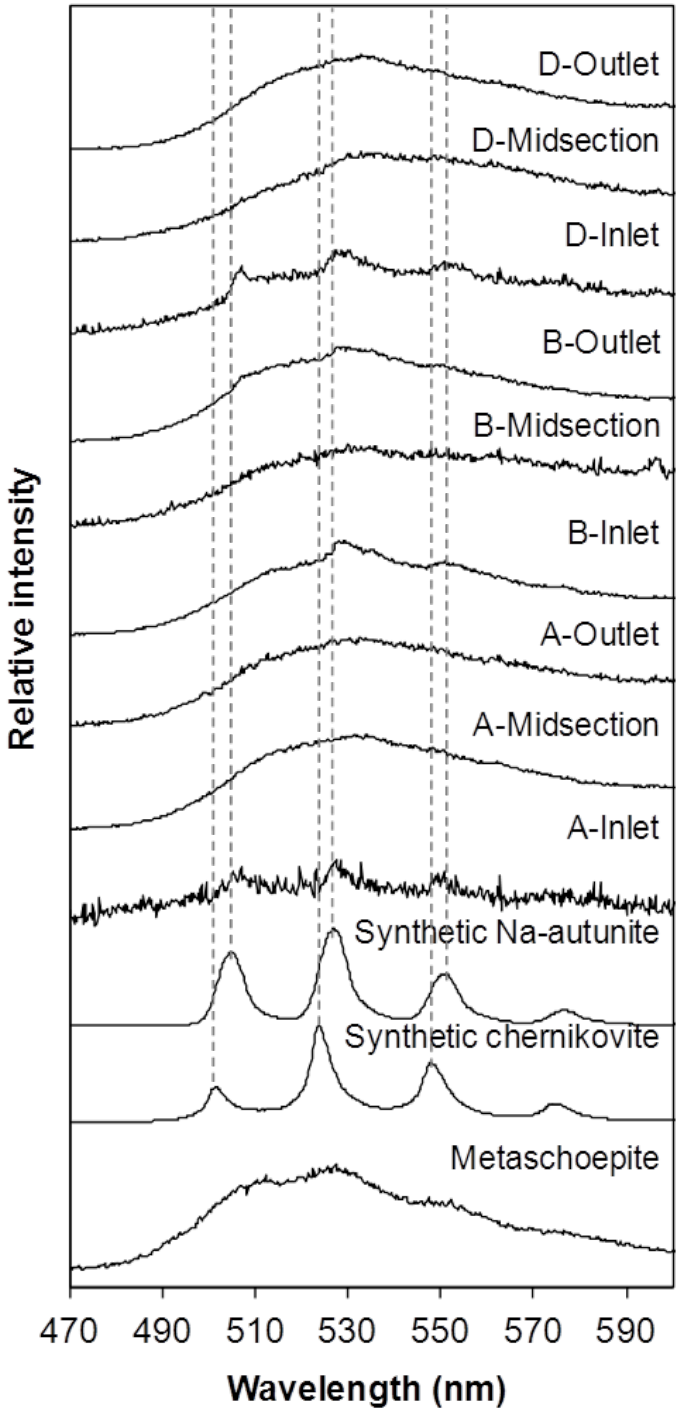

Figure 4.7. Fluorescence spectra of samples obtained from different depths within the columns. Inlet, midsection, and outlet represent samples obtained from different portions of the columns. Spectra of metaschoepite, chernikovite and sodium autunite reference materials are included for comparison.

spectral broadening at room temperatures (Wang et al. 2005). However, analyzing the samples at lower temperatures did not improve spectral intensities or resolution thereby suggesting that fluorescence quenching was likely the result of the presence of surface complexes.

Fluorescence spectra for samples from Columns B and D had similar features (weak, broad spectral background) to those for the samples from Column A. However, an additional weak feature was observed for the sample obtained from the inlet end of column D, one of the columns amended with phosphate (Figure 4.7). This additional feature does not match any of the peaks observed for uranyl phosphate solids and thus suggests the presence of a different uranyl species in addition to the surface complexes seen in samples from Column A. Addition of phosphate might have resulted in formation of ternary uranyl phosphate complexes that led to improved retention within the columns during the release phase or the precipitation of calcium-phosphate solid onto which uranium was then bound. These results imply that uranium immobilization occurred via adsorption. If the dominant mechanism had been precipitation, then uranium distribution within the column should have been uneven or sediments should have had distinct fluorescence spectral characteristics.

4.4 Conclusion

Aqueous phase and solid phase measurements demonstrate the enhanced retention of uranium caused by phosphate addition to sediments. Sequential

extractions revealed that uranium was distributed uniformly within the columns. Higher retention in the presence of phosphate could be due to enhanced adsorption of uranium through the formation of ternary surface complexes. Batch sorption experiments confirmed that the K_d for uranium adsorption increases by up to a factor of 6 upon phosphate addition. Stopped flow events performed during the column experiments confirmed that non-equilibrium processes were involved in controlling the U(VI) transport during the adsorption and desorption modes. The non-equilibrium behavior is believed to result from physical mass transfer processes and is attributed to intragrain diffusional mass transfer limitations existing within local micro-environments.

A one-dimensional non-equilibrium CDE model was used to fit uranium and bromide profiles and calculate the transport parameters. Fitting of the uranium and bromide profiles yielded a retardation factor of 10.85 for uranium. Based on this retardation factor value, a distribution coefficient (K_d) was calculated that suggests that the Rifle sediments are relatively weak adsorbents for uranium. The uranium adsorption capacity of sediments can be a function of water chemistry. For SRGW, in the presence or absence of phosphate, the U(VI) predominantly exist as $Ca_2UO_2(CO_3)_3$ (~ 87 %) followed by $CaUO_2(CO_3)_3^{2-}$ (~ 13 %). Hence, the extent of immobilization at the Rifle site is likely limited due to the high carbonate concentration. At low carbonate concentrations and at pH conditions ranging from slightly acidic to mildly alkaline, phosphate amendments may be more effective for *in situ* uranium immobilization than that would be at the Rifle site.

The current study represents a scenario of phosphate addition to a site with most of the uranium hosted within the sediments. The results from the examined scenario clearly suggest that, under such circumstances, only modest uranium retention would be attained. An alternative scenario to study is treatment of a uranium-contaminated site using phosphate addition to uranium-rich solutions upgradient of the target treatment zone at rates that would not significantly alter the natural groundwater flow.

Acknowledgements

We are grateful to the McDonnell International Scholars Academy at Washington University for providing the Ameren corporate fellowship for Vrajesh Mehta. This work was supported by the U.S. Department of Energy (DOE) Subsurface Biogeochemical Research program (Award No. DE-SC0006857). ICP-MS analysis was performed at the Nano Research Facility (NRF), a member of the National Nanotechnology Infrastructure Network (NNIN), which was supported by the National Science Foundation under Grant No. ECS-0335765. LIFS measurements were performed at the Environmental Molecular Sciences Laboratory (EMSL), a national scientific user facility sponsored by the DOE Office of Biological and Environmental Research and located at the Pacific Northwest National Laboratory. PNNL is operated for DOE by Battelle Memorial Institute under Contract # DE-AC06-76RLO-1830. Sediments were kindly provided by Ken Williams, Phil Long and the Rifle Integrated Field Research Challenge team.

Chapter 5. Uranium immobilization and remobilization in Rifle sediments in response to phosphate treatment

5.1 Introduction

Phosphate amendment to U(VI)-contaminated subsurface environments has been successfully evaluated in laboratory and field studies as a potential *in situ* remediation method (Arey et al. 1999, Beazley et al. 2011, Fuller et al. 2002, Mehta et al. 2014, Wellman et al. 2008). Phosphate addition resulted in enhanced retardation of U(VI) transport through columns loaded with Rifle field sediments as discussed in Chapter 4. The column experiments in Chapter 4 represented a scenario of phosphate addition to a site with most of the uranium initially hosted within the sediments and not present in the advecting groundwater. An additional scenario that needed to be evaluated was treatment of a uranium-contaminated site using phosphate addition to uranium-rich solutions upgradient of the site. Such a scenario is the focus of this chapter. The objective of the experiments presented here was to determine the effects of concurrent phosphate and uranium addition to sediments on

the extent and products of uranium immobilization. The experiments tested the hypothesis that phosphate addition would result in formation of sparingly soluble uranyl phosphate solids within the sediments.

5.2 Materials and Methods

5.2.1 Materials

All chemicals used in this study were ACS grade or better. Stock solutions were prepared in ultrapure water (> 18.2 MΩ-cm resistivity). Sediments, from the same batch as those used for the experiments in Chapter 4 (< 2 mm size fraction from a site in Rifle, Colorado) were used as the porous medium. Detailed characterization of these sediments has been reported previously where background sediment samples had up to 1.7 µg U/g of sediments as determined by nitric acid extraction (Campbell et al. 2012, Komlos et al. 2008). XRD analysis of the sediments revealed the presence of quartz (52 %) and plagioclase (23 %) and potassium feldspars (15 %), with lesser amounts of amphibole (2 %), calcite (2 %), and clays. The clay size fraction is dominated by illite and smectite with minor amounts of chlorite and kaolinite. Mössbauer spectroscopy shows that iron is predominantly hosted in silicates and Al-rich goethite; the iron oxides hematite, magnetite, and ferrihydrite are also present but at lesser abundance.

5.2.2 Methods

5.2.2.1 Column experiments

The experimental approach and setup of the column experiments used in this study are shown in Figures 5.1 and 5.2. Sediments were loaded into glass columns using the same protocol as described in Chapter 4 and resulted in porosity (θ) of 0.32 – 0.35. Porosity was calculated based on measured values of the mass of sediments added to the column, total volume of column, and the volume of water added to saturate the column. The experiments were conducted at room temperature (22±0.5 °C).

Table 5.1. Composition of the Synthetic Rifle Ground Water

Analyte	**Concentration (mM)**
Na	11.00/12.57[a]
Ca	5.00
Mg	4.94
K	0.33
U(VI)[b]	$0/4\times10^{-3}$
DIC[c]	7.44
SO_4	10.78
Cl	3.00
NO_3	0.53
$Si(OH)_4$	0.28
PO_4[b]	0/1.00
pH	7.10

[a] Increased concentrations as a result of phosphate amendment by adding salts of sodium phosphate

[b] Concentration of 0 corresponds to experimental conditions without any U(VI) or PO_4^{3-} in the influent

[c] DIC stands for dissolved inorganic carbon

Synthetic Rifle groundwater (SRGW) with the composition noted in Table 5.1 was prepared to simulate the conditions at the field site (Campbell et al. 2011, DOE 1999). Plastic bags (Tedlar) that were impermeable to gases were used to store

the SRGW to maintain a combination of dissolved inorganic carbon and pH that mimicked that of the actual site and that would have resulted in CO_2 exsolution to the ambient laboratory atmosphere. The SRGW was introduced into the columns in an upflow mode using a peristaltic pump at rates that correspond to groundwater flow velocities of ~ 1.1 m/d, which is in the range observed at the site(Fang et al. 2009, Moon et al. 2010, Yabusaki et al. 2007). For a field scale application, the phosphate addition to advecting groundwater would be done at flow rates that would

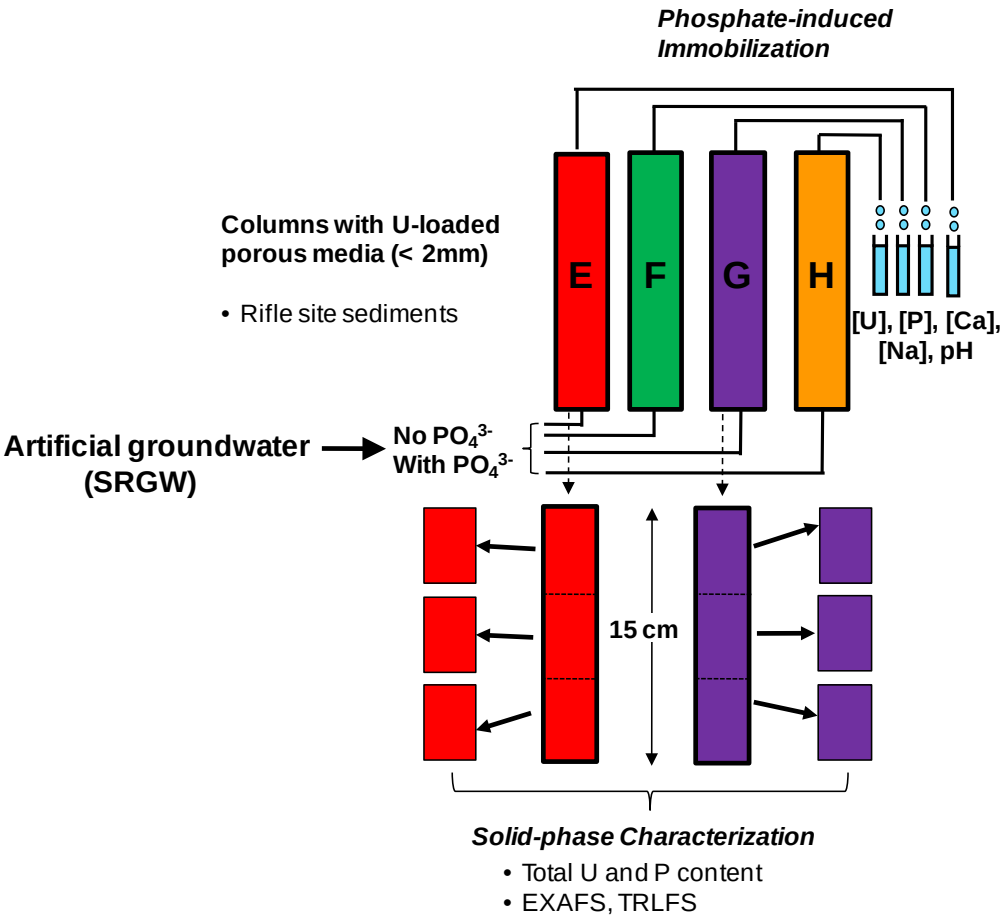

Figure 5.1. Schematic showing the experimental approach and setup of column experiments used in this study. At different time intervals, columns were stopped, sampled and analyzed using various aqueous and solid phase characterization techniques.

not influence the overall groundwater flow.

Experiments were performed in different modes (Figure 5.3) that involved feeding SRGW to the columns with or without uranium and phosphate. Similar to in the earlier study presented in Chapter 4, a conditioning mode was included to remove the background labile fraction of uranium from the sediments. Columns were then operated in the sorption mode until uranium breakthrough occurred. Following breakthrough columns were operated in an uptake mode during which SRGW containing both uranium and phosphate was fed into the sediments. The influent reservoir used to store this solution was replaced with a freshly prepared solution at least once every week. Influent samples were collected more frequently using a sampling valve placed just before the solution entered the columns and analyzed to examine the extent to which uranium may have been sequestered due to precipitation or adsorption within the bags or the tubing from the bags to the column inlets. The influent solution was undersaturated with respect to uranium-containing solids, but it was supersaturated with respect to octacalcium phosphate (SI = 2.21). Over the course of the uptake mode, three columns (E, F, and G) were stopped and sampled for further analysis after 61, 170, and 334 pore volumes of phosphate treatment. Column H was operated for another 223 PV in a release mode during which SRGW containing uranium but no phosphate was fed into the column. This step helped evaluate the uranium behavior that could be expected in actual field applications when phosphate amendment would be stopped after a prescribed treatment duration.

5.2.2.2 Chemical analysis of influent and effluent

Influent and effluent samples were regularly collected, analyzed for pH, saved for dissolved inorganic carbon (DIC) analysis, and preserved for elemental analysis by acidifying to 1% nitric acid. Dissolved concentrations of uranium, phosphorus, calcium, sodium, magnesium, potassium and silica were measured using inductively coupled plasma-mass spectrometry (ICP-MS, Perkin Elmer Elan DRC II).

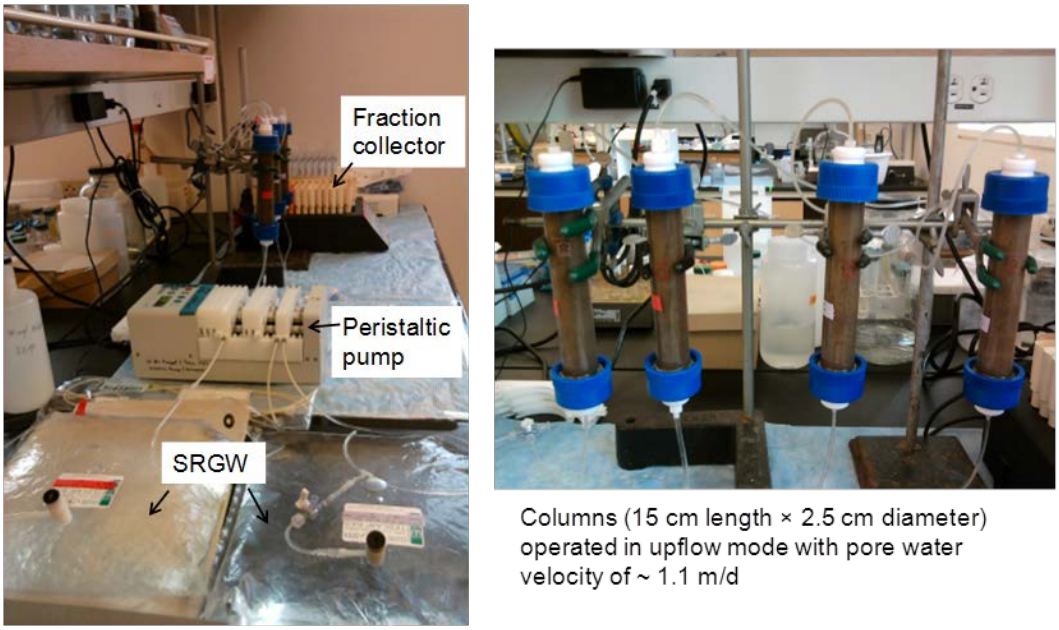

Figure 5.2. Photographs of the experimental setup showing all the components used in this study. The Tedlar bags filled with SRGW, peristaltic pump and fraction collector are shown on the left. The right side shows four glass columns loaded with wet sediments used for the study.

The detection limit was 0.2 µg/L for uranium, 10 µg/L for phosphorus, and 50 µg/L for other measured elements. DIC was measured using a TOC analyzer (Shimadzu, TOC-$L_{CPH/CPN}$ PC-controlled model). Samples for influent DIC measurement were regularly collected using the sampling valve placed just before the influent enters the columns, whereas effluent samples were periodically collected using an airtight syringe to avoid any loss of uptake of inorganic carbon between sampling and

analysis. The effluent DIC samples were then stored in glass vials and analyzed within 24 hours.

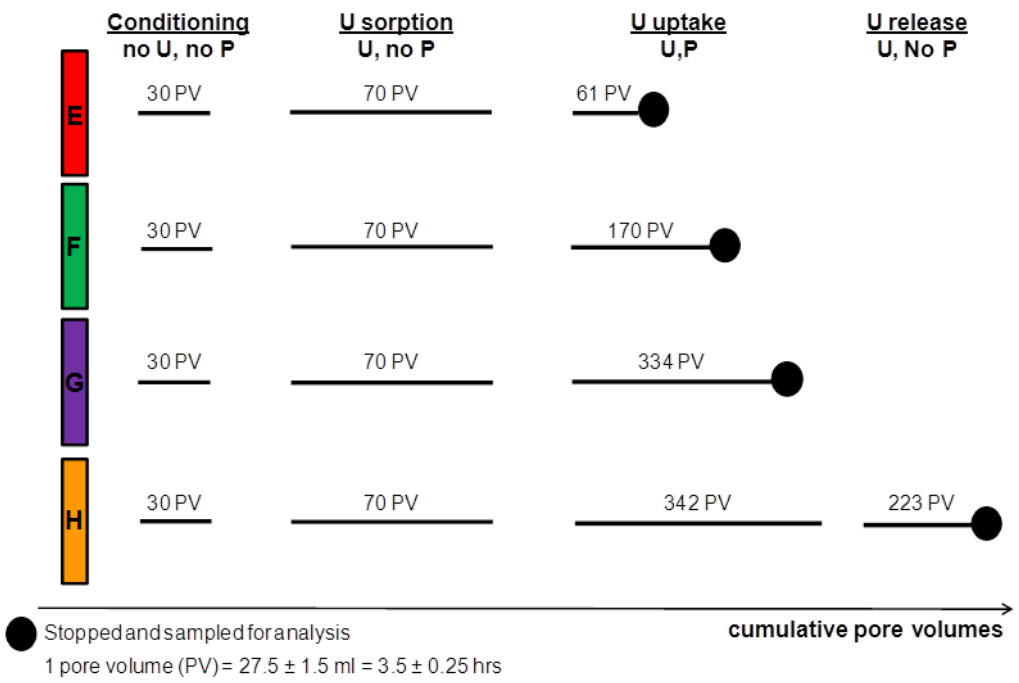

Figure 5.3. Experimental modes of operation to study U(VI)-phosphate reactions in sediments amended with phosphate to induce *in situ* uranium immobilization.

5.2.2.3 Sequential extractions

A procedure similar to that used for the columns discussed in Chapter 4 was used wherein sediments were collected in roughly three equal sections (~ 45 g) along the length of the column and classified as those from the inlet, midsection, and outlet. Extractions were performed in duplicate for all the column samples. Duplicate samples weighing 2 g each were obtained from different locations within each section to see if significant differences in speciation occurred within the section. A four step sequential extraction method (Table 5.2) modified from Tessier et al. (1979) with a solid to solution ratio of 40 g/L (34 g dry weight/L based on moisture content

measurements) in 50-mL reactors was used to evaluate the solid phase speciation and spatial distribution of uranium. A single step total digestion using a mixture of nitric acid and hydrochloric acid at 100° C for 4 h was also performed to get a more direct measure of the total uranium that could be compared with the sum of the uranium amounts from the four steps.

Table 5.2. Steps in the sequential extraction method

Step	Target phase	Extractant composition	pH	Procedure
1	Water soluble	Ultrapure water	5.5	Shake suspension 16 h.
2	Ion exchangeable	1 M ammonium acetate	7.0	Shake suspension 16 h. Rinse with ultrapure water.
3	Acid soluble	1 M acetic acid	5.0[#]	Shake suspension 16 h. Rinse with ultrapure water.
4	Residual solids	8 mL HNO_3 acid + 2 mL HCl acid + 40 mL DI water	--	Digest in heated block held at 100°C for 4 h.

[#] pH adjusted to desired level using NaOH

5.2.2.4 Equilibrium speciation calculations

Equilibrium calculations were performed using MINEQL+ v 4.6 (Schecher and McAvoy 2007) with the thermodynamic database customized to use the aqueous reactions and thermodynamic constants listed in Table A.1 of Appendix A. Potentially relevant solids include metaschoepite [$UO_3 \cdot 2H_2O$], chernikovite, sodium autunite, uranyl orthophosphate, autunite, and various calcium phosphates. The dissolution reactions and associated equilibrium constants are listed in Table A.2 of Appendix A. The log K_{sp} values of several of the relevant uranium-containing

minerals were included from a recent publication (Singh et al. 2010) wherein the compilation of these constants was based on earlier reviews of solubility studies (Gorman-Lewis et al. 2008a, Gorman-Lewis et al. 2008b, Gorman-Lewis et al. 2009).

5.2.2.5 Laser induced fluorescence spectroscopy (LIFS) analysis

LIFS analysis was performed using the same protocol that was used for the samples discussed in Chapter 4.

5.2.2.6 Uranium speciation using EXAFS analysis

Samples for EXAFS analysis were sealed in polycarbonate sample holders with Kapton tape and then heat-sealed in polyethylene bags for secondary containment. U L_{II}-edge EXAFS spectra for samples from the inlet and midsection of column G were collected at room temperature on beamline 20-BM-B at the Advanced Photon Source at Argonne National Laboratory. Spectra were collected at the U L_{II}-edge instead of the more commonly used U L_{III}-edge to avoid interferences from Rb in the sediments. The beamline employed a Si(111) fixed-offset, double-crystal monochromator and a torroidal focusing mirror to increase usable flux on the sample (Heald 2011, Heald et al. 1999). Fluorescence-yield data were collected using a 12-element solid-state Ge energy dispersive detector. The U L_{III}-edge EXAFS spectrum of the <2 um clay size fraction of sediments from the Rifle site reacted with 100 uM U(VI) in SRGW was collected for use as a spectral standard at

the Stanford Synchrotron Radiation Lightsource on beamline 11-2. This beamline employs a cryogenically cooled Si (200) double crystal monochromator. Data were collected in fluorescence-yield using a 100-element solid state Ge energy dispersive detector. Data were processed using the Athena interface (Ravel and Newville 2005) to the IFEFFIT software package (Newville 2001); linear-combination fitting was also performed in Athena.

5.3 Results and Discussion

Figure 5.4 represents the U(VI) profiles for columns E–H obtained during the different modes of operation. Sections 5.3.1, 5.3.2, and 5.3.3 systematically examine the U(VI) behavior during the different modes of operation.

5.3.1 Uranium release and sorption on sediments in the absence of phosphate

The mass balance approach described by Equation 8 in Chapter 4 and schematically represented in Figure 5.5 was used to calculate the amounts of labile uranium released from the background sediments and the amounts adsorbed by the sediments in the absence of phosphate. The conditioning mode flushed a small but measurable amount (0.34±0.05 μg/g) of labile uranium from the initial sediments (Table 5.3). This is somewhat higher than the 0.20±0.03 μg/g flushed through the same sediments from the same batch but in a separate set of experiments (Chapter 4).

The small difference in the amounts of uranium released from the background sediments used for Chapter 4 and in this chapter is possibly due to different durations (30 PV for current chapter as compared to 20 PV for experiments in Chapter 4) of conditioning. Uranium effluent profiles from all four columns (Columns E-H) looked very similar and the effluent concentrations were less than 20 μg/L by the end of the conditioning mode (Figure 5.6).

Table 5.3. Uranium concentrations in the sediments calculated using a mass balance approach

Mass of U (μg/g)	Column E	Column F	Column G	Column H
Released during conditioning mode	0.38±0.03	0.32±0.02	0.32±0.02	0.33±0.02
Adsorbed during sorption mode	2.16±0.15	2.03±0.15	1.97±0.14	2.08±0.15
Uptaken during uptake mode[#]	11.35±0.80	19.14±0.80	35.56±0.81	38.67±0.86
Released during release mode[*]	--	--	--	15.00±1.06
Retained or Accumulated	13.51±0.81	21.17±0.81	37.53±0.82	25.75±1.37

[#] Columns treated with 61, 170, 334 and 342 PV of phosphate for Columns E, F, G and H respectively.
[*] Column operated for 223 PV with phosphate-free SRGW influent.

Following the conditioning mode, the sorption mode resulted in uranium loadings of the sediments of up to 2.06±0.30 μg/g [Table 5.3] as compared to 1.98±0.14 μg/g observed for the earlier experiments (Chapter 4) with sediments from the same batch (Figure 5.6).

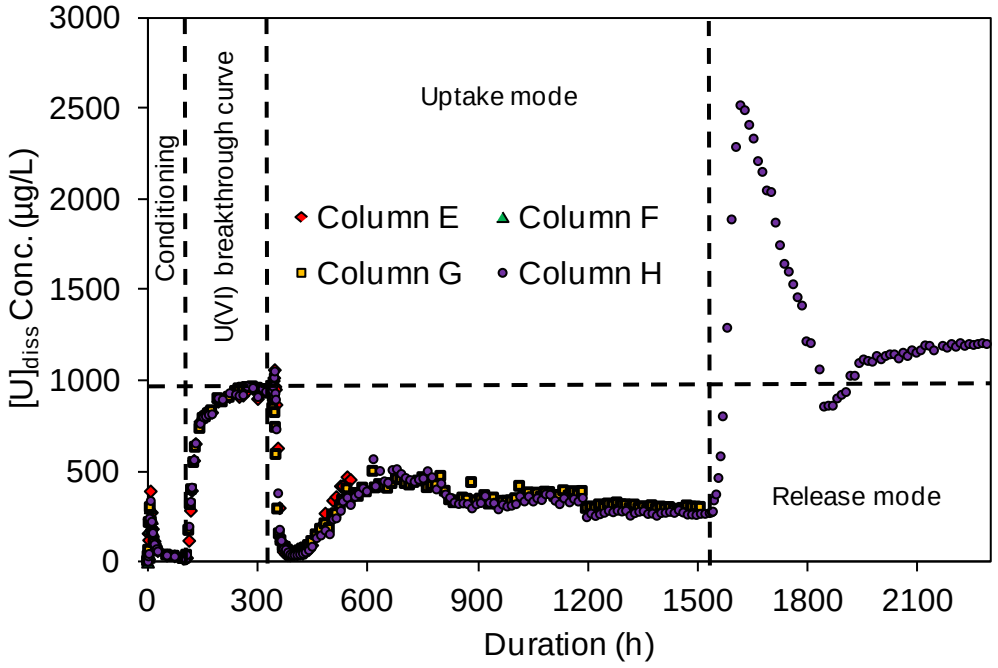

Figure 5.4. Dissolved uranium profile concentrations for Columns E, F, G, and H during various modes of operation. The horizontal dashed lines represent the target U(VI) influent concentrations in the SRGW during the breakthrough, uptake and release mode.

5.3.2 Uranium uptake in the presence of phosphate

Following uranium breakthrough in the sorption mode, the columns were operated in an uptake mode (SRGW containing U and P, Figure 5.3) before being stopped and sampled for further analysis at various time intervals. The influent uranium concentrations during the uptake mode were lower than anticipated and were possibly lost from solution before the influents entered the columns. Hence the measured influent concentrations just before the solution entered the columns were used for the uptake calculations. The phosphate amendment resulted in sustained uranium removal from the SRGW within the columns. On addition of phosphate, the

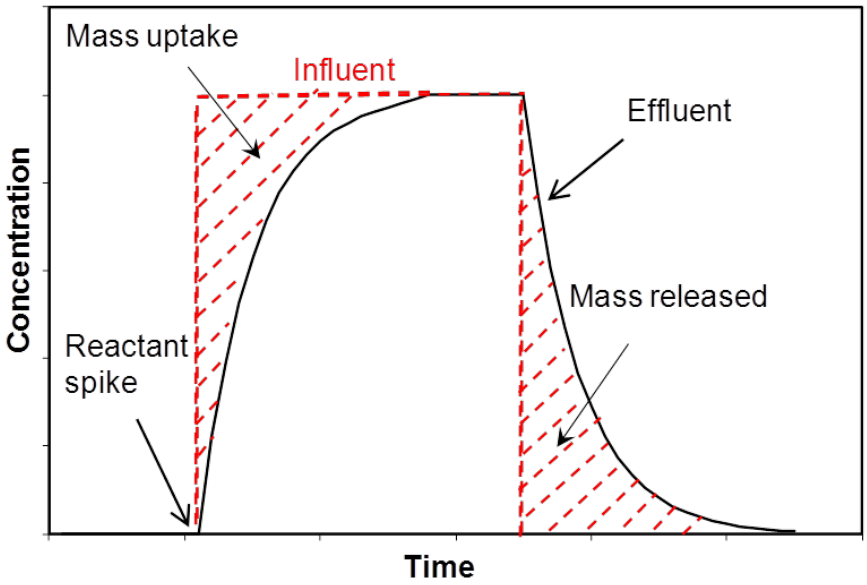

Figure 5.5. Schematic representation showing the approach used to estimate the masses taken up and released for a typical effluent concentration profile of a particular solute of interest. The vertical and horizontal dashed lines represent the concentration profile of a non-reactive tracer. The difference between masses taken up and released gives the net accumulation of a particular species within the system.

uranium concentrations quickly dropped to ~ 40 µg/L before increasing and stabilizing at levels of 400 µg/L (Figure 5.7). As phosphate amendment continued, the estimated uranium content of the sediments increased from 11.35±0.80 µg/g for column E during the first 61 PV of phosphate treatment to 38.67±0.86 µg/g for column H after 342 PV of phosphate treatment (Table 5.3). The initial rapid decrease in uranium concentrations followed by steady uranium concentrations significantly lower than influent concentrations suggest the presence of different U(VI) uptake mechanisms as compared to those observed for the set of column experiments in Chapter 4. Adsorption reactions typically occur rapidly with equilibrium being attained within minutes. On addition of phosphate, the effluent uranium

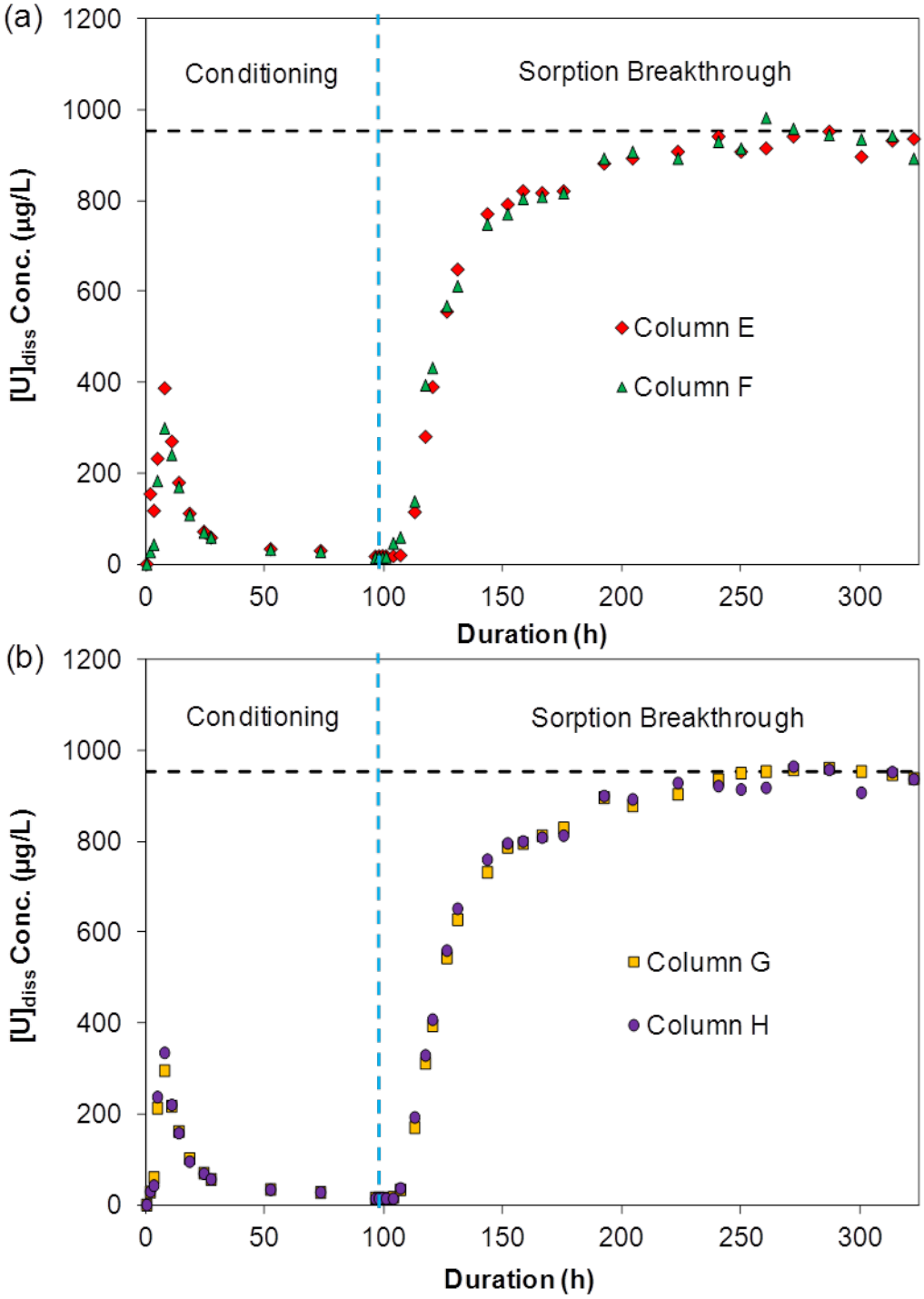

Figure 5.6. Conditioning and sorption phase profiles of U(VI) for (a) Columns E and F and (b) Columns G and H. The horizontal dashed lines represent the U(VI) influent concentrations included in the SRGW during the sorption breakthrough phase. The vertical dashed line indicates the transition from conditioning to sorption breakthrough mode.

concentrations decreased by more than 90 % within a few pore volumes. The decrease occurred over about 10 PV and not instantaneously, which would be expected from the physical non-equilibrium adsorption/desorption process discussed in Chapter 4. Hence, the initial decreasing trend can be associated with adsorption as the dominant uptake process. The steady effluent concentration profile that followed that was lower than the influent could be a result of uranium removal via precipitation.

The potential for precipitation in the influent reservoir and in the columns was assessed by considering the saturation indices of possible precipitating solids in the SRGW influent and in the column effluents. Calculations done using the initial measured influent concentrations of SRGW containing uranium and phosphate at the start of the uptake mode suggested that the solution was undersaturated with respect to autunite (-0.45) and sodium autunite (-2.50) but supersaturated with respect to octacalcium phosphate (2.21). Saturation calculations done using the measured effluent concentrations after more than 600 hours (170 PV) of the uptake mode (at 1000 h in Figure 5.7b) resulted in SI values of -1.5, -3.56 and 2.18 for autunite, sodium autunite and octacalcium phosphate respectively. Previous studies have shown the formation of uranyl phosphate solids for undersaturated conditions via surface mineralization (Murakami et al. 1997, Ohnuki et al. 2004). For the current study, U(VI) removal could have occurred due to formation of autunite via surface mineralization or adsorption on calcium phosphate solids. The LIFS and EXAFS analysis discussed in later sections (5.3.5 and 5.3.6) confirm the presence of autunite and other species of uranium. The uranium could have been removed via

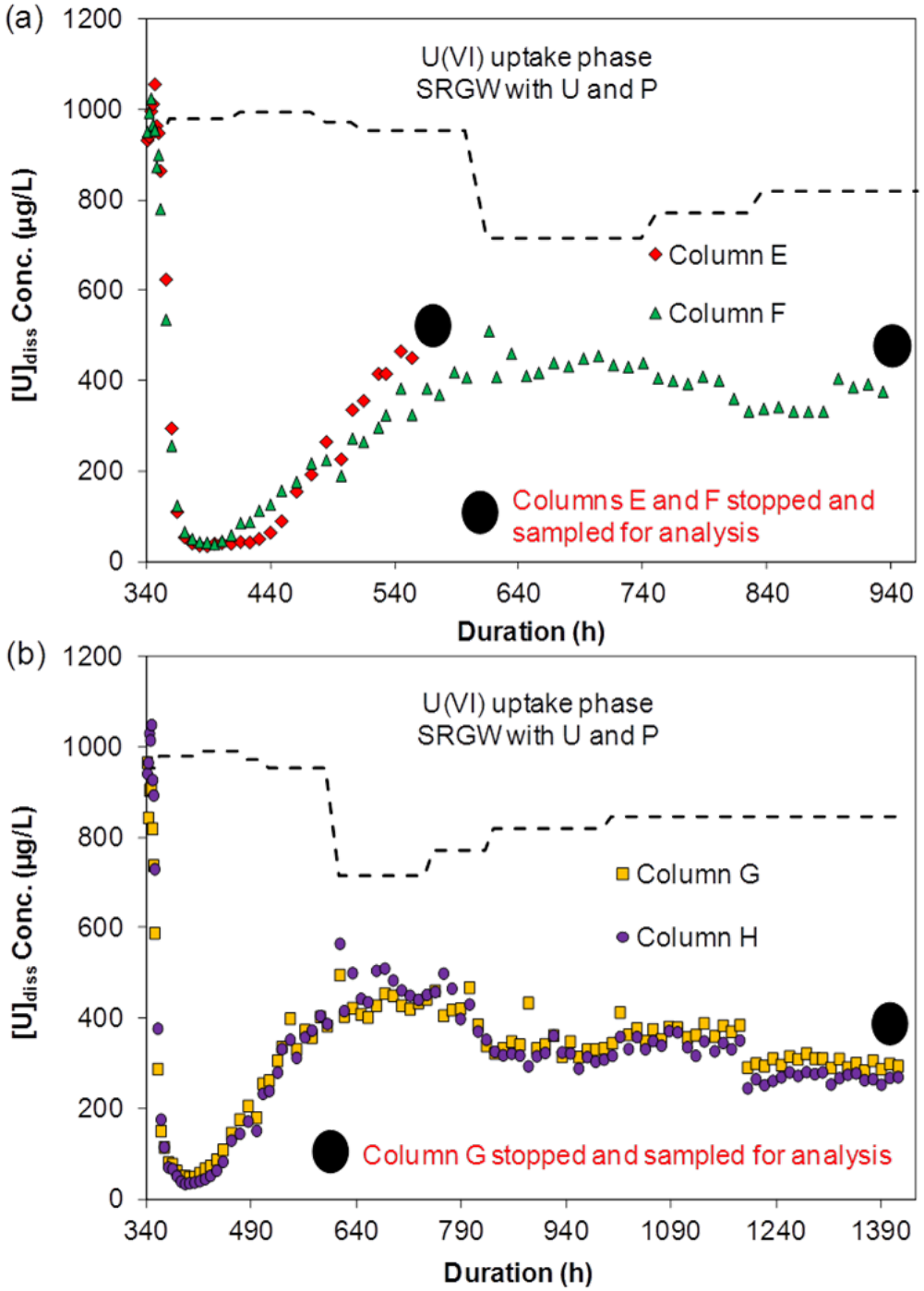

Figure 5.7. Uptake mode profiles of U(VI) for (a) Columns E and F and (b) Columns G and H in the presence of phosphate. Columns E-G were stopped at different times (shown by stars) and sampled for further analysis, whereas column H was continued. The dashed line represents the measured U(VI) influent concentration.

incorporation into calcium-phosphate solids as seen for the set of experiments in Chapter 3 in which 5 mM Ca, 1 mM DIC, 100 µM U and 1 mM P were all added simultaneously at pH 7.5.

5.3.3 Uranium release in the absence of phosphate

When phosphate-free SRGW containing uranium was introduced into a column (Column H) after an extended period of phosphate treatment, the effluent uranium concentrations sharply increased and peaked at concentrations more than twice the influent levels (2500 µg/L) before falling back to close to influent levels (Figure 5.8). As the release mode continued, a slow uranium release with

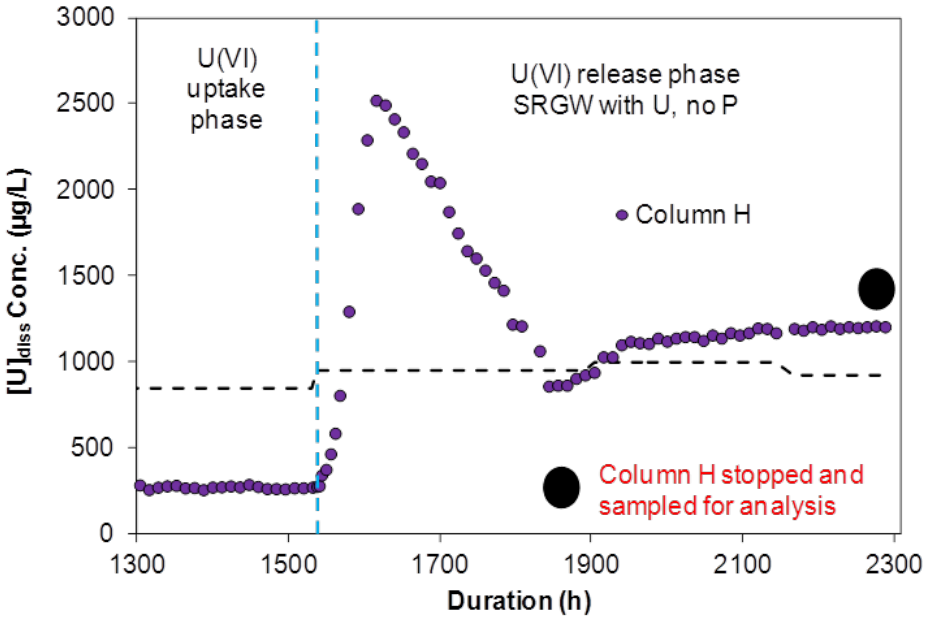

Figure 5.8. U(VI) concentration profile for Column H from the end of the uptake mode and into the release mode. The vertical dashed line indicates the transition from uptake to release mode. The horizontal dashed line represents measured influent U(VI) concentration.

concentrations slightly higher than the influent levels was observed for several days before the column was stopped and sampled for further analysis. Even with the dramatic spike in effluent uranium, only one third of the uranium that had accumulated during the sorption and uptake modes was released in the spike; the phosphate-treated sediments retained a significant amount of uranium after phosphate addition had stopped (Table 5.3). The uranium release profiles include a fast rapid release of uranium followed by the slower release. The distinct periods in the release profiles suggest the presence of different uranium species associated with the sediments. The rapid release could have been due to desorption of uranium adsorbed during the uptake mode and the slower release could have been due to dissolution of a precipitated solid. The SI calculation done using the measured concentrations at ~ 2000 hours (after 135 PV of phosphate free U(VI)-influent) resulted in SI values of -4.29, -6.5 and 0.79 for autunite, sodium-autunite and octacalcium phosphate respectively. The SI values for autunite are lower than they were during the uptake mode. Although the SI values were negative even for the uptake mode, the spectroscopic results presented later do indicate the presence of autunite in the samples; consequently, the even decrease in the autunite SI values (i.e. to more negative values) when phosphate was removed suggest that the period of slow continuing release could have been due to dissolution of a precipitate like autunite.

5.3.4 Sequential extractions

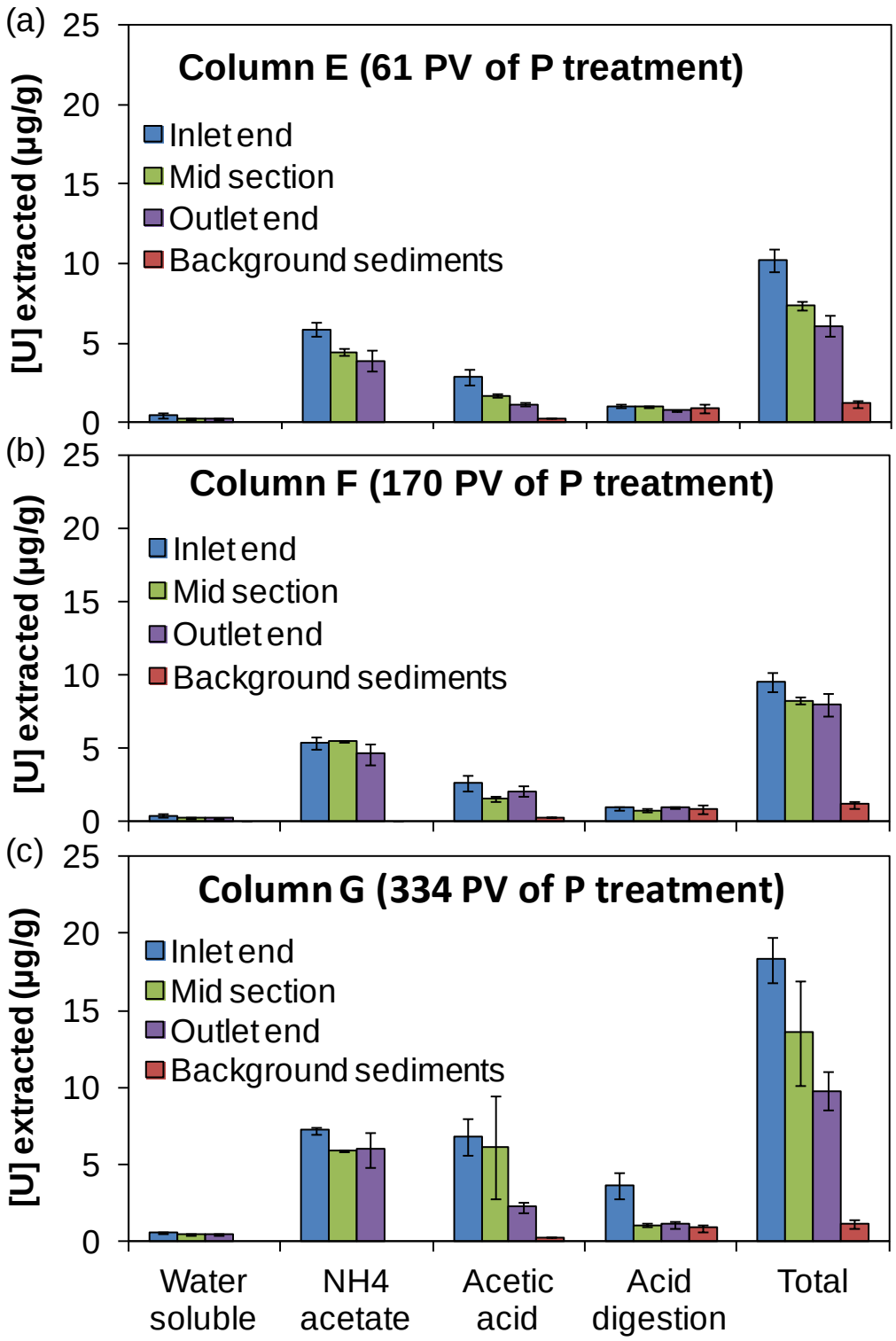

Figure 5.9. Sequential extraction results for uranium extracted from three depth increments of (a) Column E, (b) Column F, and (c) Column G. Results of background sediments are shown for reference. Error bars represent standard error for the data obtained through duplicate samples.

Sequential extractions were performed to provide information on the amounts and speciation of uranium in the sediments. Negligible amounts of uranium were extracted in the water soluble step. The dominant fractions of labile uranium were extracted in the step targeting ion exchangeable species and then in the weak acid extraction step. As expected from the aqueous phase profiles, the total uranium content increased with the duration of phosphate treatment (61 PV for column E to 342 PV for Column G) (Figure 5.9). Interestingly, with the increase in time, the uranium accumulation shifted toward the less easily extractable (i.e., more immobile) fractions. This shift is indicated by the relative amounts of accumulated uranium extracted in the acetic acid and hot acid digestion steps being highest for Column G, then Column F, and finally Column E. Although the calculations based on influent-effluent mass balance for the amount of uranium accumulated (~ 11, 19, 35, and 23 μg/g for Column E, F, G, and H respectively) have the same trend as the values determined from sequential extractions (~ 9, 10, 15, and 6 μg/g for Columns E, F, G and H respectively), the exact quantitative amounts determined from the two approaches are not in agreement. The difference in calculated uranium accumulations by the two approaches could be a result of multiple factors. It is possible that the sediment sub-samples used for the extractions were not representative of the overall 5-cm long subsections. Another factor was the possible loss of uranium from solution before the influents contacted the sediments in the columns. The lower measured influent samples than the target concentrations, especially for longer durations, indicate that some U was lost upstream of the influent sampling ports on the columns. While this measured loss is accounted for in

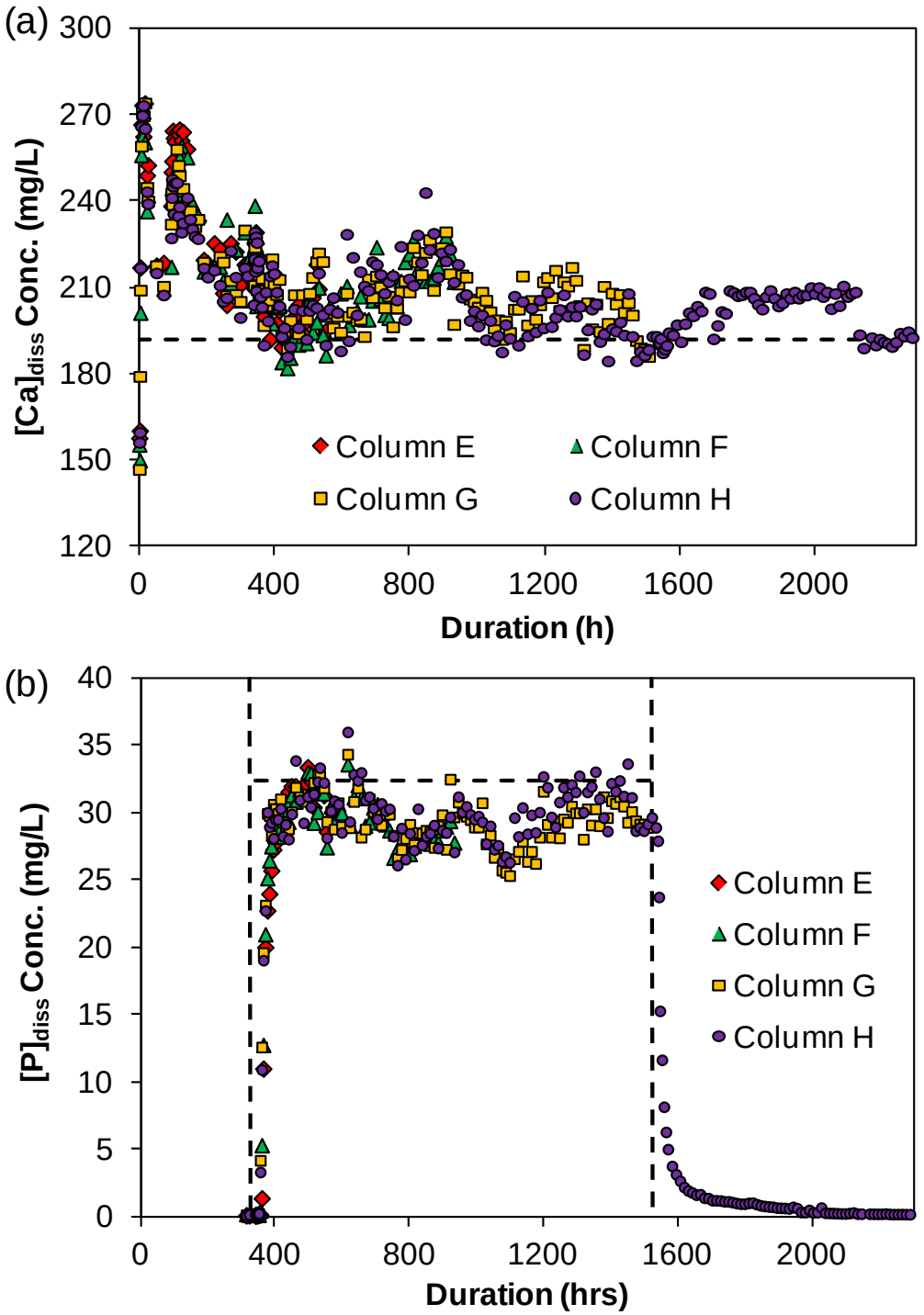

Figure 5.10. Dissolved calcium (a) and phosphate (b) profiles through Columns E, F, G, and H. Horizontal dashed line represent measured calcium and phosphate influent concentrations. Vertical dashed line in (b) represents the transition from sorption mode to uptake mode and from uptake mode to release mode.

the mass balance calculations, any further loss of uranium from solution between the influent sampling port and the actual sediments (inlet cap and fittings, tubing section, column walls) could bias the results. Despite the large differences, the similarity of the trends observed for both the approaches still suggests that uranium removal during the later stages occurred via precipitation.

The extraction results also indicate that considerable phosphate accumulated in the sediments (48 μg/g in the first two stages of the sequential extractions). However the accumulations were not as much as those observed in other studies in which significant phosphate precipitation affected the flow. For example, laboratory column experiments using phosphate treatment of Hanford field sediments observed large amounts of phosphate mineral precipitation when phosphate was added in the form of water soluble amendments. The rapid extensive precipitation occurred after the displacement of one pore volume thus making it infeasible to pass additional volumes of phosphate amendments through the column (Wellman et al. 2006). For a field application extensive precipitation could potentially deflect subsequently injected amendment solutions around the target area; consequently other studies were conducted to inhibit the formation of phosphate minerals using organic phosphates or micro-organisms that would control the release of phosphate in subsurface environments (Beazley et al. 2009, Beazley et al. 2011). However, the current set of experiments did not experience any clogging issues. Sequential extractions of samples obtained from Columns E, F, G and H show relatively less calcium (data not shown) than in the background sediments, which indicate that there

was a small amount of net calcium loss from the sediments over the course of the experiment. It should be noted that this is a net loss and that it is possible that calcium phosphate amounts actually increased while calcium loss from other species were more than enough to offset those gains. In contrast, phosphate accumulation did occur over the course of the phosphate treatment period. However, the similarity of the influent and effluent phosphate concentrations indicates that any phosphate precipitation was not too extensive (Figure 5.10), and this is consistent with the lack of qualitatively observable changes in sediment porosity or permeabilty.

The total uranium content was much lower (~ 6 µg/g based on sequential extractions as compared to ~ 23 µg/g based on influent-effluent mass balance approach) for samples obtained from Column H following the release mode in which SRGW with U but no P was flushed through the system (Figure 5.11). The

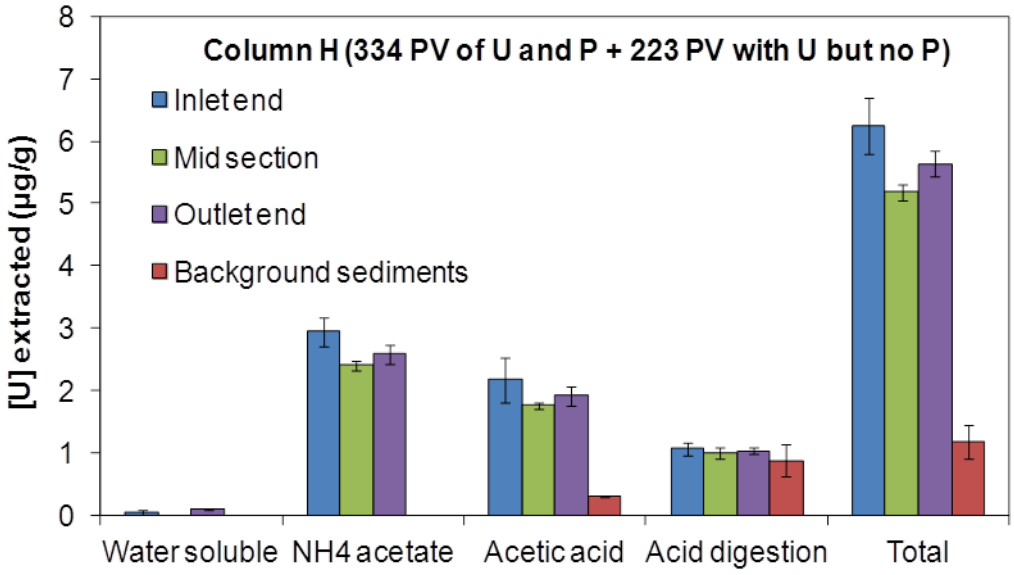

Figure 5.11. Sequential extraction results for uranium extracted from three depth increments of Column H. Results of background sediments are shown for reference. Error bars represent standard error for the data obtained through duplicate samples.

uranium retained in the sediments was primarily in a form that could be extracted with ammonium acetate and acetic acid. During the release mode, approximately 8.5 μg/g of accumulated uranium was released from the system suggesting around 45 % retention based on sequential extractions as compared to ~ 67 % based on influent-effluent mass balance. The uranium released was in different forms with roughly equal amounts being extracted using ammonium acetate and acetic acid. The equal contributions from different extraction (ammonium acetate and acetic acid) steps suggest that at least two types of uranium species were probably present in the sediments with one primarily being extracted with ammonium acetate and the other with acetic acid. The uranium extracted by ammonium acetate could have been adsorbed to sediments or to the phosphate solids formed during the reaction whereas the uranium extracted from acetic acid extraction could be the uranium existing in solid forms.

5.3.5 Laser induced fluorescence spectroscopy analysis

Samples from Columns E, G, and H were analyzed using LIFS to complement the observations made using aqueous phase analysis and sequential extractions. Relatively small differences were observed between Column E and F from extraction results which suggested that uranium speciation was very similar in both the columns. Since LIFS analysis only provides information on the uranium speciation, Column F samples were not analyzed for LIFS because the speciation was anticipated to be very similar to that in Column E. Fluorescence spectra showed

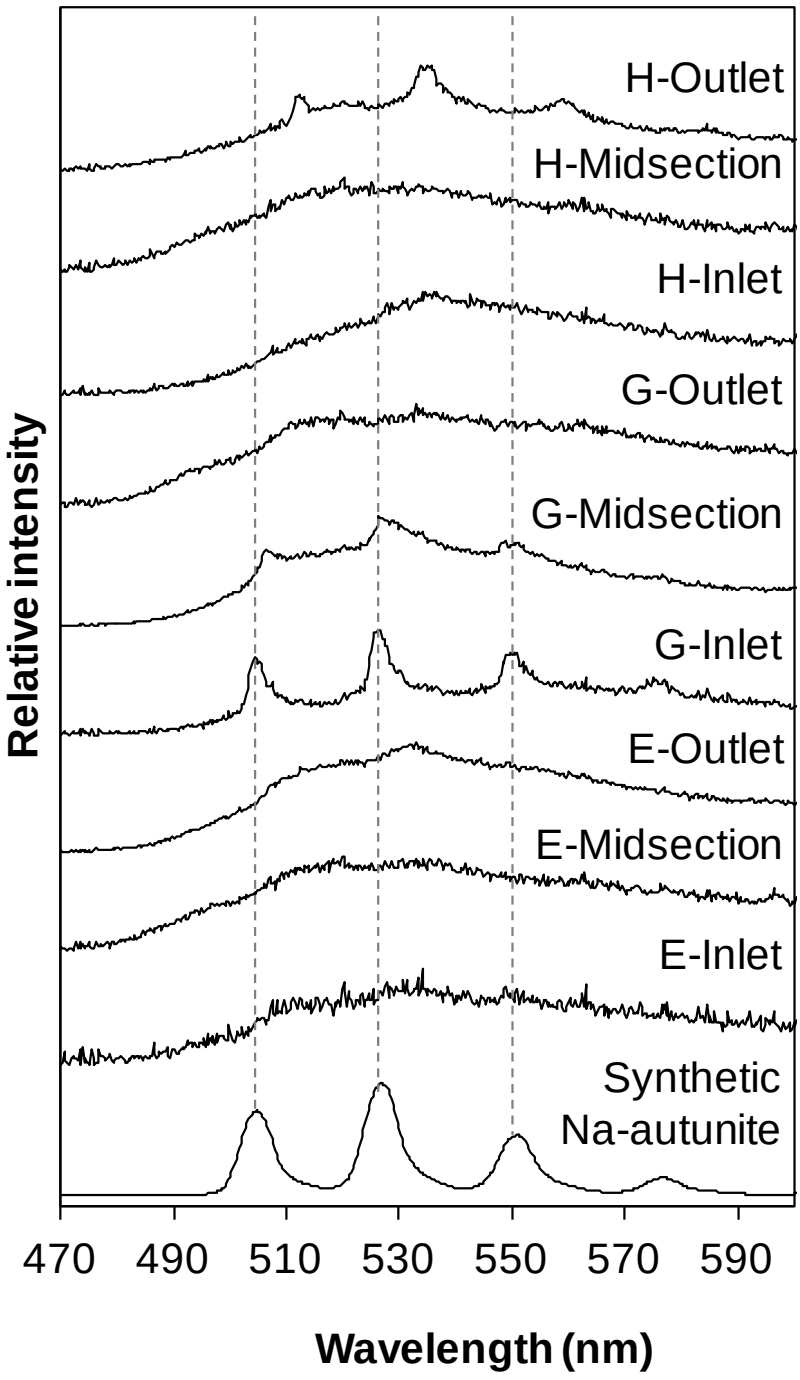

Figure 5.12. Fluorescence spectra of samples obtained from different depths within Columns E, G and H. Inlet, midsection, and outlet represent samples obtained from different portions of the columns. A spectrum of synthetic sodium autunite is included as a reference surrogate for autunite.

very little or no discernible fluorescence spectral intensity (Figure 5.12). The low spectral intensities or resolution despite analyzing the samples at low temperatures (8 ± 2 K) rules out fluorescence quenching by mechanisms discussed in Section 4.3.4 and suggest the presence of adsorbed uranium for most samples. However, the

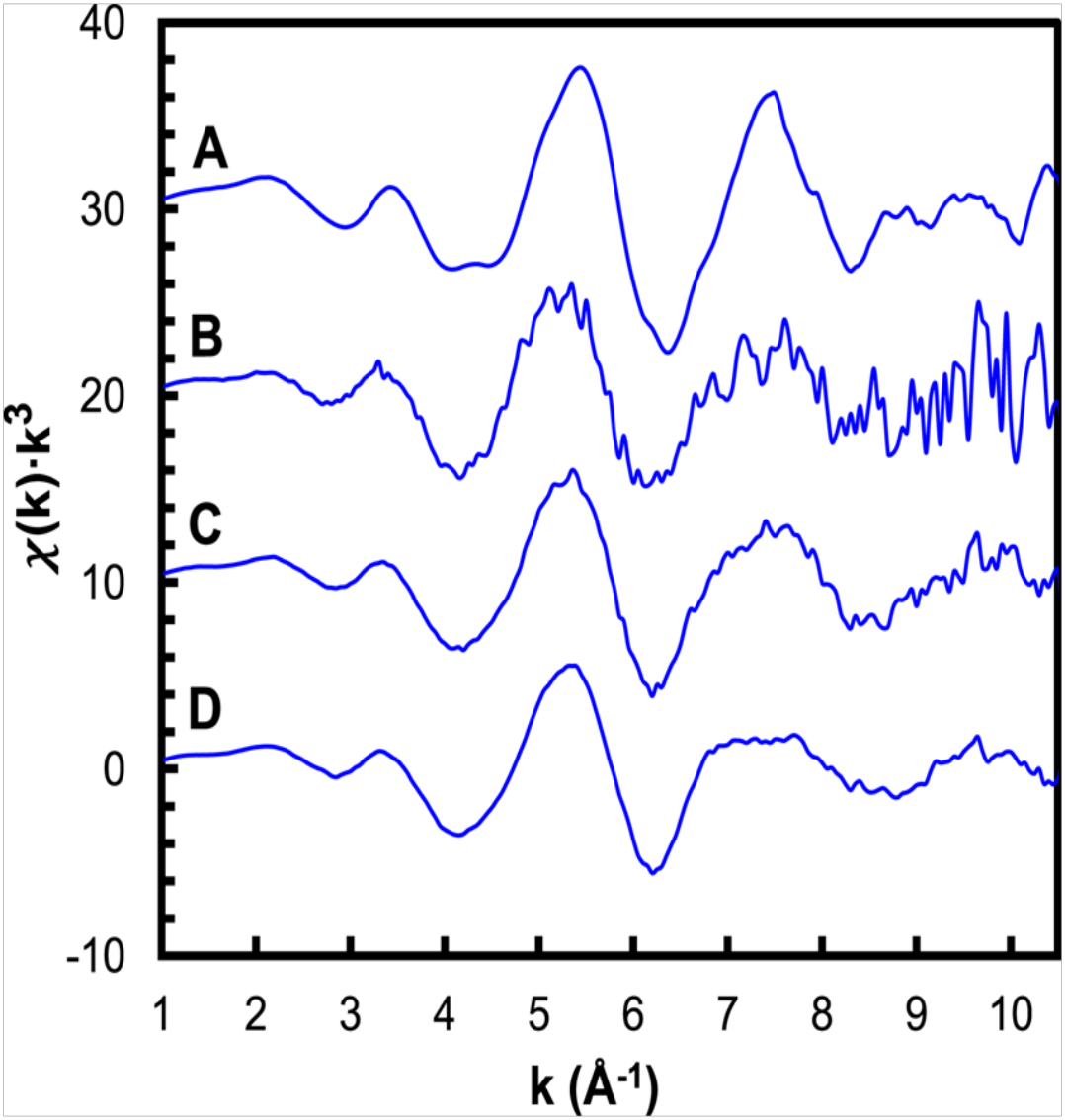

Figure 5.13. EXAFS spectral standards used in linear combination fitting: (A) chernikovite, (B) U(VI) adsorbed to the clay size fraction of Rifle sediments, (C) U(VI) adsorbed to amorphous calcium-phosphate, and (D) U(VI) incorporated with amorphous calcium-phosphate.

sample from the inlet end and midsection of Column G (column that underwent maximum duration of phosphate treatment) had additional weak features that match well with a synthetic sodium-autunite reference spectrum (used as a surrogate for autunite solids). The peak intensity was higher for the sample from the inlet end. The results are in agreement with those of sequential extractions (Figure 5.9) in which more uranium was extracted from the inlet end than the outlet end. The results corroborate the observation made from aqueous phase analysis and the sequential extractions that uranium uptake occurred through a combination of adsorption and precipitation. Fluorescence spectra for samples from Column H (following the release mode) showed a distinct behavior. The inlet and midsection samples suggest the uranium to be predominantly adsorbed whereas the sample from the outlet end had additional weak features that do not match any of the reference peaks or peaks for those of inlet end and midsection samples from column G. This suggests that following the release mode, the form of uranium accumulated during the uptake mode changed when phosphate amendment was stopped and a different form of uranium species was at least partially responsible for retaining the uranium within the column.

5.3.6 EXAFS analysis

EXAFS analysis was used to further probe the speciation of the solid-associated uranium in the sediments. Samples from Column G (i.e. the sediments that received the longest phosphate treatment and contained the most uranium) were

analyzed via linear combination fitting using four spectral standards: U(VI) in the autunite group mineral chernikovite (Singh et al. 2012), U(VI) adsorbed to the clay fraction of Rifle sediments in the absence of phosphate, U(VI)-adsorbed to amorphous calcium-phosphate, and U(VI) incorporated into calcium-phosphate (Figure 5.13). The spectral standard for U(VI)-adsorbed to amorphous calcium-phosphate was obtained from the pre-formed study of Chapter 3 where uranium solution was reacted with pre-formed amorphous calcium-phosphate solids. The standard for U(VI) incorporated into calcium-phosphate was obtained using a

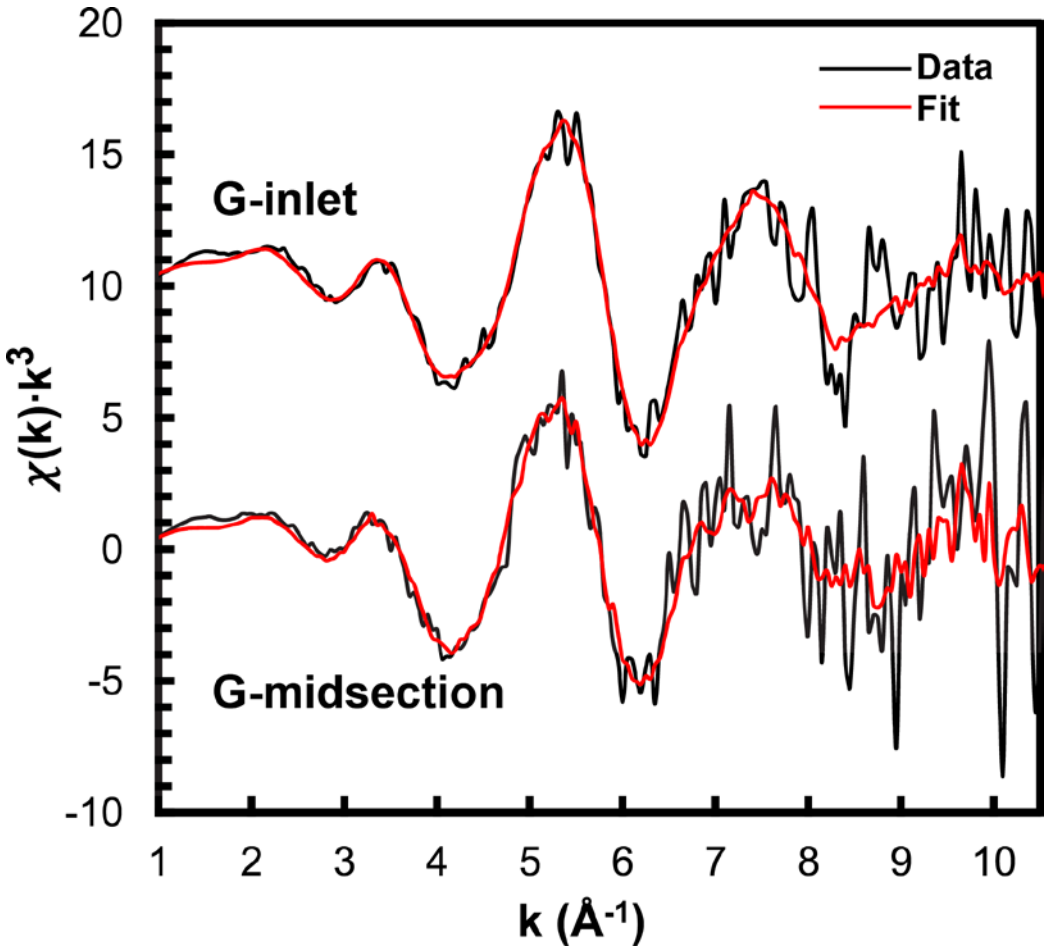

Figure 5.14. EXAFS spectra of samples obtained from two depths (inlet end and midsection) of Column G and associated linear combination fits.

spectrum of a pH 7.5 sample when all Ca, U and P were added together (also from Chapter 3). Only spectra obtained for samples from the inlet and midsection were analyzed because the U concentration in the sample from the outlet end was too low to obtain data of the needed quality. The spectral fits (Figure 5.14) determined the U speciation in the inlet as 29±6% autunite, and 46±17% adsorbed to calcium-phosphate or similar solid; the percentages adsorbed to the clay-sized fraction Rifle sediments (3±6%) and incorporated in calcium phosphate (22±23%) were statistically indistinguishable from 0. The uranium contents of the samples were close to what could be detected by EXAFS and interferences from other elements in the sediments affected the collection of spectra, which led to more uncertainty than in the linear combination fitting of the spectra of higher concentration samples from simpler systems presented in Chapter 3. The fitting for the midsection sample suggest uranium speciation as 46±11% adsorbed to Rifle sediments and 54±17% incorporated in calcium-phosphate. The autunite and U(VI) adsorbed to calcium-phosphate components for the midsection spectrum both refined to 0% and were thus excluded from the final fit (Figure 5.14).

The analysis suggests that uranium was predominantly removed via adsorption on calcium-phosphate or Rifle sediments and incorporation into calcium-phosphate from the inlet end and the midsection of the column. Additionally, a fraction of uranium uptake occurred via formation of autunite in the inlet end of the column, which is expected to have the most supersaturated conditions as the solutions enter the column. The EXAFS spectra fitting helped quantify the uranium speciation and also confirmed the LIFS results that suggested that uranium uptake

occurred through a combination of precipitation (via autunite) and adsorption. It also suggests that interaction with calcium-phosphate is an important contribution to the enhanced uptake of U(VI) upon phosphate addition.

5.4 Conclusions

The integrated approach of aqueous phase analysis, sequential extractions, and spectroscopic characterization of sediments demonstrated that phosphate amendment can result in significant *in situ* uranium immobilization in subsurface environments. The current study mimics a scenario with treatment of a uranium-contaminated site using phosphate addition to uranium-rich solutions upgradient of target treatment zones at rates that would not significantly alter the natural groundwater flow characteristics. The concurrent presence of high uranium and phosphate concentrations resulted in significant and continuous uranium immobilization within the columns via removal mechanisms that likely included adsorption, incorporation in calcium phosphate solids, and precipitation of autunite.

On cessation of phosphate amendment, a spike of uranium release with effluent concentrations reaching more than twice the influent concentration occurred. However, a significant amount of uranium that had accumulated during the uptake mode was still retained (67 % based on influent-effluent mass balance and 45 % based on sequential extraction results) within the column after 223 PV (770 h) of phosphate-free operation. For a real world application, a continued treatment of phosphate (at much lower concentrations) would be required to maintain the uranium

levels below the influent levels and prevent any major release of uranium from the system. The insights gained through the experiment can help understand the effects of precipitation of other phosphate solids (e.g., calcium phosphates) on uranium immobilization.

Chapter 6. Conclusions and Recommendations for Future Work

6.1 Conclusions

This doctoral thesis research investigated the dominant mechanisms of uranium-phosphate interactions and their implications for uranium fate and transport in subsurface environments. The focus of the work was on reactions relevant to *in situ* remediation. This project provided fundamental information about various interaction pathways between uranium and phosphate that involve adsorption-precipitation, desorption-dissolution, and incorporation. A comprehensive description of various interactions was provided using different experimental configurations, spectroscopy, microscopy, chemical extraction and modeling approaches. Specific conclusions from each task are described below.

Subtask 1A: Homogeneous batch experiments on uranium phosphate precipitation

In the first task, batch experiments were performed to study the effect of pH and co-solutes (DIC, Na^{+} and Ca^{2+}) on the products and solubility of U(VI)

precipitated with phosphate. The presence of DIC increases the uranium solubility as compared to systems that do not contain DIC. The increase is especially significant for neutral or alkaline conditions due to the formation of uranyl-carbonate complexes. In the absence of co-solute cations, chernikovite [$H_3O(UO_2)(PO_4)\cdot 3H_2O$] precipitated despite uranyl orthophosphate [$(UO_2)_3(PO_4)_2\cdot 4H_2O$] being the most thermodynamically favorable solid at pH 6.0 and 7.5 conditions. The presence of Na^+ as a co-solute led to the precipitation of sodium autunite [$Na_2(UO_2)_2(PO_4)_2$], thereby decreasing uranium solubility by several orders of magnitude especially at pH 6.0 and 7.5 conditions. Many contaminated sites are known to have circumneutral pH conditions and thus the presence of sodium as a co-solute can be beneficial for successful *in situ* uranium immobilization.

Subtask 1B: Batch experiments studying U(VI) uptake mechanisms for uranium–calcium–phosphate systems

The presence of calcium resulted in different uranium uptake mechanisms depending on the experimental conditions. Specific batch studies were conducted to investigate the dependence of U(VI) uptake mechanisms on the starting forms of calcium and phosphate at concentrations relevant to field sites. Uptake mechanisms were interpreted by consideration of solid-water equilibrium speciation and characterization of solids by X-ray absorption spectroscopy and laser induced fluorescence spectroscopy. When U(VI) was reacted with dissolved calcium and phosphate at pH 4 and 6, uranium uptake occurred via precipitation of autunite

irrespective of the order of reactant addition. At pH 7.5 the uptake mechanisms depended on the order of reactant addition. When dissolved uranium, calcium, and phosphate were simultaneously added to a reactor, uranium was incorporated into an amorphous calcium phosphate solid. When dissolved uranium was contacted with pre-formed amorphous calcium phosphate solids, adsorption was the dominant U(VI) uptake mechanism. When U(VI) was added to a suspension containing amorphous calcium phosphate solids as well as dissolved calcium and phosphate, then uptake occurred through precipitation (57±4 %) of autunite and adsorption (43±4 %) onto calcium phosphate.

Task 2: Column experiments simulating phosphate addition to uranium-contaminated sediments at groundwater flow conditions

Task 2 investigated the effect of phosphate amendment on uranium immobilization for sediments obtained from a field site in Rifle, Colorado. Batch sorption studies were performed to probe the effect of phosphate addition on Rifle sediments under equilibrium conditions. The results provided vital information on the U(VI)-phosphate reactions under equilibrium conditions, which when compared with the results from column experiments helped in interpreting the presence of non-equilibrium processes that can control U(VI) fate and transport in subsurface environment. Batch sorption experiments confirmed that the K_d for uranium adsorption increased by up to a factor of 6 upon phosphate addition, however

uranium sorption was still weak relative to other sediment-groundwater combinations due to the dominance of the aqueous speciation by Ca-U(VI)-carbonate complexes.

Column experiments were performed under conditions that simulated the subsurface environment with corresponding groundwater velocity of 1.1 m/day. In the absence of phosphate, the sediments took up to 1.98±0.14 μg U/g of sediments when the influent of synthetic groundwater contained 4 μM U(VI). When U(VI)-free influents were then introduced, more than 75 % of the adsorbed uranium was retained over 100 PV of operation if phosphate was present in the influent. In contrast, all the adsorbed uranium was released from the sediments if phosphate was not present in the U(VI)-free influent. Sequential extractions revealed that uranium was distributed uniformly within the columns and was primarily in forms that could be extracted by ion exchange and by contact with a weak acid. Laser induced fluorescence spectroscopy (LIFS) analysis along with sequential extraction results suggested adsorption as the dominant uranium uptake mechanism.

A one-dimensional non-equilibrium CDE model was used to fit uranium and bromide profiles, which yielded a retardation factor of 10.85 for uranium. Based on this retardation factor value, a distribution coefficient (K_d) of 1.90 – 2.03 mL/g was calculated, which was in general agreement with batch sorption results and thus confirmed that the Rifle sediments are relatively weak adsorbents for uranium. The response of dissolved uranium concentrations to stopped-flow events and the comparison of experimental data with a simple reactive transport model indicated that uranium transport was controlled by non-equilibrium processes; intraparticle

diffusion was probably the rate-limiting process. This set of column experiments represented a scenario of phosphate addition to a site with most of the uranium hosted within the sediments and low concentraitons of dissolved uranium. The results from the examined scenario suggest that under such circumstances, only modest uranium retention is attained.

An alternative scenario studied was treatment of a uranium-contaminated site using phosphate addition to uranium-rich solutions upgradient of the target treatment zone. Column experiments were performed such that phosphate addition was done to the columns with the synthetic Rifle groundwater influent that also contained dissolved uranium. When uranium and phosphate were added concurrently, significant uranium uptake was observed, increasing from 11.35±0.80 μg/g during the first 61 pore volumes (PV) of phosphate treatment to 38.67±0.86 μg/g after 342 PV of phosphate treatment. When phosphate amendment was stopped as would be done in a real world application, the column retained significant amounts (~ 67 %) of uranium after 221 PV (> 30 days) of phosphate-free column operation.

6.2 Recommendations for Future Work

The information gained from this research project provided insights and advanced our understanding of U(VI)-phosphate reactions that can be used to identify and manipulate the conditions that lead to the greatest reductions in U(VI) mobility. Recommended future work includes but is not limited to (1) investigating the effect of phosphate amendment on other sediments at their groundwater

compositions (e.g., Hanford sediments); (2) evaluating the presence of a microbial community and its effects on U-P interactions; (3) performing experiments to evaluate the effect of other co-solutes like potassium and magnesium on uranium-phosphate reactions and resolving the uncertainty regarding their solubility; and (4) developing a model that accounts for adsorption and precipitation for a uranium-phosphate-field sediment system.

Some of the present results involved experiments with sediments from a field site in Rifle, Colorado. It would be interesting to see uranium uptake behavior in a field test of phosphate addition at the actual site. The observations of uranium mobility after phosphate addition was stopped in the laboratory column experiments could be compared with results of extended monitoring in a field experiment after phosphate treatment ended. If uranium concentrations do stay high during the release, additional tests should be conducted to see if continued phosphate loading (relatively small concentrations as compared to initial amendment) helps prevent uranium remobilization.

It will also be helpful to perform a similar set of laboratory experiments with sediments from a field site in Hanford, Washington and to evaluate the effectiveness of phosphate addition for *in situ* uranium immobilization at this site compared to the results obtained for current study using Rifle sediments. It would be particularly interesting to see the effects of precipitation of other phosphate solids (e.g., calcium phosphates) on uranium immobilization as well as on the overall flow dynamics of the system. For systems that undergo extensive precipitation of phosphate solids and

drastic changes in flow patterns, further studies might be needed to design a better phosphate delivery mechanism.

While the primary focus of the present project was on abiotic geochemical reactions and transport processes, microorganisms could play a crucial role in phosphate-based remediation strategies. The presence of phosphate could lead to higher growth of microorganisms, which in turn could lead to higher metabolism and increase in bicarbonate. Microbial cells could also act as sorbent surfaces for uranium or could release orthophosphate by hydrolysis of organic compounds. It would be worth investigating if the U(VI)-phosphates formed on addition of phosphate amendments can be bio-reduced to U(IV)-phosphates which are generally more insoluble. Formation of U(IV)-phosphates may further decrease the uranium mobility in subsurface environment and provide a long term solution for in situ uranium remediation. U(IV)-phosphates have been identified in ore deposits in Japan, North America, Europe, and Asia (Doinikova 2007, Muto et al. 1959) and have also been identified as possible species of microbial U(VI) reduction (Bernier-Latmani et al. 2010, Khijniak et al. 2005). Bioreduction of hydrogen uranyl phosphate (HUP) by metal-reducing bacteria to U(IV)-phosphate species ningyoite [$CaU(PO_4)_2 \cdot H2O$] has also been reported recently which further reduces the uranium solubility and mobility in environment (Rui et al. 2013).

The current study highlighted the effects of sodium and calcium as co-solutes on the products and solubility of uranium-phosphate reactions. However, other cations like potassium and magnesium need to be evaluated since they are present in natural environments and can also form relatively insoluble U(VI)-phosphate solid

like potassium uranyl phosphate (ankoleite) or magnesium uranyl phosphate (saleeite). Moreover, there is significant uncertainty with the current set of thermodynamic constants for these solids. Equilibrium-based batch experiments that approach solubility from precipitation as well as dissolution in conjunction with various solid characterization tools might provide a more accurate set of thermodynamic constants.

Finally, the predictive understanding of equilibrium dissolved U(VI) concentrations on application of phosphate addition in a complex field system is one of the desired goals. It would be highly beneficial to develop an equilibrium-based model that accounts for both adsorption and precipitation for a uranium-phosphate-field sediment system. Generalized composite models have been used to model uranium adsorption on field sediments (Davis et al. 2004, Hyun et al. 2009). A model based on similar lines that also includes phosphate reactions would be required to help predict the uranium concentrations. The developed model could then be combined with precipitation reactions to enable the predictive capabilities. Additionally, the information on K_d values obtained through a set of column experiments can be incorporated into a reactive transport model that includes rates of different processes to model the uranium fate and transport more accurately. Since the column experiments in the current study suggested the occurrence of precipitation, the ultimate goal could be a reactive transport model that could account for precipitation and dissolution reactions in addition to adsorption reactions.

References

Ahmed, B., Cao, B., Mishra, B., Boyanov, M.I., Kemner, K.M., Fredrickson, J.K. and Beyenal, H. (2012) Immobilization of U(VI) from oxic groundwater by Hanford 300 Area sediments and effects of Columbia River water. Water Research 46(13), 3989-3998.

Altschuler, Z.S., Clarke, R.S., Young, E.J. and Commission, U.S.A.E. (1958) Geochemistry of uranium in apatite and phosphorite, U.S. Government Printing Office.

Ankudinov, A.L. and Rehr, J.J. (1997) Relativistic calculations of spin-dependent x-ray-absorption spectra. Physical Review B 56(4), R1712-R1715.

Arai, Y., Marcus, M.A., Tamura, N., Davis, J.A. and Zachara, J.M. (2007) Spectroscopic evidence for uranium bearing precipitates in vadose zone sediments at the hanford 300-area site. Environmental Science and Technology 41(13), 4633-4639.

Arey, J.S., Seaman, J.C. and Bertsch, P.M. (1999) Immobilization of uranium in contaminated sediments by hydroxyapatite addition. Environmental Science and Technology 33(2), 337-342.

Bargar, J.R., Reitmeyer, R. and Davis, J.A. (1999) Spectroscopic confirmation of uranium(VI)-carbonato adsorption complexes on hematite. Environmental Science and Technology 33(14), 2481-2484.

Barnett, M.O., Jardine, P.M., Brooks, S.C. and Selim, H.M. (2000) Adsorption and transport of uranium(VI) in subsurface media. Soil Science Society of America Journal 64(3), 908-917.

Baumann, N., Arnold, T., Geipel, G., Trueman, E.R., Black, S. and Read, D. (2006) Detection of U(VI) on the surface of altered depleted uranium by time-resolved laser-induced fluorescence spectroscopy (TRLFS). Science of the Total Environment 366(2–3), 905-909.

Beazley, M.J., Martinez, R.J., Sobecky, P.A., Webb, S.M. and Taillefert, M. (2009) Nonreductive biomineralization of uranium(VI) phosphate via microbial phosphatase activity in anaerobic conditions. Geomicrobiology Journal 26(7), 431-441.

Beazley, M.J., Martinez, R.J., Webb, S.M., Sobecky, P.A. and Taillefert, M. (2011) The effect of pH and natural microbial phosphatase activity on the speciation of uranium in subsurface soils. Geochimica Et Cosmochimica Acta 75(19), 5648-5663.

Bernhard, G., Geipel, G., Brendler, V. and Nitsche, H. (1998) Uranium speciation in waters of different uranium mining areas. Journal of Alloys and Compounds 271–273(0), 201-205.

Bernhard, G., Geipel, G., Reich, T., Brendler, V. and Amayri, S. (2001) Uranyl(VI) carbonate complex formation: Validation of the $Ca_2UO_2(CO_3)_3$(aq.) species. Radiochimica Acta 89(8/2001), 511-518.

Bernier-Latmani, R., Veeramani, H., Vecchia, E.D., Junier, P., Lezama-Pacheco, J.S., Suvorova, E.I., Sharp, J.O., Wigginton, N.S. and Bargar, J.R. (2010)

Non-uraninite products of microbial U(VI) reduction. Environmental Science and Technology 44(24), 9456-9462.

Bostick, B.C., Fendorf, S., Barnett, M.O., Jardine, P.M. and Brooks, S.C. (2002) Uranyl surface complexes formed on subsurface media from DOE facilities. Soil Science Society of America Journal 66(1), 99-108.

Brusseau, M.L., Hu, Q.H. and Srivastava, R. (1997) Using flow interruption to identify factors causing nonideal contaminant transport. Journal of Contaminant Hydrology 24(3-4), 205-219.

Buck, E.C., Brown, N.R. and Dietz, N.L. (1996) Contaminant uranium phases and leaching at the Fernald site in Ohio. Environmental Science and Technology 30(1), 81-88.

Burns, P.C., Finch, R. and Mineralogical Society of America. (1999) Uranium : mineralogy, geochemistry and the environment, Mineralogical Society of America, Washington, DC.

Butt, C.R.M. and Graham, J. (1981) Sodian potassian hydroxonian meta-autunite- 1st natural occurence of an intermediate member of a predcited solid-solution series. American Mineralogist 66(9-10), 1068-1072.

Campbell, K.M., Kukkadapu, R.K., Qafoku, N.P., Peacock, A.D., Lesher, E., Williams, K.H., Bargar, J.R., Wilkins, M.J., Figueroa, L., Ranville, J., Davis, J.A. and Long, P.E. (2012) Geochemical, mineralogical and microbiological characteristics of sediment from a naturally reduced zone in a uranium-contaminated aquifer. Applied Geochemistry 27(8), 1499-1511.

Campbell, K.M., Veeramani, H., Urich, K.-U., Blue, L.Y., Giammar, D.E., Bernier-Latmani, R., Stubbs, J.E., Suvorova, E., Yabusaki, S., Lezama-Pacheco, J.S., Mehta, A., Long, P.E. and Bargar, J.R. (2011) Oxidative dissolution of biogenic uraninite in groundwater at Old Rifle, CO. Environmental Science and Technology 45(20), 8748-8754.

Catalano, J.G. and Brown Jr., G.E. (2004) Analysis of uranyl-bearing phases by EXAFS spectroscopy: Interferences, multiple scattering, accuracy of structural parameters, and spectral differences. American Mineralogist 89(7), 1004-1021.

Catalano, J.G., McKinley, J.P., Zachara, J.M., Heald, S.M., Smith, S.C. and Brown, G.E. (2006) Changes in uranium speciation through a depth sequence of contaminated Hanford sediments. Environmental Science and Technology 40(8), 2517-2524.

Cerrato, J.M., Ashner, M.N., Alessi, D.S., Lezama-Pacheco, J.S., Bernier-Latmani, R., Bargar, J.R. and Giammar, D.E. (2013) Relative reactivity of biogenic and chemogenic uraninite and biogenic noncrystalline U(IV). Environmental Science and Technology 47(17), 9756-9763.

Cheng, T., Barnett, M.O., Roden, E.E. and Zhuang, J.L. (2004) Effects of phosphate on uranium(VI) adsorption to goethite-coated sand. Environmental Science and Technology 38(22), 6059-6065.

Christoffersen, M.R., Christoffersen, J. and Kibalczyc, W. (1990) Apparent solubilities of 2 amorphous calcium phosphates and of octacalcium phosphate in the temperature range 30-42^{0} C. Journal of Crystal Growth 106(2-3), 349-354.

Cornell, R.M. and Schwertmann, U. (2003) The iron oxides : structure, properties, reactions, occurrences, and uses, Wiley-VCH, Weinheim.

Crane, R.A., Dickinson, M., Popescu, I.C. and Scott, T.B. (2011) Magnetite and zero-valent iron nanoparticles for the remediation of uranium contaminated environmental water. Water Research 45(9), 2931-2942.

Davis, J.A., Meece, D.E., Kohler, M. and Curtis, G.P. (2004) Approaches to surface complexation modeling of uranium(VI) adsorption on aquifer sediments. Geochimica Et Cosmochimica Acta 68(18), 3621-3641.

DOE (1997) Linking Legacies: Connecting the cold war nuclear weapons production processes to their environmental consequences. Office of Environmental Management - The U.S. Department of Energy, Washington, D.C.

DOE (1999) Final site observational work plan for the UMTRA project old rifle site GJO-99-88-TAR. U.S Department of Energy, Grand Junction Office: Grand Junction, Colorado.

Doinikova, O.A. (2007) Uranium deposits with a new phosphate type of blacks. Geology of Ore Deposits 49(1), 80-86.

Dong, W., Tokunaga, T.K., Davis, J.A. and Wan, J. (2011) Uranium(VI) Adsorption and Surface Complexation Modeling onto Background Sediments from the F-Area Savannah River Site. Environmental Science and Technology 46(3), 1565-1571.

Dong, W.M. and Brooks, S.C. (2006) Determination of the formation constants of ternary complexes of uranyl and carbonate with alkaline earth metals

(Mg^{2+}, Ca^{2+}, Sr^{2+}, and Ba^{2+}) using anion exchange method. Environmental Science and Technology 40(15), 4689-4695.

EPA (2001) Use of uranium drinking water standards under 40 CFR 141 and 40 CFR192 as remediation goals for groundwater at CERCLA sites; EPA Directive no. 9283. 1-14.

Ewing, R.C. (1999) Radioactivity and the 20th Century. Reviews in Mineralogy & Geochemistry 38, 1-21.

Fang, Y., Yabusaki, S.B., Morrison, S.J., Amonette, J.P. and Long, P.E. (2009) Multicomponent reactive transport modeling of uranium bioremediation field experiments. Geochimica Et Cosmochimica Acta 73(20).

Fanizza, M.F., Yoon, H., Zhang, C., Oostrom, M., Wietsma, T.W., Hess, N.J., Bowden, M.E., Strathmann, T.J., Finneran, K.T. and Werth, C.J. (2013) Pore-scale evaluation of uranyl phosphate precipitation in a model groundwater system. Water Resources Research 49, 1-17.

Finch, R. and Murakami, T. (1999) Systematics and paragenesis of uranium minerals. Reviews in Mineralogy & Geochemistry 38, 91-179.

Fletcher, K.E., Boyanov, M.I., Thomas, S.H., Wu, Q., Kemner, K.M. and Loeffler, F.E. (2010) U(VI) reduction to mononuclear U(IV) by desulfitobacterium species. Environmental Science and Technology 44(12), 4705-4709.

Fox, P.M., Davis, J.A., Hay, M.B., Conrad, M.E., Campbell, K.M., Williams, K.H. and Long, P.E. (2012) Rate-limited U(VI) desorption during a small-scale tracer test in a heterogeneous uranium-contaminated aquifer. Water Resources Research 48.

Fuller, C.C., Bargar, J.R. and Davis, J.A. (2003) Molecular-scale characterization of uranium sorption by bone apatite materials for a permeable reactive barrier demonstration. Environmental Science and Technology 37(20), 4642-4649.

Fuller, C.C., Bargar, J.R., Davis, J.A. and Piana, M.J. (2002) Mechanisms of uranium interactions with hydroxyapatite: Implications for groundwater remediation. Environmental Science and Technology 36(2), 158-165.

Giammar, D.E. and Hering, J.G. (2001) Time scales for sorption-desorption and surface precipitation of uranyl on goethite. Environmental Science and Technology 35(16), 3332-3337.

Gorman-Lewis, D., Burns, P.C. and Fein, J.B. (2008a) Review of uranyl mineral solubility measurements. Journal of Chemical Thermodynamics 40(3), 335-352.

Gorman-Lewis, D., Fein, J.B., Burns, P.C., Szymanowski, J.E.S. and Converse, J. (2008b) Solubility measurements of the uranyl oxide hydrate phases metaschoepite, compreignacite, Na-compreignacite, becquerelite, and clarkeite. Journal of Chemical Thermodynamics 40(6), 980-990.

Gorman-Lewis, D., Shvareva, T., Kubatko, K.A., Burns, P.C., Wellman, D.M., McNamara, B., Szymanowski, J.E.S., Navrotsky, A. and Fein, J.B. (2009) Thermodynamic properties of autunite, uranyl hydrogen phosphate, and uranyl orthophosphate from solubility and calorimetric measurements. Environmental Science and Technology 43(19), 7416-7422.

Grenthe, I., Wanner, H., Forest, I. and Agency, O.N.E. (1992) Chemical thermodynamics of uranium, North-Holland.

Greskowiak, J., Hay, M.B., Prommer, H., Liu, C., Post, V.E.A., Ma, R., Davis, J.A., Zheng, C. and Zachara, J.M. (2011) Simulating adsorption of U(VI) under transient groundwater flow and hydrochemistry: Physical versus chemical nonequilibrium model. Water Resources Research 47(8), W08501.

Guillaumont, R., Agency, O.N.E. and Mompean, F.J. (2003) Update on the chemical thermodynamics of uranium, neptunium, plutonium, americium and technetium, Elsevier.

Heald, S.M. (2011) Optics upgrades at the APS beamline 20-BM. Nuclear Instruments & Methods in Physics Research Section a-Accelerators Spectrometers Detectors and Associated Equipment 649(1), 128-130.

Heald, S.M., Brewe, D.L., Stern, E.A., Kim, K.H., Brown, F.C., Jiang, D.T., Crozier, E.D. and Gordon, R.A. (1999) XAFS and micro-XAFS at the PNC-CAT beamlines. Journal of Synchrotron Radiation 6, 347-349.

Hsi, C.K.D. and Langmuir, D. (1985) Adsorption of uranyl onto ferric oxyhydroxides - Application of the surface complexation site-binding model. Geochimica Et Cosmochimica Acta 49(9), 1931-1941.

Hudson, E.A., Allen, P.G., Terminello, L.J., Denecke, M.A. and Reich, T. (1996) Polarized x-ray-absorption spectroscopy of the uranyl ion: Comparison of experiment and theory. Physical Review B 54(1), 156-165.

Hyun, S.P., Fox, P.M., Davis, J.A., Campbell, K.M., Hayes, K.F. and Long, P.E. (2009) Surface Complexation Modeling of U(VI) Adsorption by Aquifer

Sediments from a Former Mill Tailings Site at Rifle, Colorado. Environmental Science and Technology 43(24).

Jensen, M.P., Nash, K.L., Morss, L.R., Appelman, E.H. and Schmidt, M.A. (1996) Humic and Fulvic Acids, pp. 272-285, American Chemical Society.

Jerden, J.L. and Sinha, A.K. (2003) Phosphate based immobilization of uranium in an oxidizing bedrock aquifer. Applied Geochemistry 18(6), 823-843.

Jerden, J.L., Sinha, A.K. and Zelazny, L. (2003) Natural immobilization of uranium by phosphate mineralization in an oxidizing saprolite-soil profile: chemical weathering of the Coles Hill uranium deposit, Virginia. Chemical Geology 199(1-2), 129-157.

Jones, T.E., Wood, M.I., Corbin, R.A. and Simpson, B.C. (2001) Preliminary inventory estimates for single-shell tank leaks in B, BX, and BY Tank Farms. RPP-7389.

Kelly, S.D., Hesterberg, D. and Ravel, B. (2008) Methods of Soil Analysis, Part 5 - Mineralogical Methods. Ulery, A.L. and Drees, L.R. (eds), pp. 367-463, Soil Science Society of America, Madison, WI.

Kelly, S.D., Kemner, K.M. and Brooks, S.C. (2007) X-ray absorption spectroscopy identifies calcium-uranyl-carbonate complexes at environmental concentrations. Geochimica Et Cosmochimica Acta 71(4), 821-834.

Khijniak, T.V., Slobodkin, A.I., Coker, V., Renshaw, J.C., Livens, F.R., Bonch-Osmolovskaya, E.A., Birkeland, N.K., Medvedeva-Lyalikova, N.N. and Lloyd, J.R. (2005) Reduction of uranium(VI) phosphate during growth of the

thermophilic bacterium Thermoterrabacterium ferrireducens. Applied and Environmental Microbiology 71(10), 6423-6426.

Kohler, M., Curtis, G.P., Kent, D.B. and Davis, J.A. (1996) Experimental investigation and modeling of uranium(VI) transport under variable chemical conditions. Water Resources Research 32(12), 3539-3551.

Komlos, J., Peacock, A., Kukkadapu, R.K. and Jaffé, P.R. (2008) Long-term dynamics of uranium reduction/reoxidation under low sulfate conditions. Geochimica Et Cosmochimica Acta 72(15), 3603-3615.

Langmuir, D. (1978) Uranium solution-mineral equilibria at low-temperatures with applications to sedimentary ore-deposits. Geochimica Et Cosmochimica Acta 42(6), 547-569.

Langmuir, D. (1997) Aqueous environmental geochemistry, Prentice Hall, Upper Saddle River, N.J.

Lasaga, A.C. (1998) Kinetic theory in the earth sciences, Princeton University Press.

Liu, C.X., Zachara, J.M., Zhong, L.R., Kukkadupa, R., Szecsody, J.E. and Kennedy, D.W. (2005) Influence of sediment bioreduction and reoxidation on uranium sorption. Environmental Science and Technology 39(11), 4125-4133.

Locock, A.J. and Burns, P.C. (2003) The crystal structure of synthetic autunite, $Ca[(UO_2)(PO_4)]_2(H_2O)_{11}$. American Mineralogist 88(1), 240-244.

Locock, A.J., Burns, P.C., Duke, M.J.M. and Flynn, T.M. (2004) Monovalent cations in structures of the meta-autunite group. Canadian Mineralogist 42, 973-996.

Malinowski, E.R. (1977) Determination of number of factors and experimental error in a data matrix. Analytical Chemistry 49(4), 612-617.

Malinowski, E.R. (1978) Theory of error for target factor-analysis with applications to mass-spectrometry and nuclear magnetic-resonance spectrometry. Analytica Chimica Acta-Computer Techniques and Optimization 2(4), 339-354.

Malinowski, E.R. (2002) Factor Analysis in Chemistry, John Wiley, New York.

Manceau, A., Marcus, M.A. and Tamura, N. (2002) Quantitative Speciation of Heavy Metals in Soils and Sediments by Synchrotron X-ray Techniques. Reviews in Mineralogy & Geochemistry 49(1), 341-428.

McCullough, J., Hazen, T. and Benson, S. (1999) Bioremediation of metals and radionuclides: What it is and how it works, p. 45.

Mehta, V.S., Maillot, F., Wang, Z., Catalano, J.G. and Giammar, D.E. (2014) Effect of co-solutes on the products and solubility of uranium(VI) precipitated with phosphate. Chemical Geology 364(0), 66-75.

Meinrath, G. and Kimura, T. (1993) Behavior of U(VI) solids under conditions of natural aquatic systems. Inorganica Chimica Acta 204(1), 79-85.

Miretzky, P. and Fernandez-Cirelli, A. (2008) Phosphates for Pb immobilization in soils: a review. Environmental Chemistry Letters 6(3), 121-133.

Moon, H.S., Komlos, J. and Jaffe, P.R. (2007) Uranium reoxidation in previously bioreduced sediment by dissolved oxygen and nitrate. Environmental Science and Technology 41(13), 4587-4592.

Moon, H.S., McGuinness, L., Kukkadapu, R.K., Peacock, A.D., Komlos, J., Kerkhof, L.J., Long, P.E. and Jaffe, P.R. (2010) Microbial reduction of uranium under iron and sulfate reducing conditions: Effect of amended goethite on microbial community composition and dynamics. Water Research 44(14), 4015-4028.

Morris, D.E., Allen, P.G., Berg, J.M., ChisholmBrause, C.J., Conradson, S.D., Donohoe, R.J., Hess, N.J., Musgrave, J.A. and Tait, C.D. (1996) Speciation of uranium in Fernald soils by molecular spectroscopic methods: Characterization of untreated soils. Environmental Science and Technology 30(7), 2322-2331.

Murakami, T., Ohnuki, T., Isobe, H. and Sato, T. (1997) Mobility of uranium during weathering. American Mineralogist 82(9-10), 888-899.

Muto, T., Hirono, S. and Kurata, H. (1968) Some aspects of fixation of uranium from natural waters, Japan Atomic Energy Research Inst.

Muto, T., Meyrowitz, R., Pommer, A.M. and Murano, T. (1959) Ningyoite, a new aranous phosphate mineral from Japan. Journal Name: Am. Mineralogist; Journal Volume: Vol: 44; Other Information: Orig. Receipt Date: 31-DEC-59, Medium: X; Size: Pages: 633-650.

Newsome, L., Morris, K. and Lloyd, J.R. (2014) The biogeochemistry and bioremediation of uranium and other priority radionuclides. Chemical Geology 363(0), 164-184.

Newville, M. (2001) IFEFFIT: Interactive EXAFS analysis and FEFF fitting. Journal of Synchrotron Radiation 8, 322-324.

NRC (1993) In situ bioremediation: When does it work?, The National Academies Press.

Ohnuki, I., Kozai, N., Samadfam, M., Yasuda, R., Yamamoto, S., Narumi, K., Naramoto, H. and Murakami, T. (2004) The formation of autunite ($Ca(UO_2)_2(PO_4)_2 \cdot nH2_O$)within the leached layer of dissolving apatite: incorporation mechanism of uranium by apatite. Chemical Geology 211(1-2), 1-14.

Palmisano, A. and Hazen, T. (2003) Bioremediation of Metals and Radionuclides: What It Is and How It Works (2nd Edition), p. Medium: ED; Size: 45 pages.

Parker, J.C. and Van Genuchten, M.T. (1984) Determining Transport Parameters from Laboratory and Field Tracer Experiments, Virginia Agricultural Experiment Station.

Payne, T.E., Davis, J.A. and Waite, T.D. (1996) Uranium adsorption on ferrihydrite - Effects of phosphate and humic acid. Radiochimica Acta 74, 239-243.

Qafoku, N.P., Kukkadapu, R.K., McKinley, J.P., Arey, B.W., Kelly, S.D., Wang, C.M., Resch, C.T. and Long, P.E. (2009) Uranium in Framboidal Pyrite from a Naturally Bioreduced Alluvial Sediment. Environmental Science and Technology 43(22), 8528-8534.

Qafoku, N.P., Zachara, J.M., Liu, C.X., Gassman, P.L., Qafoku, O.S. and Smith, S.C. (2005) Kinetic desorption and sorption of U(VI) during reactive transport in a contaminated Hanford sediment. Environmental Science and Technology 39(9), 3157-3165.

Rakovan, J., Reeder, R.J., Elzinga, E.J., Cherniak, D.J., Tait, C.D. and Morris, D.E. (2002) Structural characterization of U(VI) in apatite by X-ray absorption spectroscopy. Environmental Science and Technology 36(14), 3114-3117.

Ravel, B. and Newville, M. (2005) ATHENA, ARTEMIS, HEPHAESTUS: Data analysis for X-ray absorption spectroscopy using IFEFFIT. Journal of Synchrotron Radiation 12, 537--541.

Reardon, E.J. (1981) K_d - Can they be used to describe reversible ion sorption reactions in contaminant migration? Ground Water 19(3), 279-286.

Rui, X., Kwon, M.J., O'Loughlin, E.J., Dunham-Cheatham, S., Fein, J.B., Bunker, B., Kemner, K.M. and Boyanov, M.I. (2013) Bioreduction of Hydrogen Uranyl Phosphate: Mechanisms and U(IV) Products. Environmental Science and Technology 47(11), 5668-5678.

Sani, R.K., Peyton, B.M., Dohnalkova, A. and Amonette, J.E. (2005) Reoxidation of reduced uranium with iron(III) (hydr)oxides under sulfate-reducing conditions. Environmental Science and Technology 39(7), 2059-2066.

Schecher, W.D. and McAvoy, D.C. (2007) MINEQL+, v 4.6: A chemical equilibrium modeling system, Environmental Research Software.

Senko, J.M., Kelly, S.D., Dohnalkova, A.C., McDonough, J.T., Kemner, K.M. and Burgos, W.D. (2007) The effect of U(VI) bioreduction kinetics on subsequent reoxidation of biogenic U(IV). Geochimica Et Cosmochimica Acta 71(19), 4644-4654.

Sharp, J.O., Lezama-Pacheco, J.S., Schofield, E.J., Junier, P., Ulrich, K.-U., Chinni, S., Veeramani, H., Margot-Roquier, C., Webb, S.M., Tebo, B.M., Giammar, D.E., Bargar, J.R. and Bernier-Latmani, R. (2011) Uranium speciation and stability after reductive immobilization in aquifer sediments. Geochimica Et Cosmochimica Acta 75(21), 6497-6510.

Sherman, D.M., Peacock, C.L. and Hubbard, C.G. (2008) Surface complexation of U(VI) on goethite (α-FeOOH). Geochimica Et Cosmochimica Acta 72(2), 298-310.

Simon, F.G., Biermann, V. and Peplinski, B. (2008) Uranium removal from groundwater using hydroxyapatite. Applied Geochemistry 23(8), 2137-2145.

Singer, D.M., Zachara, J.M. and Brown, G.E. (2009) Uranium speciation as a function of depth in contaminated Hanford sediments - A micro-XRF, micro-XRD, and micro- and bulk-XAFS study. Environmental Science and Technology 43(3), 630-636.

Singh, A. (2010) Geochemical Conditions Affecting Uranium(VI) Fate And Transport In Soil And Groundwater In The Presence Of Phosphate, Washington University in St. Louis, p. 324.

Singh, A., Catalano, J.G., Ulrich, K.U. and Giammar, D.E. (2012) Molecular-scale structure of uranium(VI) immobilized with goethite and phosphate. Environmental Science and Technology 46(12), 6594-6603.

Singh, A., Ulrich, K.U. and Giammar, D.E. (2010) Impact of phosphate on U(VI) immobilization in the presence of goethite. Geochimica Et Cosmochimica Acta 74(22), 6324-6343.

Sowder, A.G., Clark, S.B. and Fjeld, R.A. (2001) The impact of mineralogy in the U(VI)-Ca-PO_4 system on the environmental availability of uranium. Journal of Radioanalytical and Nuclear Chemistry 248(3), 517-524.

Stewart, B.D., Mayes, M.A. and Fendorf, S. (2010) Impact of Uranyl-Calcium-Carbonato Complexes on Uranium(VI) Adsorption to Synthetic and Natural Sediments. Environmental Science and Technology 44(3), 928-934.

Stubbs, J.E., Veblen, L.A., Elbert, D.C., Zachara, J.M., Davis, J.A. and Veblen, D.R. (2009) Newly recognized hosts for uranium in the Hanford Site vadose zone. Geochimica Et Cosmochimica Acta 73(6), 1563-1576.

Stumm, W. and Morgan, J.J. (1996) Aquatic chemistry : chemical equilibria and rates in natural waters, Wiley, New York.

Tang, G., Mayes, M.A., Parker, J.C., Yin, X.L., Watson, D.B. and Jardine, P.M. (2009) Improving parameter estimation for column experiments by multi-model evaluation and comparison. Journal of Hydrology 376(3-4), 567-578.

Tessier, A., Campbell, P.G.C. and Bisson, M. (1979) Sequential extraction procedure for the speciation of particulate trace-metals. Analytical Chemistry 51(7), 844-851.

Toride, N., Leij, F.J. and van Genuchten, M.T. (1995) The CXTFIT Code for Estimating Transport Parameters from Laboratory or Field Tracer Experiments. Version 2.0.

Tripathi, V.S. (1984) Uranium(VI) transport modeling: geochemical data and submodels, Department of Applied Earth Sciences, p. 319, Stanford University, California.

Vermeul, V.R., Bjornstad, B.N., Fritz, B.G., Fruchter, J.S., Mackley, R.D., Newcomer, D.R., Mendoza, D.P., Rockhold, M.L., Wellman, D.M. and Williams,

M.D. (2009) 300 Area Uranium Stabilization Through Polyphosphate Injection: Final Report.

Vesely, V., Pekarek, V. and Abbrent, M. (1965) A study on uranyl phosphates-III solubility products of uranyl hydrogen phosphate, uranyl orthophosphate and some alkali uranyl phosphates. Journal of Inorganic and Nuclear Chemistry 27(5), 1159-1166.

Wang, Z., Lee, S.-W., Kapoor, P., Tebo, B.M. and Giammar, D.E. (2013) Uraninite oxidation and dissolution induced by manganese oxide: A redox reaction between two insoluble minerals. Geochimica Et Cosmochimica Acta 100(1), 24-40.

Wang, Z., Tebo, B.M. and Giammar, D.E. (2014) Effects of Mn(II) on UO2 Dissolution under Anoxic and Oxic Conditions. Environmental Science and Technology 48(10), 5546-5554.

Wang, Z.M. and Giammar, D.E. (2013) Mass Action Expressions for Bidentate Adsorption in Surface Complexation Modeling: Theory and Practice. Environmental Science and Technology 47(9), 3982-3996.

Wang, Z.M., Zachara, J.M., Boily, J.F., Xia, Y.X., Resch, T.C., Moore, D.A. and Liu, C. (2011) Determining individual mineral contributions to U(VI) adsorption in a contaminated aquifer sediment: A fluorescence spectroscopy study. Geochimica Et Cosmochimica Acta 75(10), 2965-2979.

Wang, Z.M., Zachara, J.M., Gassman, P.L., Liu, C.X., Qafoku, O., Yantasee, W. and Catalano, J.G. (2005) Fluorescence spectroscopy of U(VI)-silicates and U(VI)-contaminated Hanford sediment. Geochimica Et Cosmochimica Acta 69(6), 1391-1403.

Wang, Z.M., Zachara, J.M., Yantasee, W., Gassman, P.L., Liu, C.X. and Joly, A.G. (2004) Cryogenic laser induced fluorescence characterization of U(VI) in hanford vadose zone pore waters. Environmental Science and Technology 38(21), 5591-5597.

Wasserman, S.R., Allen, P.G., Shuh, D.K., Bucher, J.J. and Edelstein, N.M. (1999) EXAFS and principal component analysis: a new shell game. Journal of Synchrotron Radiation 6, 284-286.

Webb, S.M. (2005) SIXPack: A graphical user interface for XAS analysis using IFEFFIT. Physica Scipta T115, 1011-1014.

Wellman, D.M., Catalano, J.G., Icenhower, J.P. and Gamerdinger, A.P. (2005) Synthesis and characterization of sodium meta-autunite, $NaUO_2PO_4 \cdot 3H2_O$. Radiochimica Acta 93(7), 393-399.

Wellman, D.M., Glovack, J.N., Parker, K., Richards, E.L. and Pierce, E.M. (2008) Sequestration and retention of uranium(VI) in the presence of hydroxylapatite under dynamic geochemical conditions. Environmental Chemistry 5(1), 40-50.

Wellman, D.M., Gunderson, K.M., Icenhower, J.P. and Forrester, S.W. (2007) Dissolution kinetics of synthetic and natural meta-autunite minerals, $X_{3-n}^{(n)+}[(UO_2)(PO_4)]_2 \cdot xH_2O$, under acidic conditions. Geochemistry Geophysics Geosystems 8, 1-16.

Wellman, D.M., Icenhower, J.P. and Owen, A.T. (2006) Comparative analysis of soluble phosphate amendments for the remediation of heavy metal contaminants: Effect on sediment hydraulic conductivity. Environmental Chemistry 3(3), 219-224.

Wright, K.E., Hartmann, T. and Fujita, Y. (2011) Inducing mineral precipitation in groundwater by addition of phosphate. Geochemical Transactions 12.

Wu, W.-M., Carley, J., Luo, J., Ginder-Vogel, M.A., Cardenas, E., Leigh, M.B., Hwang, C., Kelly, S.D., Ruan, C., Wu, L., Van Nostrand, J., Gentry, T., Lowe, K., Mehlhorn, T., Carroll, S., Luo, W., Fields, M.W., Gu, B., Watson, D., Kemner, K.M., Marsh, T., Tiedje, J., Zhou, J., Fendorf, S., Kitanidis, P.K., Jardine, P.M. and Criddle, C.S. (2007) In situ bioreduction of uranium (VI) to submicromolar levels and reoxidation by dissolved oxygen. Environmental Science and Technology 41(16), 5716-5723.

Xie, L. and Giammar, D.E. (2007) Equilibrium solubility and dissolution rate of the lead phosphate chloropyromorphite. Environmental Science and Technology 41(23), 8050-8055.

Yabusaki, S.B., Fang, Y., Long, P.E., Resch, C.T., Peacock, A.D., Komlos, J., Jaffe, P.R., Morrison, S.J., Dayvault, R.D., White, D.C. and Anderson, R.T. (2007) Uranium removal from groundwater via in situ biostimulation: Field-scale modeling of transport and biological processes. Journal of Contaminant Hydrology 93(1-4).

Yang, X., Zhang, L., Chen, X., Yang, G., Gao, C., Yang, H. and Gou, Z. (2012) Trace element-incorporating octacalcium phosphate porous beads via polypeptide-assisted nanocrystal self-assembly for potential applications in osteogenesis. Acta biomaterialia 8(4), 1586-1596.

Zachara, J.M., Davis, J.A., Liu, C.X., McKinley, J.P., Qafoku, N.P., Wellman, D.M. and Yabusaki, S.B. (2005) Uranium geochemistry in vadose zone and aquifer

sediments from the 300 area uranium plume; PNNL-15121; Pacific Northwest National Laboratory: Richland, WA.

Zheng, Z.P., Wan, J.M., Song, X.Y. and Tokunaga, T.K. (2006) Sodium meta-autunite colloids: Synthesis, characterization, and stability. Colloids and Surfaces a-Physicochemical and Engineering Aspects 274(1-3), 48-55.

Appendix A. Relevant thermodynamic data

Table A.1. Relevant aqueous reactions and stability constants at 298 K and I = 0 M

Reaction	Log K[a]
Uranium hydrolysis:	
$UO_2^{2+} + H_2O = UO_2OH^+ + H^+$	-5.25
$UO_2^{2+} + 2H_2O = UO_2(OH)_{2(aq)} + 2H^+$	-12.15
$UO_2^{2+} + 3H_2O = UO_2(OH)_3^- + 3H^+$	-20.25
$UO_2^{2+} + 4H_2O = UO_2(OH)_4^{2-} + 4H^+$	-32.40
$2UO_2^{2+} + H_2O = (UO_2)_2OH^{3+} + H^+$	-2.70
$2UO_2^{2+} + 2H_2O = (UO_2)_2(OH)_2^{2+} + 2H^+$	-5.62
$3UO_2^{2+} + 4H_2O = (UO_2)_3(OH)_4^{2+} + 4H^+$	-11.90
$3UO_2^{2+} + 5H_2O = (UO_2)_3(OH)_5^+ + 5H^+$	-15.55
$3UO_2^{2+} + 7H_2O = (UO_2)_3(OH)_7^- + 7H^+$	-32.20
$4UO_2^{2+} + 7H_2O = (UO_2)_4(OH)_7^+ + 7H^+$	-21.90
Uranyl phosphates:	
$UO_2^{2+} + PO_4^{3-} = UO_2PO_4^-$	13.23
$UO_2^{2+} + PO_4^{3-} + H^+ = UO_2HPO_{4(aq)}$	19.59
$UO_2^{2+} + PO_4^{3-} + 2H^+ = UO_2H_2PO_4^+$	22.82
$UO_2^{2+} + PO_4^{3-} + 3H^+ = UO_2H_3PO_4^{2+}$	22.46
$UO_2^{2+} + 2PO_4^{3-} + 4H^+ = UO_2(H_2PO_4)_{2(aq)}$	44.04
$UO_2^{2+} + 2PO_4^{3-} + 5H^+ = UO_2(H_2PO_4)(H_3PO_4)^+$	45.05
Uranyl Carbonates:	
$UO_2^{2+} + CO_3^{2-} = UO_2CO_{3(aq)}$	9.94
$UO_2^{2+} + 2CO_3^{2-} = UO_2(CO_3)_2^{2-}$	16.61
$UO_2^{2+} + 3CO_3^{2-} = UO_2(CO_3)_3^{4-}$	21.84
$3UO_2^{2+} + 6CO_3^{2-} = (UO_2)_3(CO_3)_6^{6-}$	54.00
$2UO_2^{2+} + 3H_2O + CO_3^{2-} = (UO_2)_2CO_3(OH)_3^- + 3H^+$	-0.86
$3UO_2^{2+} + 3H_2O + CO_3^{2-} = (UO_2)_3CO_3(OH)_3^+ + 3H^+$	0.65
$11UO_2^{2+} + 12H_2O + 6CO_3^{2-} = (UO_2)_{11}(CO_3)_6(OH)_{12}^{2-} + 6H^+$	36.41

$UO_2^{2+} + 2Ca^{2+} + 3CO_3^{2-} = Ca_2UO_2(CO_3)_{3(aq)}$	30.70[b]
$UO_2^{2+} + Ca^{2+} + 3CO_3^{2-} = CaUO_2(CO_3)_3^{2-}$	27.18[b]
Uranyl Nitrates:	
$UO_2^{2+} + NO_3^- = UO_2NO_3^+$	0.30
Phosphate acid-base:	
$PO_4^{3-} + H^+ = HPO_4^{2-}$	12.35
$PO_4^{3-} + 2H^+ = H_2PO_4^-$	19.56
$PO_4^{3-} + 3H^+ = H_3PO_{4(aq)}$	21.70
Carbonate acid-base:	
$CO_3^{2-} + H^+ = HCO_3^{2-}$	10.327
$CO_3^{2-} + 2H^+ = H_2CO_3^*{}_{(aq)}$	16.68
$CO_3^{2-} + 2H^+ = CO_{2(g)} + H_2O$	18.152

[a] From (Guillaumont et al. 2003) unless otherwise noted
[b] From (Dong and Brooks 2006)

Table A.2. Relevant solids and their solubility products at 298 K and I = 0 M

Uranium solids:	**Log K**	**Mineral name**
$UO_3 \cdot 2H_2O_{(s)} + 2H^+ = UO_2^{2+} + 3H_2O$	5.60[a]	Metaschoepite
$UO_3 \cdot 2H_2O_{(s)} + 2H^+ = UO_2^{2+} + 3H_2O$	4.81[b]	Schoepite
$UO_2HPO_4 \cdot 4H_2O_{(s)} = UO_2^{2+} + H^+ + PO_4^{3-} + 4H_2O$	-25.50[c]	Chernikovite
$(UO_2)_3(PO_4)_2 \cdot 4H_2O_{(s)} = 3UO_2^{2+} + 2PO_4^{3-} + 4H_2O$	-49.36[b,c]	Uranyl-orthophosphate
$UO_2(H_2PO_4)_2 \cdot 3H_2O_{(s)} = UO_2^{2+} + 4H^+ + 2PO_4^{3-} + 3H_2O$	-45.10[b]	Uranylphosphate
$Ca(UO_2)_2(PO_4)_{2(s)} = 2UO_2^{2+} + Ca^{2+} + 2PO_4^{3-}$	-48.36[c]	Autunite
$Na_2(UO_2)_2(PO_4)_{2(s)} = 2UO_2^{2+} + 2Na^+ + 2PO_4^{3-}$	-47.41[d]	Sodium autunite
$UO_2CO_{3(s)} = UO_2^{2+} + CO_3^{2-}$	-14.76[e]	Rutherfordine
$Ca(PO_4)_{0.74}H_{0.22(s)} = Ca^{2+} + 0.22H^+ + 0.74PO_4^{3-}$	-13.102[f]	Octacalcium phosphate
$Ca_5(PO_4)_3OH + H^+ = 5\,Ca^{2+} + 3PO_4^{3-} + H_2O$	-44.33[g]	Hydroxylapatite

[a] From Gorman-Lewis et al., (2008b)
[b] From Grenthe et al., (1992)
[c] From Gorman-Lewis et al., (2009)
[d] The values of Log K for sodium autunite were reported by Langmuir (1978). The author had calculated the Log K values of various autunites using the ΔG_f^0 values reported by Muto et al., (1968)
[e] From Meinrath and Kimura (1993)
[f] Van't Hoff equation was used to calculate the Log K values at 298 K using the $\Delta H°$ values and the Log K values at 303 K reported by Christoffersen et al. (1990)
[g] From Schecher and McAvoy (2007)

Appendix B. Additional batch experiments using simulated groundwater

Batch equilibrium experiments were conducted to evaluate uranium-phosphate interactions with simulated groundwater composition (Table B.1) of field sites in Rifle, Colorado and Hanford, Washington (Campbell et al. 2011, DOE 1999, Zachara et al. 2005). Experiments were performed in capped stirred glass reactors (250 mL) at room temperature (22±0.5 °C). A reactor bottle was sacrificed at 0, 1, 4 and 10 d for aqueous and solid phase measurements using the methods described in Chapter 2.

Excess phosphate (1000 µM to provide a molar ratio of P:U of 10:1) was added to solutions. The high P:U ratio provided favorable conditions for the solutions to be supersaturated with respect to uranyl phosphate solids. Excess phosphate relative to uranium would also be used in remediation strategies to promote precipitation and overcome other pathways for phosphate removal such as adsorption to sediment minerals, precipitation of phosphate containing non uranyl compounds like calcium-phosphate.

Table B.1: Composition of Simulated Hanford Groundwater (SHGW) and Simulated Rifle Groundwater used for the batch experiments.

Constituent	SHGW	SRGW
pH	8.07	7.10
	Concentration (mM)	
Na	2.00/3.85[a]	11.00/12.57[a]
Ca	1.00	5.00
Mg	0.50	4.94
K	0.20	0.33
U(VI)[b]	0.10	0.10
DIC[c]	1.00	7.44
SO_4	1.45	10.78
Cl	1.00	3.00
NO_3	0.50	0.53
$Si(OH)_4$	0.50	0.28
PO_4	1.00	1.00
Ionic strength	8.56	52.36

[a] Increased concentrations as a result of phosphate amendment by adding salts of sodium phosphate.

[b] Uranium concentrations of 100 μM were selected to provide sufficient solid mass for performing solids characterization at the end of the experiment.

[c] DIC stands for dissolved inorganic carbon

Aqueous phase analysis: Figure B.1 represents the concentrations of major constituents (U, P, Ca and Na) observed as a function of time following phosphate addition. Results clearly show that phosphate addition effectively removed uranium from both SHGW and SRGW solution within 10 days of reaction. The uranium concentrations reached levels of 0.2 μM for SHGW as compared to 3.9 μM for SRGW. Uptake of phosphorus, calcium and sodium was less extensive as compared to uranium. The phosphorus removal was however much more than would be expected stoichiometrically for uranyl phosphate precipitation. This observation

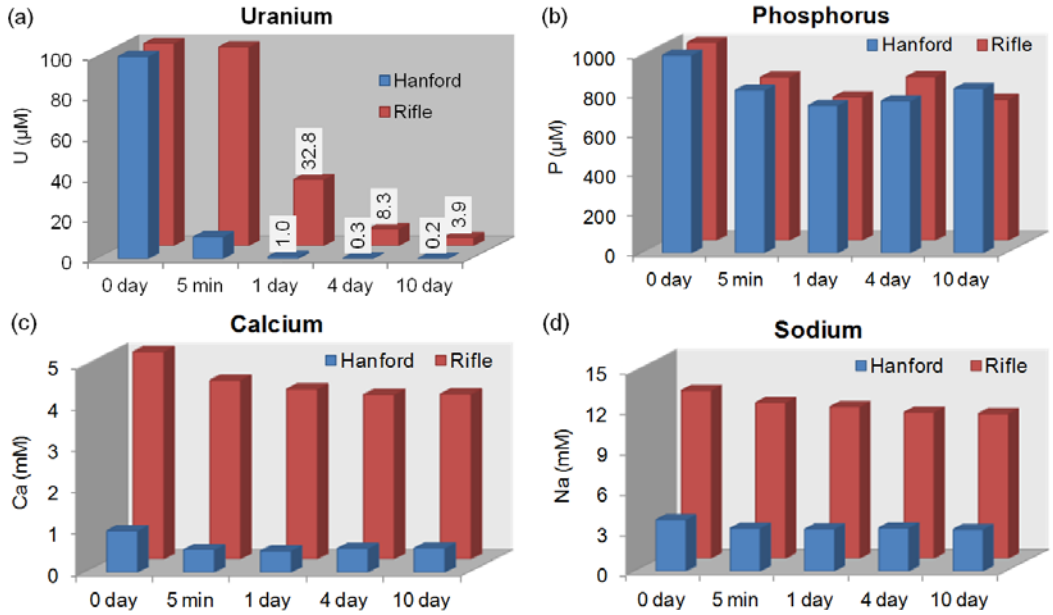

Figure B.1. Concentration profiles for uranium (a), phosphorus (b), calcium (c) and sodium (d) observed as a function of time for both Hanford (SHGW) and Rifle (SRGW) batch studies.

along with the decreasing trends for calcium and sodium suggest that different types of solids must have formed.

To further examine what solids may have formed, saturation index calculations (SI) were carried out for the starting compositions of SHGW and SRGW. The calculations were done using the set of reactions and the respective formation constants shown in Table A.1 and A.2. The SI values suggested that the solution was supersaturated with different solids (Table B.2) initially on addition of phosphate amendment. For SRGW, The SI calculations suggest that the solution was undersaturated with respect to saleeite and anhydrite and supersaturated with respect to autunite and sodium autunite. For SHGW, the solution was supersaturated with respect to saleeite, autunite and sodium autunite. Both the solutions were also supersaturated with various calcium-phosphate solids.

Table B.2: Saturation indices for starting composition of SHGW and SRGW

Saturation Index	SHGW	SRGW
Metaschoepite [$UO_3 \cdot 2H_2O$]	-1.63	-4.33
Rutherfordine [UO_2CO_3]	-2.82	-3.64
Chernikovite [$UO_2HPO_4 \cdot 4H_2O$]	-2.16	-3.39
Uranyl orthophosphate [$(UO_2)_3(PO_4)_2 \cdot 4H_2O$]	-1.97	-7.15
Saleeite [$Mg(UO_2)_2(PO_4)_2$]	0.93	-2.6
Sodium autunite [$Na_2(UO_2)_2(PO_4)_2$]	3.38	0.03
Autunite [$Ca(UO_2)_2(PO_4)_2$]	5.95	2.08
Anhydrite [$CaSO_4$]	-1.78	-0.58
Octacalcium phosphate [$Ca(PO_4)_{0.74}H_{0.22}$]	2.60	2.28
Calcium phosphate [$Ca_3(PO_4)_2$]	4.41	3.08
Hydroxylapatite [$Ca_5(PO_4)_3OH$]	14.05	11.30

XRD and SEM analysis: X-ray spectra of solids obtained at the end of the experiment (10 d) confirmed the presence of multiple solids (Figure B.2) for the SRGW sample. The XRD pattern included the features that suggested the presence of magnesium autunite (saleeite), anhydrite, and some other solids. SEM-EDS analysis on the other hand clearly suggested the presence of at least two different types of solids. One type had needle shaped structures and were much smaller than 1 μm in size, and the other type were thin plate like structures with sizes greater than 1 μm (Figure B.3). The needle shaped solids contained higher amounts of calcium, phosphate and sodium as confirmed through EDS whereas the plates had higher contents of uranium, phosphate and magnesium and relatively smaller contents of sodium and calcium. The needle shaped structures could be the anhydrite formed during the experiment whereas the thin plates have typical characteristics of autunite

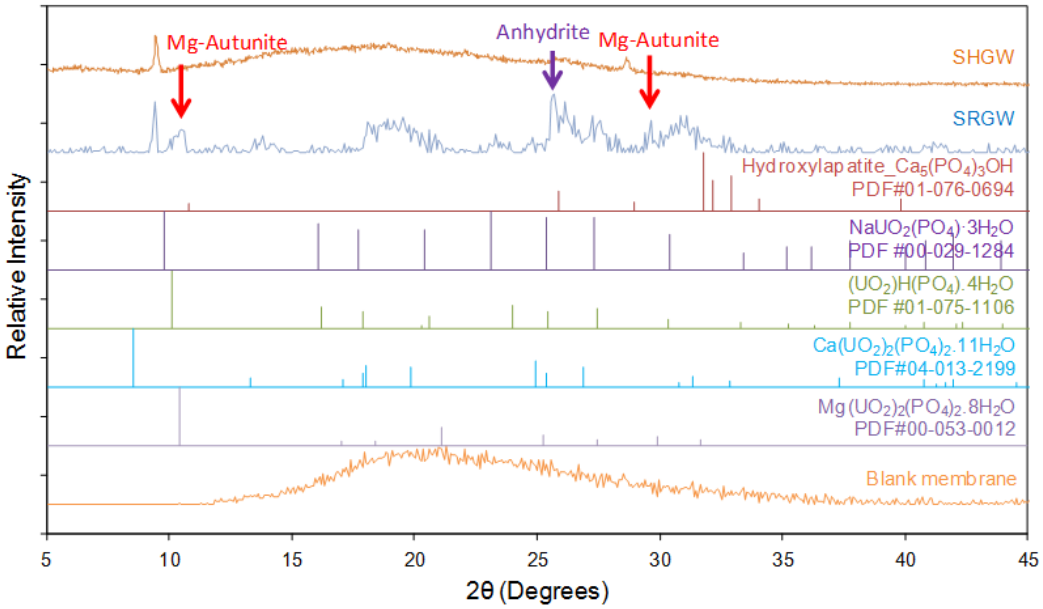

Figure B.2. X-ray diffraction patterns of solids collected after 10 days of reaction following phosphate addition to SHGW and SRGW composition. For reference, the standard patterns obtained from the International Crystal Diffraction Database with the respective PDF card numbers are included. A spectrum of blank membrane filter onto which solids were collected via vacuum filtration and used for analyzing the samples is also included.

group of minerals (Chapter 2) and suggest the formation of autunite as the dominant uranium removal pathway.

For SHGW though, the XRD pattern (Figure B.2) only showed two distinct peaks along with a broad membrane background. The strongest peak observed at around 10° matched well with the peak observed from SRGW, however both these peaks did not match correctly with any of the reference peaks. Both these peaks were very close to that of other autunite minerals peaks and this minor shift could have possibly occurred due to different extent of hydration of the interlayers of the autunite solids. SEM analysis for SHGW solids did not provide any information on the shape and morphology of the solids [Figure B.3]. EDS analysis however suggested the presence of calcium, phosphate and uranium with U:Ca:P ratios of

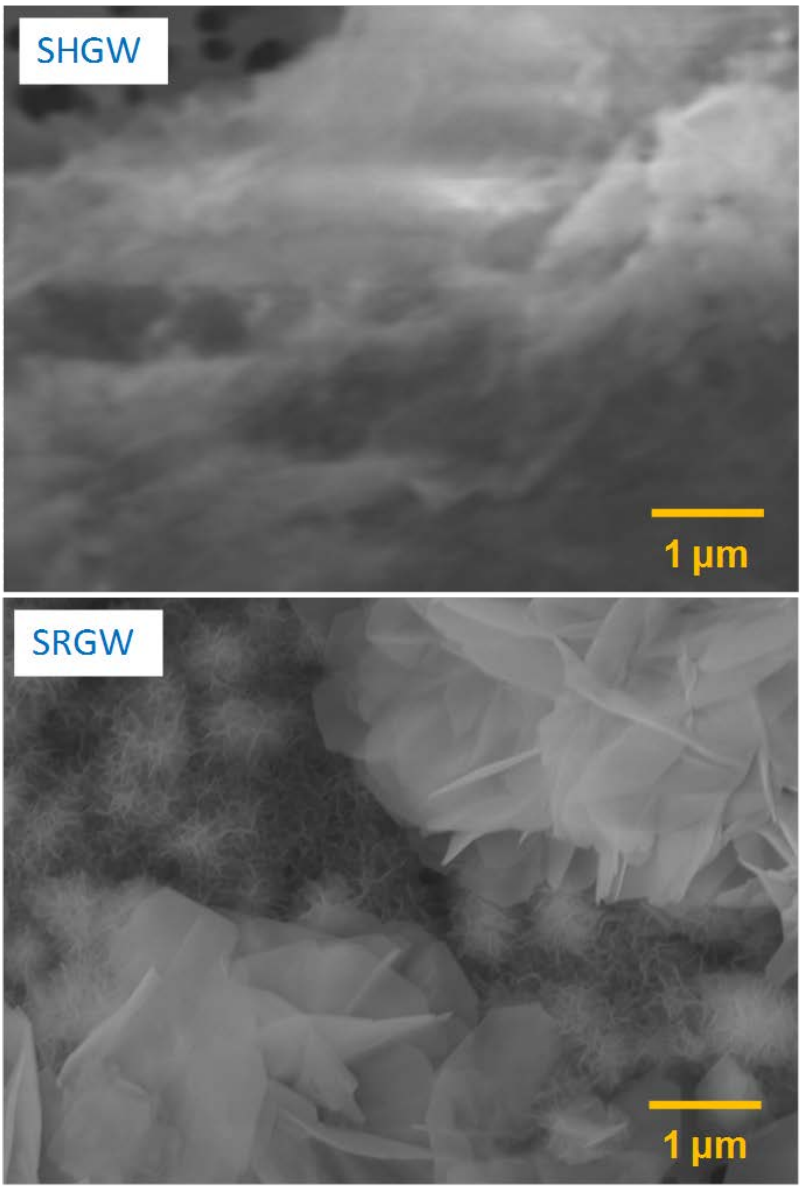

Figure B.3. Scanning electron microscopy (SEM) images of the solids collected after 10 days of reaction following phosphate addition to SHGW (top image) and SRGW (bottom image) composition.

1.00:1.63:2.35 suggesting the presence of calcium phosphate minerals which is in agreement with SI calculations. Stoichiometrically, the U:Ca:P ratios for autunite are expected to be 2:1:2.

The observations thus suggest that phosphate was effective in removing uranium from solution phase possibly via a combination of different mechanisms.

While uranyl phosphate (different autunite group minerals) precipitation seems to be the dominant mechanism in case of SRGW, the removal might have occurred through combination of autunite precipitation, adsorption or incorporation of uranium on calcium phosphates formed during the reaction in case of SHGW. Further detailed characterization studies would be needed to quantify the mode of immobilization and to evaluate whether similar results are obtained with lower starting concentration of uranium. With lower starting uranium concentrations, the solutions will remain highly undersaturated with respect to various uranyl phosphate solids and might not result in any uranyl phosphate precipitation. Under those conditions, adsorption and/or incorporation of uranium onto calcium-phosphates might be the primary removal mechanism as seen from results of Chapter 3. Experiments with lower starting uranium concentrations would also provide some insights on the critical saturation index required to overcome the energy barrier of nucleation.

Appendix C. Equilibrium-based model for solid-water partitioning in U(VI)-PO_4^{3-}-goethite system

The experiments for the U(VI)-PO_4^{3-}-Goethite system for different pH conditions (pH 4, 6, and 8) and at different solid loadings (0.15, 0.6, 1 g/L) were performed by a collaborator on this project, Dr. Fabien Maillot, when he was working in Professor Catalano's laboratory. The experimental data were then used to develop the model presented in this appendix. Goethite was synthesized using the methods described previously (Cornell and Schwertmann 2003). A separate batch of goethite which was synthesized by Singh et al. (2010) had been previously characterized and resulted in a specific surface area (SSA) of 39.9 m^2/g. A constant capacitance model was then developed considering these values and a site density (N) of 1.68 sites/nm^2 was then obtained using a fitting exercise that provided the best fit to the data (Singh et al. 2010). For the current study, the SSA of the synthesized solids was assumed to be similar to that in the previous study. Similarly, the site density values obtained by the fitting exercise for the previous study (Singh et al. 2010) were used for the current model.

An equilibrium model was used to examine the solid-water partitioning of uranium and phosphate to the goethite over a range of conditions that spanned those for which adsorption and precipitation were expected. Different solid loadings (0.15, 0.6 and 1 g/L) were used to calculate the respective total surface site concentrations in mol/L. In contrast to the previous study, the present work used a diffuse double-layer model (DDLM). The model was implemented in MINEQL+ 4.6 (Schecher and McAvoy 2007). The model includes two acid-base reactions on the goethite surface, three monodentate phosphate adsorption reactions, one bidentate uranyl adsorption reaction, a ternary uranyl-phosphate-goethite surface complexation reaction, relevant precipitation reactions, and a number of aqueous acid-base and complexation reactions. The aqueous reactions used in the model are listed in Appendix A. The surface complexation reactions and the relevant precipitation reactions used in this model are listed in Table C.1.

The bidentate surface complexation reaction has not yet been implemented in the model in the most appropriate manner. First, the mole balance for the site concentration is set up so that the bidentate surface complex will only occupy one site and not the two that is expected. This occurs because in MINEQL the same coefficients are used for species in the mole balance and mass action equations. This leads to the second sub-optimal part of the model implementation. For the bidentate adsorption reaction, an exponent of 1 was used for the molar-based activity of $\equiv Fe(OH)_2$ in the mass action expression. This will introduce less error than using an exponent of 2 and the molar-based activity, but improvements can be made to allow for proper handling of both the mole balance and mass action expressions (Wang and

Giammar 2013). Since the input equilibrium constants in MINEQL are with respect to a standard state of 1 mol/L and are not intrinsically independent of the specific surface areas and the site densities as could be achieved using a model for which surface species activities are determined based on fractional site occupancy, further work is needed to optimize the model with improved equilibrium constants that account for the complexity of including surface reactions in a model that also includes aqueous reactions.

Table C.1. Surface complexation reactions, precipitation reactions and their stability constants included in the model at 298 K and I = 0 M

Equilibrium Reactions	**Log K_{int}**[a]	
Goethite protonation and deprotonation		
$\equiv FeOH + H^+ \rightleftharpoons \equiv FeOH_2^+$	7.58	
$\equiv FeOH \rightleftharpoons \equiv FeO^- + H^+$	-9.62	
Phosphate adsorption		
$\equiv FeOH + 3H^+ + PO_4^{3-} \rightleftharpoons \equiv FePO_4H_2 + H_2O$	32.27	
$\equiv FeOH + 2H^+ + PO_4^{3-} \rightleftharpoons \equiv FePO_4H^- + H_2O$	26.83	
$\equiv FeOH + H^+ + PO_4^{3-} \rightleftharpoons \equiv FePO_4^{2-} + H_2O$	19.64	
Uranyl adsorption		
$\equiv Fe(OH)_2 + UO_2^{2+} \rightleftharpoons \equiv FeO_2UO_2 + 2H^+$	-4.36	
Uranyl phosphate ternary complex		
$\equiv FeOH + UO_2^{2+} + H^+ + PO_4^{3-} \rightleftharpoons \equiv FePO_4UO_2 + H_2O$	30.49	
Relevant precipitation reactions	**Log K_{sp}**[a]	**Mineral**
$2UO_2^{2+} + 2Na^+ + 2PO_4^{3-} \rightleftharpoons Na_2(UO_2)_2(PO_4)_{2(s)}$	47.41	Na-autunite
$UO_2^{2+} + H^+ + PO_4^{3-} + 4H_2O \rightleftharpoons UO_2HPO_4.4H_2O_{(s)}$	25.52	Chernikovite
$UO_2^{2+} + 3H_2O \rightleftharpoons UO_3.2H_2O_{(s)} + 2H^+$	-5.60	Metaschoepite

[a] Molar concentration based equilibrium constants, as input in MINEQL (I = 0 M, @ 298 K). These constants for surface reactions correspond to the site density (N = 1.68 sites/nm^2) and specific surface area (A = 39.9 m^2/g).

Results: The fittings for the model developed for different solid loadings, different pH and varying phosphate concentrations are presented as isotherm-style plots and shown in Figures C.1 – C.7. Additionally, the observed data and model predictions were plotted as adsorption edge style plots showing % uranium uptake as a function of pH as shown in Figure C.8.

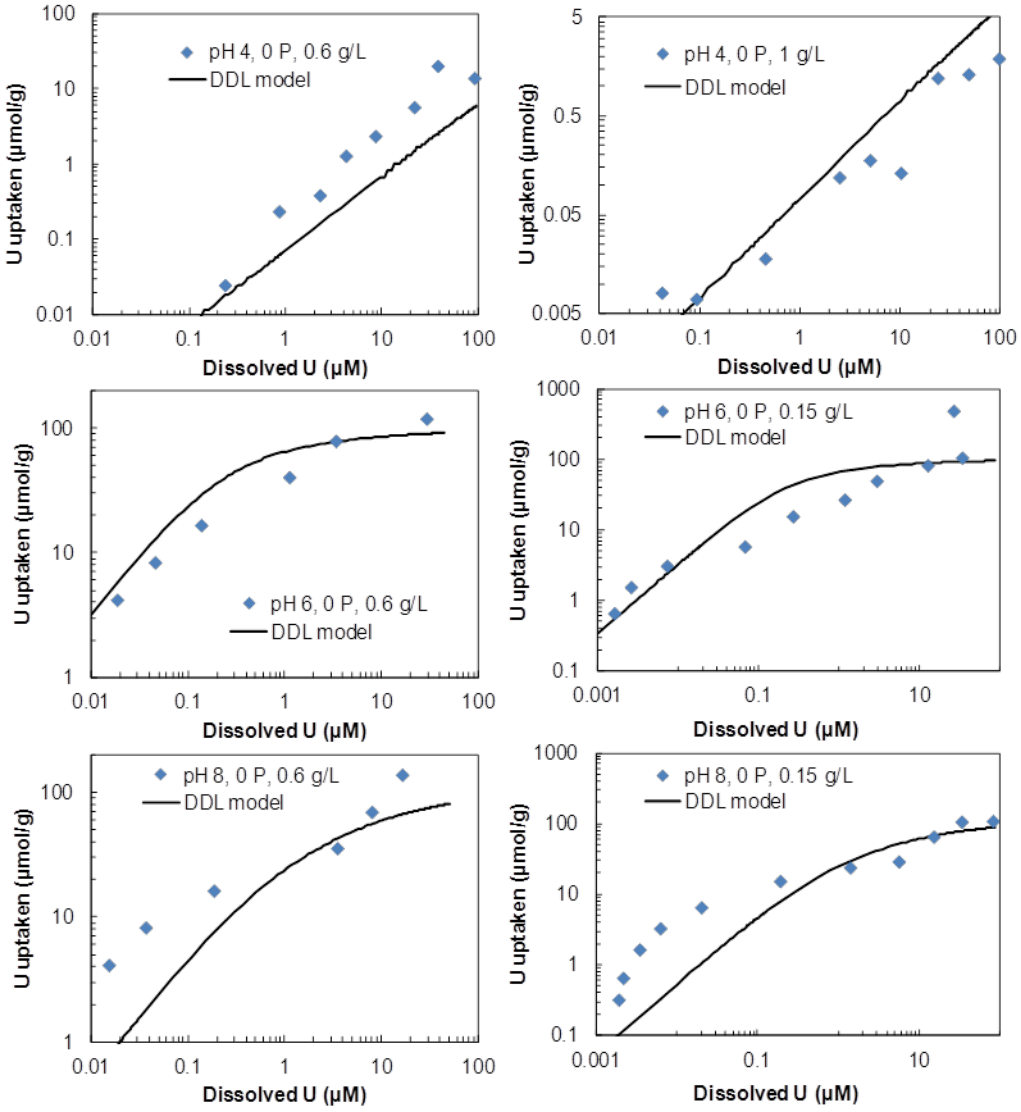

Figure C.1. U(VI) sorption at pH 4 (goethite solid loading of 0.6 and 1.0 g/L), pH 6 and pH 8 (goethite solid loading of 0.60 and 0.15 g/L) in the absence of phosphate. The datapoints represent the observed concentrations for starting U(VI) concentrations of 0 – 100 µM. The solid line represents the diffuse double layer model predictions.

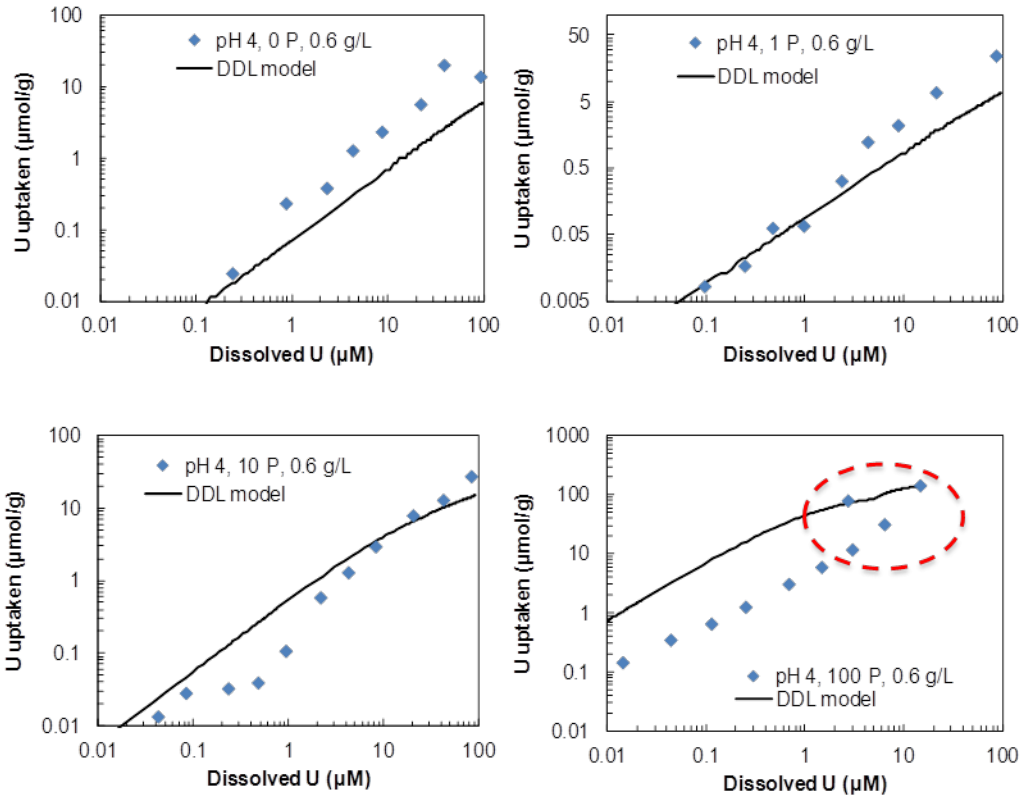

Figure C.2. U(VI sorption at pH 4, goethite solid loading of 0.60 g/L and starting phosphate concentrations of 0, 1, 10 and 100 µM. The datapoints represent the observed concentrations for starting U(VI) concentrations of 0 – 100 µM. The solid line represents the diffuse double layer model predictions. SI calculations were made using the measured dissolved concentrations of uranium, phosphate and sodium. The dotted oval shows datapoints for which SI calculations suggested that a precipitate might have formed.

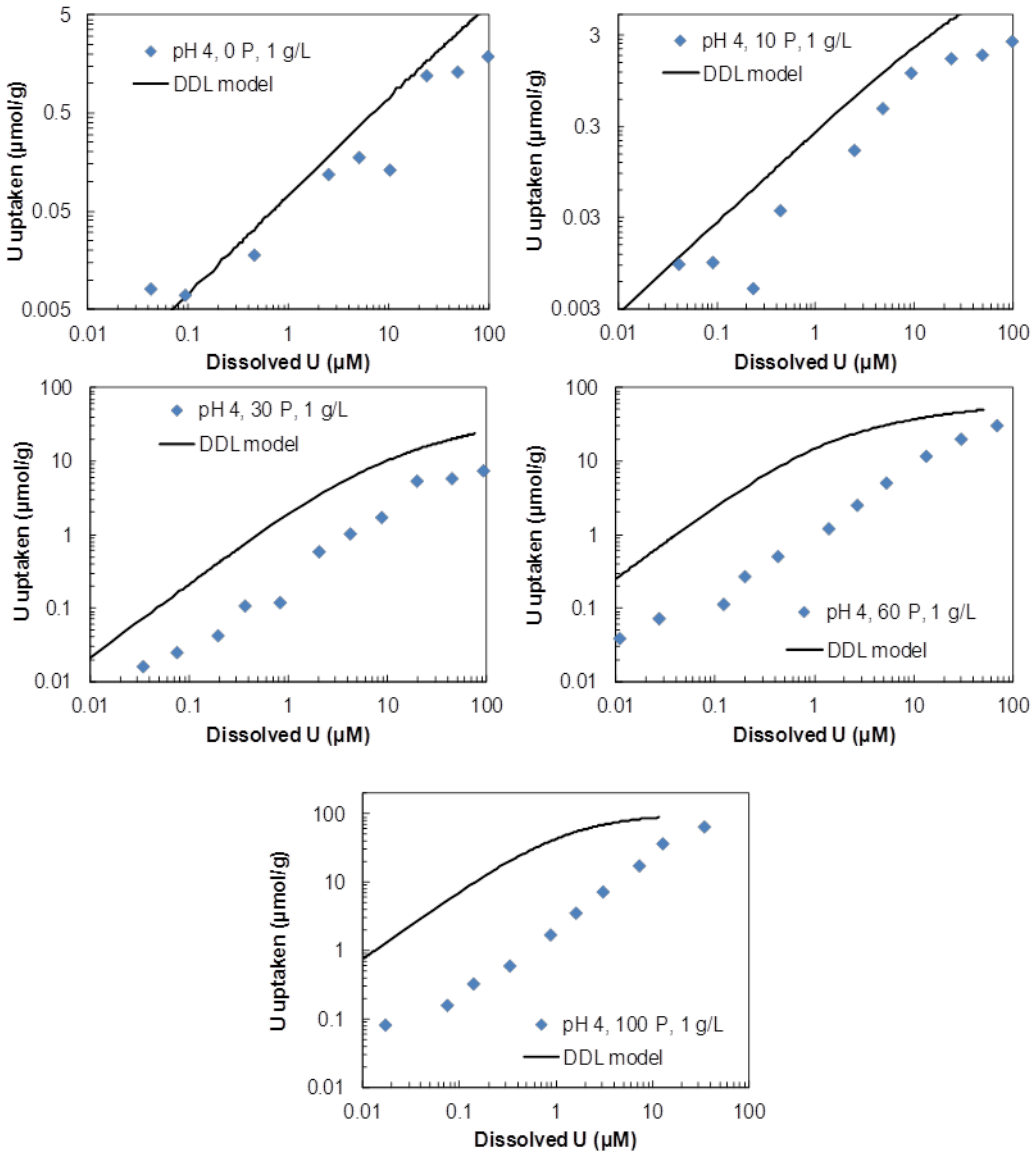

Figure C.3. U(VI) sorption at pH 4, goethite solid loading of 1 g/L and starting phosphate concentrations of 0, 1, 30, 60 and 100 µM. The datapoints represent the observed concentrations for starting U(VI) concentrations of 0 – 100 µM. The solid line represents the diffuse double layer model predictions.

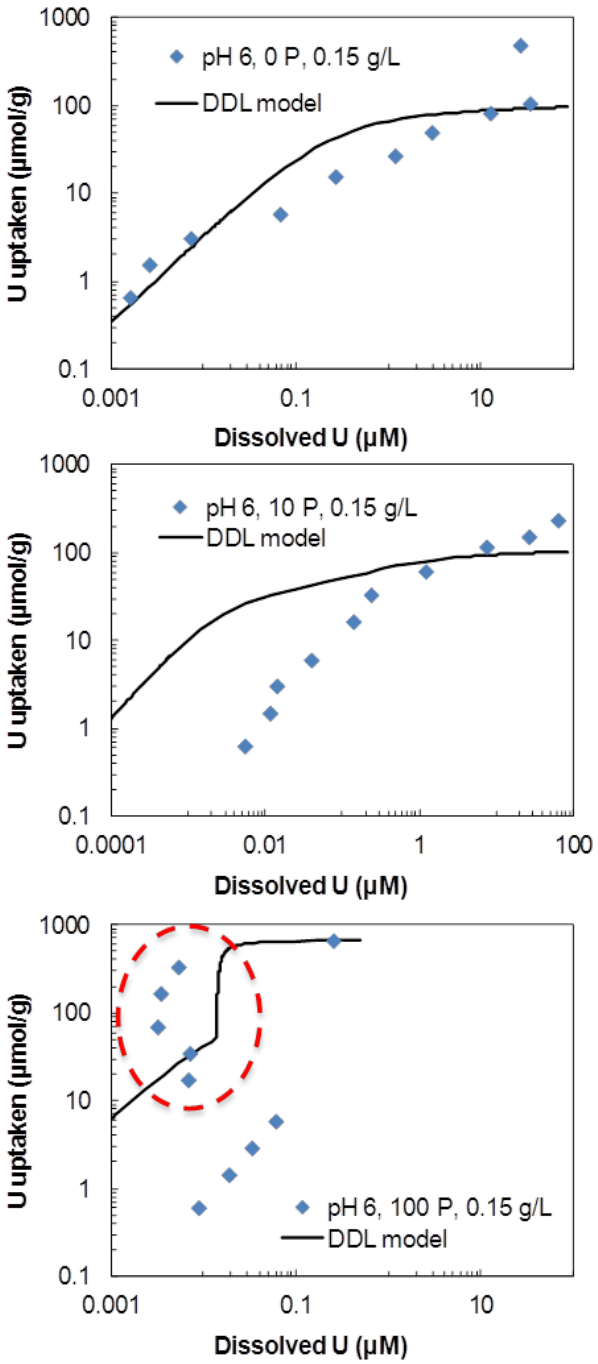

Figure C.4. U(VI) sorption at pH 6, goethite solid loading of 0.15 g/L and starting phosphate concentrations of 0, 10, and 100 µM. The datapoints represent the observed concentrations for starting U(VI) concentrations of 0 – 100 µM. The solid line represents the diffuse double layer model predictions. SI calculations were made using the measured dissolved concentrations of uranium, phosphate and sodium. The dotted oval shows datapoints for which SI calculations suggested that a precipitate might have formed.

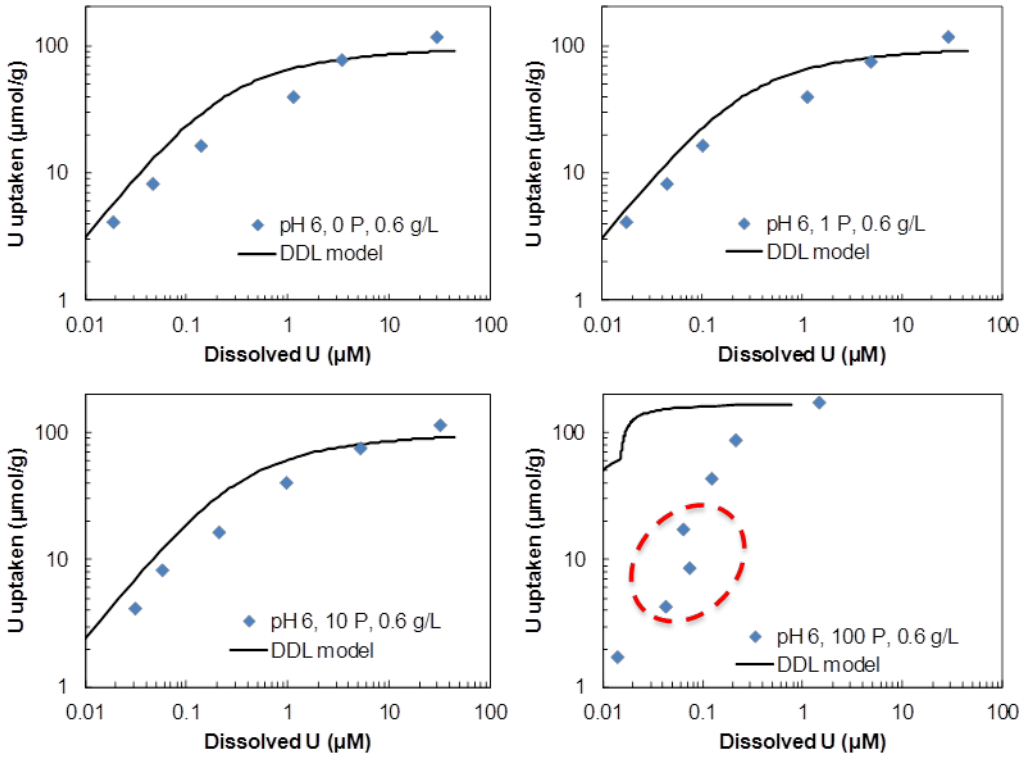

Figure C.5. U(VI) sorption at pH 6, goethite solid loading of 0.6 g/L and starting phosphate concentrations of 0, 1, 10, and 100 µM. The datapoints represent the observed concentrations for starting U(VI) concentrations of 0 – 100 µM. The solid line represents the diffuse double layer model predictions. SI calculations were made using the measured dissolved concentrations of uranium, phosphate and sodium. The dotted oval shows datapoints for which SI calculations suggested that a precipitate might have formed.

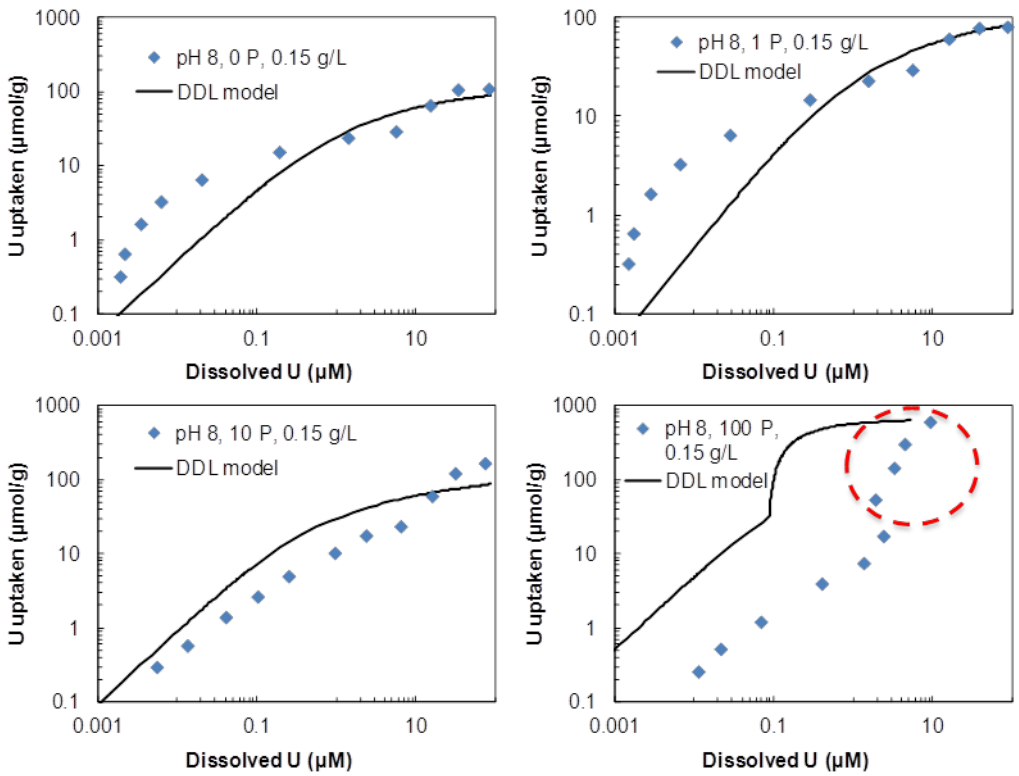

Figure C.6. U(VI) sorption at pH 8, goethite solid loading of 0.15 g/L and starting phosphate concentrations of 0, 1, 10, and 100 µM. The datapoints represent the observed concentrations for starting U(VI) concentrations of 0 – 100 µM. The solid line represents the diffuse double layer model predictions. SI calculations were made using the measured dissolved concentrations of uranium, phosphate and sodium. The dotted oval shows datapoints for which SI calculations suggested that a precipitate might have formed.

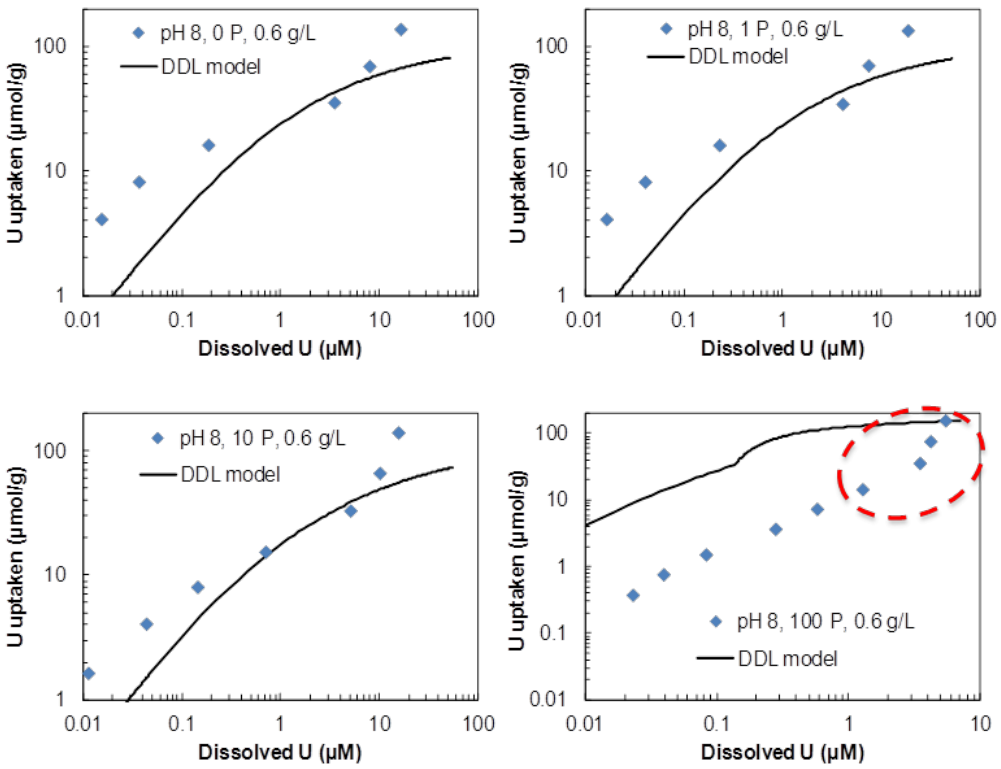

Figure C.7. U(VI) sorption at pH 8, goethite solid loading of 0.6 g/L and starting phosphate concentrations of 0, 1, 10, and 100 µM. The datapoints represent the observed concentrations for starting U(VI) concentrations of 0 – 100 µM. The solid line represents the diffuse double layer model predictions. SI calculations were made using the measured dissolved concentrations of uranium, phosphate and sodium. The dotted oval shows datapoints for which SI calculations suggested that a precipitate might have formed.

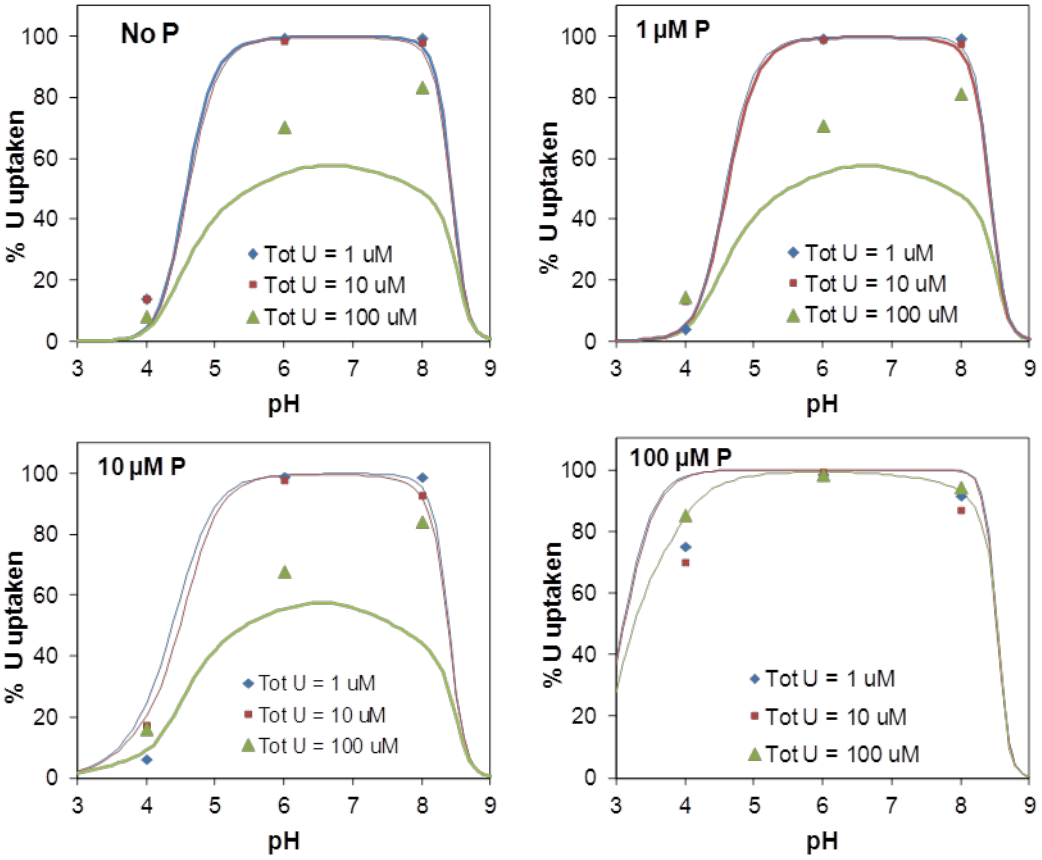

Figure C.8. Observed vs predicted % uranium uptake for a solid loading of 0.6 g/L as a function of pH and starting phosphate concentrations of 0, 1, 10, and 100 µM and starting U(VI) concentrations of 1, 10, and 100 µM. The datapoints represent the observed concentrations whereas the solid line represents the diffuse double layer model predictions.

Key observations

Model prediction for adsorption of uranium onto goethite (no phosphate):

In the absence of phosphate, uranium adsorption was simulated using a single bidentate uranyl adsorption reaction. The model predictions were generally in good agreement with observed uptake for all the pH conditions (4, 6 and 8) and solid loadings of 0.15 g/L, 0.6 g/L or 1 g/L. Under all the conditions, the solution was undersaturated with metaschoepite (the solid most likely to precipitate in the absence of phosphate under favorable conditions) based on model calculations. The observed uptake/sorption data agree well with the model prediction suggesting no precipitation for all the conditions except one. At pH 6 and 0.15 g/L the observed profile suggests the precipitation of some solid at the highest uranium loading (Figure C.1). The saturation index (SI) calculations with respect to metaschoepite indicate that the solution is close to saturation (-0.189) with respect to metaschoepite at this particular condition, which means that dissolved concentrations could be controlled by equilibrium. This behavior was not observed for any other conditions. The results thus suggest that the only adsorption reaction (bidentate uranyl adsorption) included to simulate the uranyl adsorption onto goethite is sufficient to predict the behavior in the absence of phosphate without any needs for additional changes to the logK values.

Model prediction for adsorption of phosphate onto goethite (very low concentrations of uranium): Phosphate adsorption onto goethite was simulated using three monodentate phosphate adsorption reactions. The low starting uranium concentration (0.05 – 5 μM) set of experiments at different pH (4, 6, and 8) and their respective solid loadings as mentioned earlier were used for comparison with the model predictions since they represent the case in which U(VI) would have the least impact on phosphate adsorption and the adsorption of phosphate would be most similar to that in uranium-free experiments. Overall, for all the pH conditions and solid loadings, model predictions were in good agreement (data not shown) with the observed uptake especially with high equilibrium phosphate concentrations. The model slightly overpredicted the phosphate uptake at pH 4 for both solid loadings. At pH 6 and 8 though, the model predictions did not follow a consistent trend at different solid loadings. The model predictions were intentionally compared with only low starting uranium concentrations to rule out the conditions where uranyl phosphate solids could likely precipitate. This mode of comparison helped validate the monodentate phosphate adsorption reactions and suggested that these three reactions do not need any additional changes to equilibrium constants and are sufficient to explain the behavior of phosphate onto goethite under wide range of pH conditions and solid loadings.

Model prediction for uptake of uranium in the presence of phosphate: Model prediction for uranium uptake in the presence of phosphate was simulated

using one ternary U(VI)-phosphate-goethite surface complexation reaction in addition to reactions used for uranium adsorption and phosphate adsorption individually. For all the pH conditions and solid loadings, the uranium uptake prediction matched closely with the observed uptake except at high phosphate concentrations. With increasing initial phosphate concentrations > 10 µM, the model overpredicted the uranium uptake with the highest disagreement observed at 100 µM phosphate concentrations. Interestingly, this is also the only condition where precipitation was predicted to be favorable. Although observed uptake profiles also suggest precipitation for all the solid loadings and pH conditions with 100 µM phosphate concentrations, the model systematically overpredicts the extent of uptake. To get further insights into this, SI calculations with respect to Na-autunite were performed for high phosphate (100 µM) concentration experiments. Calculations were made using MINEQL by considering the aqueous phase final concentrations of uranium and phosphate measured through experiments while assuming all Na^+ (0.01 M) being present in aqueous phase. Although calculations were done for the whole set of data (100 µM phosphate) at different pH and solid loadings, the SI for only those datapoints are tabulated (Table C.2) which are marked in Figures C.2 - C.7 and indicate the transition from undersaturated to supersaturated solutions.

Table C.2. Saturation Index calculations with respect to sodium autunite for a set of experiments.

Figure	pH	Solid loading (g/L)	Starting concentrations		Final concentrations		
			U (μM)	P (μM)	U (μM)	P (μM)	SI
C.2	4	0.60	9.90	99.01	2.95	52.59	-0.22
			24.94	99.75	6.23	48.75	0.37
			49.51	99.01	2.66	14.86	-1.16
			98.91	98.91	14.39	9.48	-0.18
C.4	6	0.15	0.23	105.07	0.02	102.75	0.24
			0.47	105.02	0.03	102.46	0.76
			0.93	105.02	0.06	102.14	1.27
			2.59	104.50	0.01	101.03	-0.72
			5.15	104.97	0.01	94.20	-0.59
C.5	6	0.60	2.49	99.75	0.04	64.75	0.92
			4.97	99.30	0.07	70.11	1.42
			9.79	97.99	0.06	58.85	1.28
C.6	8	0.15	9.89	98.91	1.89	90.06	2.13
			24.79	99.16	3.24	77.05	2.30
			49.63	99.26	4.40	51.58	2.12
			98.72	98.72	9.20	12.62	1.28
C.7	8	0.60	9.89	98.91	1.28	64.15	1.61
			24.89	99.16	3.47	62.59	2.16
			49.65	99.26	4.18	44.29	1.96
			98.81	98.72	5.43	20.37	1.43

Observations pertaining to SI (Na-autunite) based on SI calculations (Table C.2)

- pH 4, 100 μM phosphate: The SI suggested the solution was undersaturated and that it approached saturation with increasing uranium concentrations. When the solution was supersaturated (SI = ~ 0.4), a transition occurred wherein the SI decreased, i.e. the solution became undersaturated before approaching saturation again.
- pH 6, 100 μM phosphate: Similar trends to those seen at pH 4 conditions were observed with the transition occurring at SI = ~ 1.3-1.4 for both the solid loadings.
- pH 8, 100 μM phosphate: Similar trends to those seen at pH 4 and 6 conditions were observed with the transition occurring at SI = ~ 2.1-2.3 for both the solid loadings.

Implications of SI calculations: The SI calculations combined with the observed uptake profiles and model predictions suggest that the precipitation only occurred when the solution achieved a certain level of supersaturation to be able to nucleate. In other words, @ pH 4, 6 and 8, although the solution was supersaturated, Na-autunite did not precipitate until the solution reached critical SI values of 0.4, 1.3 and 2.1 respectively.

Overall, Figure C.8 compares model predictions with experimental observations for different pH, different starting phosphate (0 –100 μM) and total uranium (1 –100 μM) concentrations for a solid loading of 0.6 g/L. The model predictions are generally in good agreement for all the conditions except at high pH (6 and 8) for 100 μM total

uranium and low phosphate (0, 1, and 10 μM) concentrations where the model under predicted the % uptake. The observed uranium uptake that is systematically higher than the model predictions for phosphate concentrations suggests that further work is needed to improve the model prediction.